

MINNESOTA GEOLOGICAL SURVEY  
Harvey Thorleifson, *Director*

---

**PRELIMINARY DESCRIPTION AND  
INTERPRETATION OF THE "HATTENBERGER"  
DEEP TEST WELL, CARLTON COUNTY, MINNESOTA**

**David L. Southwick**  
*Minnesota Geological Survey*

**G.B. Morey**  
*Minnesota Geological Survey*

**J.M. Christopher**  
*Stillwater Area Schools*

**Peter L. McSwiggen**  
*McSwiggen and Associates*

**Terrence J. Boerboom**  
*Minnesota Geological Survey*

*Report of Investigations 63*  
*ISSN 0076-9177*

UNIVERSITY OF MINNESOTA  
Saint Paul — 2005



**PRELIMINARY DESCRIPTION AND  
INTERPRETATION OF THE "HATTENBERGER"  
DEEP TEST WELL, CARLTON COUNTY, MINNESOTA**

This publication is accessible from the home page of the Minnesota Geological Survey (<http://www.geo.umn.edu/mgs>) as a PDF file readable with Acrobat Reader 4.0.

*Date of release: October, 2005*

*Recommended citation*

**Southwick, D.L., Morey, G.B., Christopher, J.M., McSwiggen, P.L., and Boerboom, T.J., 2005, Preliminary description and interpretation of the "Hattenberger" deep test well, Carlton County, Minnesota: Minnesota Geological Survey Report of Investigations 63, 63 p.**

Minnesota Geological Survey  
2642 University Avenue West  
Saint Paul, Minnesota 55114-1057

Telephone: 612-627-4780  
Fax: 612-627-4778  
E-mail address: [mgs@tc.umn.edu](mailto:mgs@tc.umn.edu)  
Web site: <http://www.geo.umn.edu/mgs>

©2005 by the Regents of the University of Minnesota

All rights reserved.

ISSN 0076-9177

The University of Minnesota is committed to the policy that all persons shall have equal access to its programs, facilities, and employment without regard to race, color, creed, religion, national origin, sex, age, marital status, disability, public assistance status, veteran status, or sexual orientation.



## CONTENTS

	<i>page</i>
INTRODUCTION .....	1
Historical background .....	1
Drilling history—The deepened Hattenberger water well (total depth 803 feet) .....	1
Drilling history—The deep exploration well (finished depth 7,440 feet) .....	1
REGIONAL GEOLOGIC SETTING .....	2
GEOLOGIC QUESTIONS .....	5
DESCRIPTIONS OF ROCKS PENETRATED BY CORE DRILLING .....	5
Introduction .....	5
Metasedimentary rocks .....	6
<i>General characteristics</i> .....	6
<i>Lithologic and structural details of the metasedimentary units</i> .....	7
Units H and F: Metamorphosed pelitic, arenaceous, and calcareous rocks .....	7
Units E (metasedimentary component) and D: Metamorphosed iron-formation and pelitic rocks .....	11
<i>Metamorphosed iron-rich rock</i> .....	11
<i>Metamorphosed pelitic rocks of various types</i> .....	15
Unit B: Metamorphosed pelitic rocks, many rich in carbonaceous material .....	15
Metaigneous rocks .....	20
<i>General characteristics</i> .....	20
<i>Lithologic and structural details of the metaigneous rocks</i> .....	23
Unit G—Metadiabase and metagabbro .....	23
Unit E—The metaigneous component of a mixed stratigraphic interval .....	23
Unit C—Metabasalt and metadiabase .....	24
Unit A—Metabasalt and metadiabase .....	24
STRATIGRAPHIC INTERPRETATION .....	25
GEOCHEMISTRY OF THE CORED BEDROCK .....	27
Introduction .....	27
Metamorphosed clastic sedimentary rocks of the Denham Formation .....	28
Metamorphosed limey mudrock and dolostone of the Denham Formation .....	31
Metamorphosed iron-rich strata of the Glen Township Formation .....	31
Metamorphosed carbonaceous mudstone and allied rocks of the Glen Township Formation .....	35
Metamorphosed mafic igneous rocks—Kettle River formation and others .....	35
Miscellaneous veins, sheared rocks, and minor intrusions .....	42
COMPOSITION OF THE WATER AND GAS PRODUCED FROM THE HATTENBERGER WELL .....	46
Introduction .....	46
Geochemical attributes of the well water .....	46

<b>Geochemical attributes of the dissolved gas</b> .....	46
<b>Discussion of the water and gas compositions</b> .....	46
<b>CONCLUSIONS</b> .....	51
<b>REFERENCES</b> .....	53
<b>APPENDIX</b> .....	56

## FIGURES

<b>Figure 1</b>	Bedrock geologic map of east-central Minnesota .....	3
<b>Figure 2</b>	Geologic setting of the Hattenberger drill hole .....	4
<b>Figure 3</b>	Stratigraphic column for the Hattenberger drill hole .....	6
<b>Figure 4</b>	Photomicrographs of mica schist .....	8
<b>A.</b>	Garnet-biotite-quartz schist with graphitic laminae .....	8
<b>B.</b>	Garnet-biotite-quartz schist .....	9
<b>C.</b>	Enlarged view of 4B .....	9
<b>Figure 5</b>	Structural geometry of an $F_2$ fold .....	11
<b>Figure 6</b>	Photomicrograph of porphyroblastic amphibole-rich iron-formation .....	12
<b>Figure 7</b>	Photomicrograph of iron-formation .....	13
<b>Figure 8</b>	Electron microprobe element scans of a garnet porphyroblast .....	17
<b>Figure 9</b>	Variation diagrams of amphibole porphyroblast composition .....	18
<b>A.</b>	AFM plot .....	18
<b>B.</b>	Amphibole classification .....	18
<b>Figure 10</b>	Photomicrographs of graphitic mica phyllite .....	21
<b>A.</b>	The microdecollement surface .....	21
<b>B.</b>	Cleavage relationships.....	21
<b>Figure 11</b>	Photomicrograph of a tectonically rotated porphyroblast .....	22
<b>Figure 12</b>	Photomicrographs of metabasalt .....	26
<b>A.</b>	Igneous texture .....	26
<b>B.</b>	Sheared, partially recrystallized metabasalt.....	26
<b>Figure 13</b>	NASC plots for metaclastic rocks .....	30
<b>A.</b>	Manganese, iron, and trace elements .....	30
<b>B.</b>	Rare earth elements.....	30
<b>Figure 14</b>	NASC plots for iron-rich rocks .....	34
<b>A.</b>	Manganese, iron, and trace elements .....	34
<b>B.</b>	Rare earth elements.....	34
<b>Figure 15</b>	NASC plots for metapelitic rocks .....	36
<b>A.</b>	Manganese, iron, and trace elements .....	36
<b>B.</b>	Rare earth elements.....	37
<b>Figure 16</b>	Geochemical discrimination diagram for iron-formation depositional environments .....	37

<b>Figure 17</b>	Major-element ratio diagram for iron-rich and metasedimentary rocks .....	38
<b>Figure 18</b>	K <sub>2</sub> O–SiO <sub>2</sub> variation diagram for mafic metaigneous rocks .....	42
<b>Figure 19</b>	Cation plot of mafic metaigneous rocks.....	42
<b>Figure 20</b>	Spider plot of minor and trace elements in mafic metaigneous rocks .....	43
<b>Figure 21</b>	Rare earth element plot of data from metaigneous rocks .....	43
<b>Figure 22</b>	Discrimination diagrams for assigning putative tectonic environments .....	44
<b>A.</b>	Y—Ti—Zr diagram.....	44
<b>B.</b>	AFM plot.....	44
<b>Figure 23</b>	Scattergram plot of TiO <sub>2</sub> vs. Mg number for mafic metaigneous rocks .....	44
<b>Figure 24</b>	Stable isotope abundances in the Hattenberger well water .....	49
<b>Figure 25</b>	Fields of hydrocarbon ratio vs. carbon isotope ratio for natural gas .....	50

## TABLES

<b>Table 1</b>	Log of the Hattenberger water well .....	2
<b>Table 2</b>	Core-drilling chronology .....	3
<b>Table 3</b>	Electron microprobe analyses of stilpnomelane in iron-formation .....	14
<b>Table 4</b>	Electron microprobe analyses of garnets in iron-rich rocks .....	16
<b>Table 5</b>	Electron microprobe analyses of amphibole in iron-rich rocks .....	19
<b>Table 6</b>	Chemical analyses of schistose metaclastic rocks .....	29
<b>Table 7</b>	Chemical analyses of calcareous schist and marble .....	32
<b>Table 8</b>	Chemical analyses of metamorphosed iron-rich sedimentary rocks.....	33
<b>Table 9</b>	Chemical analyses of metamorphosed carbonaceous mudstone, iron-rich rocks, and pelites ..	39
<b>Table 10</b>	Chemical analyses of low-K metamorphosed mafic volcanic rocks .....	40
<b>Table 11</b>	Chemical analyses of high-K metamorphosed mafic volcanic rocks .....	41
<b>Table 12</b>	Chemical analyses of altered, veined, or sheared rocks .....	45
<b>Table 13</b>	Chemical analyses of ground water from the Hattenberger well .....	47
<b>Table 14</b>	Isotopic analyses of gas and water from the Hattenberger well .....	48
<b>Table 15</b>	Analyses of gas from the Hattenberger well .....	48
<b>Table 16</b>	Abundance of helium and light hydrocarbons dissolved in well water .....	49

## APPENDIX

<b>Appendix Figure 1</b>	Simplified graphic log of the Hattenberger core .....	56
<b>Appendix Table 1</b>	Geochemical analyses of the Hattenberger core .....	58

## NOTE ON MEASUREMENTS USED IN THIS REPORT

Although the metric system is preferred in scientific writing, certain measurements are still routinely made in English customary units; for example, distances on land are measured in miles and depths in drill holes are measured in feet. Preference was given in this report to retaining the units in which measurements were made. To assist readers, conversion factors for some of the common units of measure are provided below.

### English units to metric units:

To convert from	to	multiply by
inch	millimeter	25.40
inch	centimeter	2.450
foot	meter	0.3048
mile	kilometer	1.6093

### Metric units to English units:

To convert from	to	multiply by
millimeter	inch	0.03937
centimeter	inch	0.3937
meter	foot	3.2808
kilometer	mile	0.6214

# PRELIMINARY DESCRIPTION AND INTERPRETATION OF THE "HATTENBERGER" DEEP TEST WELL, CARLTON COUNTY, MINNESOTA

David L. Southwick, G.B. Morey, J.M. Christopher, Peter L. McSwiggen, and Terrence J. Boerboom

## INTRODUCTION

### Historical background

In 1994, the Minnesota Geological Survey received for study and interpretation 6,637 feet (2,023.5 meters) of drill core obtained from a deep exploration test well named Hattenberger Number 1. The test hole, located in T. 46 N., R. 21 W., sec. 2, SE 1/4, SE 1/4, Carlton County, Minnesota (46-21-2DD), was financed by Turmoil, Incorporated, a group of local investors who were exploring for natural gas. It was drilled and cored continuously by the E.J. Longyear Company between 1978 and 1979. Although commercial quantities of gas were not found, the hole provides a geologically valuable depth-dimension view of deformed, metamorphosed Paleoproterozoic rocks in an area of very limited bedrock exposure. Furthermore, it is the longest continuously cored hole ever drilled in Minnesota, and the human-interest story that led to its drilling is a significant piece of local history.

The drilling was done on the farm of Mr. Lee Hattenberger, a principal of Turmoil, Inc. After drilling ceased in 1979, the Turmoil group stored the core in a barn in the Kettle River area in the hope its availability would be an incentive for additional public or private funding of the gas exploration venture. No further capital was forthcoming, and in 1994 the principals decided to donate the drill core to the Minnesota Geological Survey for scientific study. The core survived 15 years of storage intact.

The occurrence of gas on the Hattenberger property was much publicized in the press in the 1970s. Prior to 1971, a shallow well on the Hattenberger farm produced only limited quantities of potable water. In 1971, the Hattenbergers drilled a new well 803 feet deep in an effort to obtain an improved yield of better-quality water. The deepened well produced a limited supply of salty-tasting water and also gave constant problems with "air" in the plumbing system. Five years later, in the winter of 1976, a minor explosion occurred in the bathroom when a candle was lit during a power outage. This demonstrated rather emphatically that the "air" in the pipes was in fact flammable gas, and

precipitated a flurry of studies of the well and the gas it was producing. Later Mr. Hattenberger and others, attracted to the prospect of a commercial gas well in east-central Minnesota, decided to drill a deep core hole to test the possibilities. Although no commercial quantities were found, the deep core hole was still producing a small and steady volume of gas at last report.

### Drilling history—The deepened Hattenberger water well (total depth 803 feet)

The Anderson Drilling Company of Duluth, Minnesota extended the Hattenberger water well to a depth of 803 feet in 1971. A brief driller's log of that operation filed with the Minnesota Geological Survey (Table 1) shows that "saline" water was encountered at depths of 530 and 780 feet. Apparently, excess "air" was encountered at a depth of 800 feet. The driller's record also shows that a water sample, presumably from the original shallow well, had been submitted to the Minnesota Department of Health in 1970 for chemical analysis, but reports no analytical results. The well water evidently was sampled again about five years later, some months after the bathroom-explosion incident. A Department of Health water analysis dated July 12, 1976, and attached to the 1971 driller's log in the Minnesota Geological Survey well log files, reports 1,100 milligram per liter chloride, 480 milligram per liter sodium, 9.3 milligram per liter potassium, 9.5 milligram per liter sulfate, and alkalinity equivalent to 150 milligram per liter calcium carbonate. This analytical report also states that the "air" from the well probably was methane, or if not methane, perhaps propane that had leaked from tanks or pipelines somewhere in the area. The statement on gas composition appears to have been an opinion rather than the result of an actual gas analysis.

### Drilling history—The deep exploration well (finished depth 7,440 feet)

In early 1978, a decision was made to extend the Hattenberger water well to search for additional hydrocarbons at depth, and the venture name "Hattenberger Number 1" (abbreviated "HB-1" in the remainder of this report) was assigned. Drilling

**Table 1.** Annotated driller's log of the deepened Hattenberger water well drilled in 1971. There are no cuttings available from which to verify the driller's interpretations of the rock types penetrated by this drilling. The rock recovered at depth 803 feet in the 1978 core drilling (the top of the cored interval) is a metadiabase. Therefore it is possible the 1971 driller misidentified the black rock above 803 feet. It also is possible that the driller's labels were correct, inasmuch as there are substantial intervals of slaty rocks ("shale") and iron-formation interdigitated with metavolcanic rocks deeper in the 1978 core hole.

Depth (feet)	Thickness (feet)	Material and conditions reported by Anderson Drilling Company
0 – 20	20	Clay
20 – 530	510	Very hard drilling in a gray rock described as iron-formation and shale
530	—	Saline water
530 – 780	250	Gray shale and iron-formation (depth and thickness of shale and iron-formation layers not recorded)
780	—	Saline water
780 – 803	23	Same rock; excess air encountered at 800 feet

contractor E.J. Longyear Company started core drilling at the bottom of the 803-foot water well on August 14, 1978, using a NQWL drill stem (Table 2). A considerable flow of gas, presumably methane, was encountered at a depth of 2,400 to 2,500 feet. The gas-producing interval was grouted off and redrilled using a NXWL drill stem. Gas was reportedly encountered again at a depth of 2,700 to 2,800 feet and that interval was also grouted off and redrilled using a BQWL drill stem, the core size used to the bottom of the hole. Periodic gas flow continued to be a problem downward from 2,800 feet to the bottom of the hole.

Although the drilling contractor encountered numerous technical problems, most involving uncontrolled gas flow, core recoveries were excellent, approaching 100 percent over most of the hole.

## REGIONAL GEOLOGIC SETTING

HB-1 was drilled into coarsely interstratified metasedimentary and metavolcanic rocks that were deposited, deformed, and metamorphosed during the tectonic evolution of the Penokean orogen, between 2,200 and 1,800 Ma. The portion of the Penokean orogen in which HB-1 is situated (Fig. 1) is an allochthonous or para-allochthonous fold-and-thrust belt that contains several geophysically defined structural discontinuities interpreted as zones of thrusting. The discontinuities bound discrete structural panels or domains that display regionally consistent internal stratigraphy and small-scale structural features consistent with north–northwest-verging nappes (Holst, 1984; Southwick and others, 1988; Southwick and Morey, 1991). This belt of

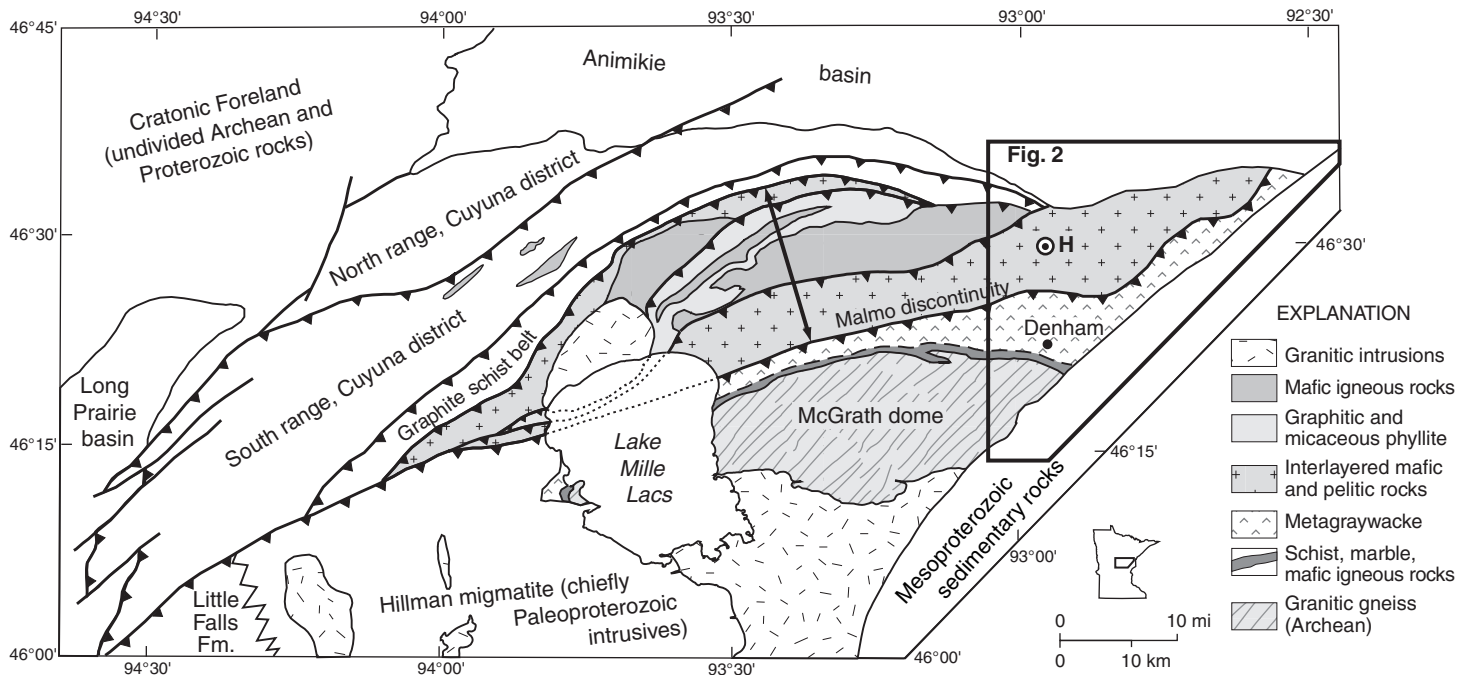
strongly deformed rocks flanks a tectonic foreland basin that extends to the Mesabi Iron Range in northern Minnesota, where rocks of the Animikie Group are exposed.

HB-1 is located in the Moose Lake–Glen Township structural panel (Figs. 1, 2), which occupies a medial or internal position in the fold-and-thrust belt (Southwick and others, 1988). Bedrock crops out in only a few places (Fig. 2; McSwiggen, 1987) and most of the rock types present beneath glacial cover generate only weak, non-diagnostic geophysical expressions. These limitations, plus very sparse drilling coverage and swampy ground conditions that restrict surface access, create substantial difficulties in interpreting the geology at scales more detailed than the regional-reconnaissance level.

Nevertheless, it is relatively certain from the limited geologic and geophysical observations available that coarsely interstratified metavolcanic rocks, metadiabase, graphitic schist, and iron-formation assignable to the Glen Township Formation of Morey (1978) occupy the western part of the Moose Lake–Glen Township panel at the surface (Fig. 1; also Boerboom and others, 1999a, b; Southwick and others, 2001). To the east, the panel contains a sequence of graphitic muscovite-chlorite phyllite and schist exposed near Barnum and Atkinson, and a sequence of metamorphosed volcanic and hypabyssal rocks exposed near Kettle River. A sequence of locally garnetiferous mica schist and metagraywacke exposed near Moose Lake, formerly mapped within the Moose Lake–Glen Township panel (Southwick and others, 1988), has been reinterpreted to lie outside the panel on the south (Boerboom and others, 1999a). Hole

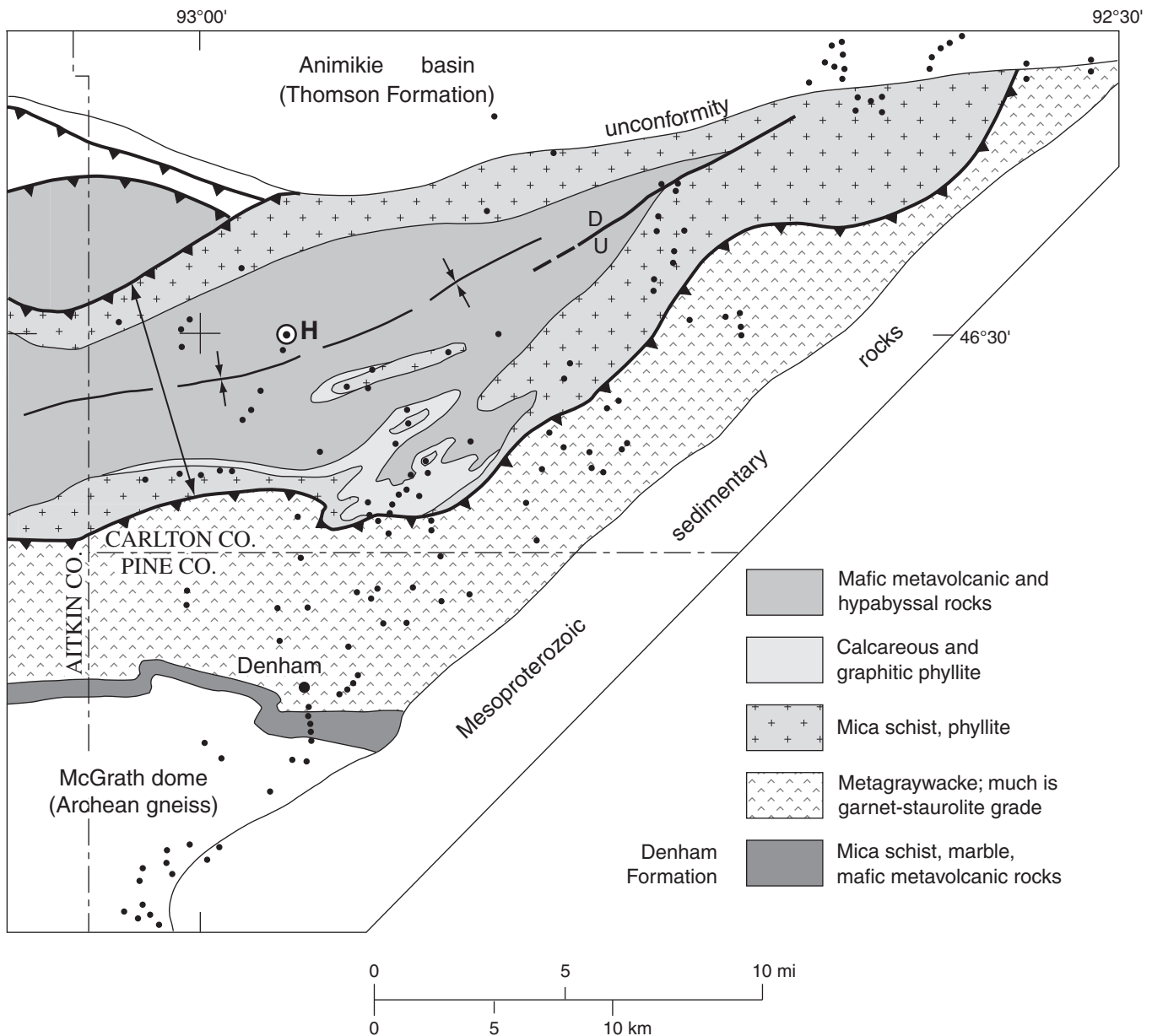
**Table 2.** Chronology of core-drilling operations on the Hattenberger Number 1 deep test well, 1978 to 1979.

Date (M/D/Y)	Reported depth in feet	Bit size	Remarks
8/14/78			Mobilized rig, one 12-hour shift
8/16/78 to 9/14/78			Prepared water well for wire-line core drilling NQWL
9/15/78	803	NQWL	Started drilling
9/30/78	1,275		
10/31/78	1,800		
11/1/78	2,400–2,500	NXWL	Encountered large volume of gas; cased off and redrilled NXWL
11/17/78	2,700–2,800	BQWL	Large volume of gas reappeared; cased off and redrilled BQWL. Gas flow continued to be a problem from 2,800 feet downward
11/17/78	3,080		Second 12-hour shift added
11/23/78	3,301		
11/30/78	3,471		
12/31/78	4,299		
1/26/79	5,062		
1/29/79 to 4/8/79			Demobilized for winter; removed rig from site
4/8/79			Remobilized with larger rig. One 12-hour shift.
4/9/79 to 5/9/79			Prepared site for start up of drilling, second 12-hour shift added
5/10/79	5,092		
5/31/79	5,838		
6/29/79	6,808		
7/31/79	7,410		
8/2/79	7,440		
8/8/79 to 8/21/79			Reduced to single 8-hour shift, miscellaneous breakdowns, repairs, false startups
8/21/79	7,440		Demobilized rig



**Figure 1.** Generalized tectonostratigraphic map of east-central Minnesota showing the principal geologic units in the Penokean fold-and-thrust belt and the location of the Hattenberger exploration drill hole (H); modified from Boerboom and others (1999a, b). The breadth of the Moose Lake–Glen Township structural panel is indicated by the double-headed arrow; the area of Figure 2 is enclosed by the heavy frame.





**Figure 2.** Geologic sketch map of the eastern end of the Moose Lake–Glen Township structural panel (breadth indicated by double-headed arrow) and portions of surrounding panels. Solid dots are locations of substantive bedrock observations, either outcrop or drill core. The Hattenberger drill hole (H) is located in a broad area where first bedrock is mainly metabasalt or closely allied metadiabase. The regional synform portrayed here is a new structural interpretation based loosely on previous mapping by McSwiggen (1987), Southwick and others (1988), and Boerboom and others (1999a).

HB-1 is collared in metadiabase and metabasalt of lower amphibolite grade that are within the sequence of volcanic strata near Kettle River (Fig. 2).

The belt of basaltic and andesitic metavolcanic rocks in which HB-1 is collared is more or less central to the Moose Lake–Glen Township structural panel toward its eastern end (Fig. 2) and is traceable along regional strike at least 40 miles (64 kilometers) west

of the drill site (Fig. 1). In the eastern part of the panel, informally known as the Kettle River area, the metavolcanic belt is flanked on the north and south by belts of mica schist and phyllite derived principally from thin-bedded argillaceous sedimentary rocks and fine-grained graywacke (Fig. 2). Also present in the southern metasedimentary belt are significant but local thicknesses of calcareous and graphitic phyllite



that greatly resemble sequences in the type locality of the Glen Township Formation (Morey, 1978) in the northern sub-panel of the Moose Lake–Glen Township panel north of Lake Mille Lacs (Fig. 1).

Regionally, the belt of graphitic rocks mapped along the northern side of the Moose Lake–Glen Township panel can be traced westward over a strike length of more than 80 miles (129 kilometers) on the basis of sparse drilling and characteristic geophysical signature (Fig. 1). Some of the material in this belt is lithologically similar to the Glen Township type, but neither physical nor temporal correlations with the Glen Township type section have been established. The belt of metagraywacke and related rocks mapped south of the Malmo discontinuity and north of the McGrath dome (Fig. 1) can be projected westward with far less confidence than the graphite schist belt, owing to the lack of drilling control or distinctive geophysical definition. Distinctive quartz-rich metaclastic rocks and dolomitic calcareous strata south of the metagraywacke belt are reliably assigned to the Denham Formation (Morey, 1978; Boerboom and Jirsa, 2001). However, the rocks of the metagraywacke belt proper, including those exposed near Moose Lake, cannot be correlated confidently with any of the named formations of the Mille Lacs Group as defined by Morey (1978). Boerboom and Jirsa (2001) suggested that some or all of these unassigned strata may correlate with the Little Falls Formation, the type locality of which is about 85 miles (142 kilometers) along regional strike to the southwest of the Kettle River–Denham–Moose Lake area.

## GEOLOGIC QUESTIONS

The results obtained from drilling core hole HB-1 and the peculiar circumstances leading up to the drilling pose several questions of scientific interest. Among them are:

1. *What does the core reveal about the stratigraphic, structural, and metamorphic evolution of the Moose Lake–Glen Township panel, or more broadly, of the Minnesota segment of the Penokean orogen?*
2. *What are the implications, if any, of the core-hole findings for mineral exploration strategies in east-central Minnesota?*
3. *What is the origin of the gas that emanated from the pre-coring water well and from various deeper levels in the cored hole? Are rock–fluid interactions involved, and if so, to what extent?*

In this report we contribute to the resolution of these questions by furnishing preliminary

descriptions of the sequence, composition, and structural condition of rock units encountered in the drilling, and a summary of available data (all acquired in the 1970s) on the chemical attributes of the well water and the emanating gas. We expect that this information will be used as the foundation for future, more detailed research.

## DESCRIPTIONS OF ROCKS PENETRATED BY CORE DRILLING

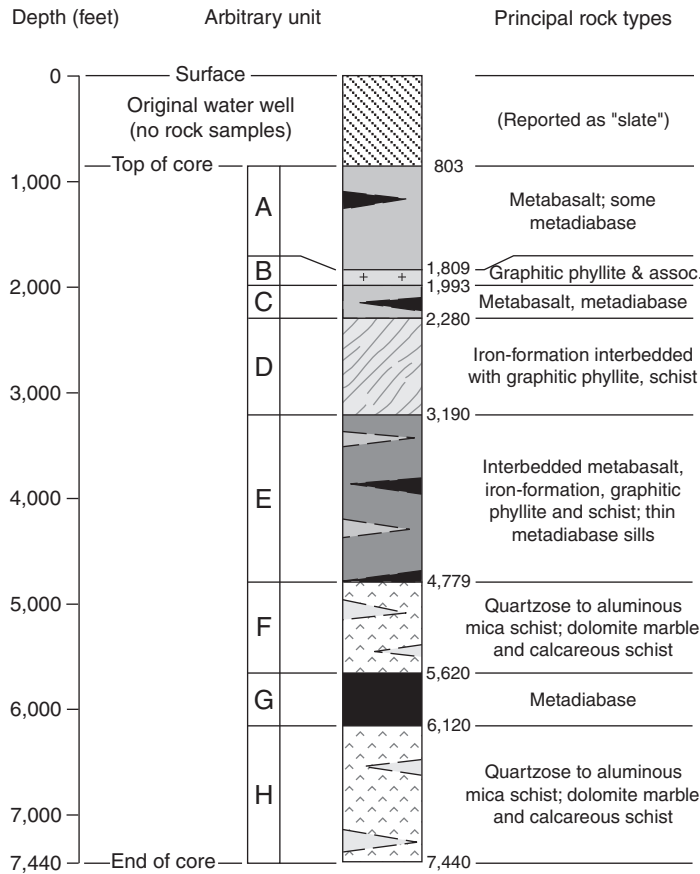
### Introduction

Core hole HB-1 was drilled vertically to a total depth of 7,440 feet (2,268.3 meters). However, because core drilling started at a depth of 803 feet, only 6,637 feet of rock were actually cored. Although there are clear indications of small-scale, inclined to recumbent folding and low-angle faulting in portions of the core, particularly near the contacts of mechanically competent rocks with less competent rocks and within certain of the incompetent sequences, there is no definitive evidence of significant stratigraphic inversion or repetition. The section penetrated by HB-1 therefore is interpreted and described as an essentially upright stratigraphic sequence of interlayered metasedimentary and dominantly mafic metavolcanic rocks (Fig. 3). Sills of metadiabase or metagabbro petrologically related to the mafic volcanic rocks are also relatively abundant. With the exception of two minor dikes of fresh diabase that are interpreted to be manifestations of Mesoproterozoic Midcontinent-rift magmatism (Fig. 1), all of the rocks in the core have been metamorphosed to the upper greenschist or lower amphibolite facies and exhibit deformational fabrics.

For descriptive purposes, the core is divided into eight stratigraphic intervals labeled A (top) through H (Fig. 3, Appendix Fig. 1). The lithologic attributes of these intervals are summarized in the following sections. A generalized graphic log appears in Appendix Figure 1 for reference.

Units B, D, F, and H of the section cut by drill hole HB-1 are predominantly metasedimentary rock, units A, C, and G are predominantly mafic metaigneous rock in the form of metabasalt flows and closely allied sills of metadiabase and metagabbro, and unit E is a mixed interval composed of about 75 percent metaigneous rock and 25 percent metasedimentary rock. We describe the metasedimentary rocks first and the metaigneous rocks second, and describe the units of both types in apparent stratigraphic order, from oldest (deepest) to youngest.

**SCHEMATIC LOG**  
HATTENBERGER CORE



**Figure 3.** Highly generalized stratigraphic column for the Hattenberger exploration drill hole. Units A through H are arbitrary lithostratigraphic subdivisions erected for convenience in logging and describing the core. See Appendix Figure 1 for greater detail.

**Metasedimentary rocks**

*General characteristics*

**Unit H**, from depth 6,120 feet to the end of the core at 7,440 feet, and **unit F**, between the depths of 4,779 and 5,620 feet, are composed principally of variably calcareous, quartz-rich pelitic and semi-pelitic mica schist and phyllite; metamorphosed feldspathic arenite, quartz arenite, and arkose, plus fine-grained metaconglomerate of similar compositions; quartz-rich metasiltstone; calcareous, phyllosilicate-rich, laminated to thin-bedded metasiltstone and metagraywacke; and marble that contains as much as 90 modal percent carbonate minerals. These rock types are interbedded on scales of decimeters to meters. Modally, the rocks consist primarily of quartz, alkali feldspar, plagioclase, muscovite, biotite, and carbonate minerals (calcite and/or dolomite) in variable proportions. Garnet is present in the more aluminous layers, and chlorite is a moderately abundant retrograde phase in parts of both units. In addition to these principal rock types, Unit H contains scattered laminae or very thin beds of iron-

formation composed principally of recrystallized chert and subhedral to anhedral magnetite. Garnet, graphitic or carbonaceous material, biotite, and pyrite are minor but ubiquitous constituents of the iron-formation layers.

Units H and F are lithologically very similar, and are distinguished only by their positions below (H) or above (F) a thick metadiabase sill termed unit G. The top of unit F is placed arbitrarily at the base of another prominent metadiabase sill assigned to unit E (Fig. 3). This horizon marks an abrupt transition in the metasedimentary record in that fine-grained, dark gray to black mudrocks of various types above the sill supplant the calcareous quartz-rich rocks characteristic of units H and F below the sill. The F-E contact also marks an upward transition to more volcanic rock in the cored sequence.

The principal metasedimentary rock types in **unit E**, between depths 3,190 and 4,779 feet, and **unit D**, between depths 2,280 and 3,190 feet, are quartz-poor, fine-grained pelitic and semipelitic mica schist and phyllite; graphitic or carbonaceous schist and phyllite;

and various types of actinolite- or garnet-bearing iron-formation. Metasedimentary rock accounts for about 25 percent of the thickness of unit E and consists chiefly of actinolitic iron-formation; the remainder of unit E consists of mafic metavolcanic rocks and metadiabase sills.

The base of **unit D** is placed arbitrarily at the upper contact of a massive metadiabase sill assigned to unit E (Appendix Fig. 1). Unit D consists predominantly of metamorphosed mudrock and iron-formation in approximately equal proportions. These are interbedded on scales ranging from centimeters to tens of meters. A thin sill of metadiabase occurs in the lower quarter of the unit, and some of the chloritic and/or actinolitic schists in the middle of the unit, within an interval designated as "mixed schist" in Appendix Figure 1, may originally have been in part tuffaceous. These metaigneous components amount to no more than 10 to 15 percent of the drilled thickness of unit D. The top of unit D is placed arbitrarily at the base of a dominantly metavolcanic sequence assigned to unit C.

The quartz-poor pelitic and semipelitic schists (metamorphosed mudrocks) of units E and D are chiefly of two types—chlorite-biotite schist and graphitic garnet-biotite schist. Although thoroughly recrystallized and affected by at least two periods of metamorphism, they contain local primary sedimentary features indicative of deposition in relatively quiescent water that was affected periodically by weak turbidity currents. These features include minor erosional discontinuities, slump structures, thin beds of intraformational microconglomerate, and graded beds. The size-graded particles in graded beds are mainly quartz and feldspar in the fine-grained sand to silt range.

Particularly striking within the pelitic section are thin beds and groups of thin beds that are rich in graphite or carbonaceous material and contain prominent porphyroblasts of garnet. The garnet occurs in clusters within irregular layers as thin as 1 to 3 millimeters or as scattered grains over intervals as thick as 0.5 meter. The dark pink to red garnet crystals are subhedral to anhedral and range in diameter from 1 to 7 millimeters. Individual porphyroblasts are typically rotated and the associated pressure shadows are filled with carbonate. The garnet is poikiloblastic and contains inclusions of quartz, calcite, and rare pyrite. Graphite or carbonaceous material is a principal constituent of the garnetiferous layers, ranging from a few to as much as 50 modal percent. Where relatively sparse, the graphitic material occurs along foliation planes as lens-shaped

stringers. The stringers merge across foliation planes to form irregularly shaped masses within the beds that are relatively graphite-rich.

Two long intervals (a few tens of meters) and several short intervals (ten meters or less) of distinctive iron-rich metasedimentary rocks occur in units D and E (Fig. 3). Iron-rich layers occur over a total core intercept of about 1,900 feet, within which they are interleaved with several thin to thick sequences of ordinary pelitic rocks and mafic volcanic rocks and intruded by diabase sills. The iron-rich rocks contain abundant very fine-grained opaque material, including graphite, and their iron-rich character is not easily recognized without chemical analyses. Much of the iron apparently resides in ultra-fine-grained oxide and sulfide minerals.

The iron-rich intervals are bedded on the scale of centimeters to meters, are generally black to dark greenish-gray, and are characterized by the local presence of centimeter-size garnet or amphibole porphyroblasts that are confined to specific beds of appropriate bulk composition. Abundantly porphyroblastic beds are interspersed with beds or groups of beds that are porphyroblast-free. The dark color of the rock is due to the presence of abundant graphite, iron sulfides, and iron oxides along with fine- to medium-grained amphibole and biotite. The proportions of mafic silicate minerals, sulfides, oxides, and graphite vary widely and abruptly from bed to bed, but all beds are essentially black.

**Unit B**, between the depths of 1,809 and 1,993 feet, is the uppermost core interval that is predominantly metasedimentary rock (Fig. 3). It consists chiefly of graphitic phyllite, metasiltstone, and quartz-mica schist. Thin beds of graphitic sulfide iron-formation are present locally. The rock just above the basal contact with the underlying metabasalt of unit C is a strongly foliated chlorite schist that may be in part tectonized metaigneous rock. The upper contact of unit B is placed at a shear zone within a section of rock in which metasedimentary strata and metabasalt flows are interbedded. The interstratified interval is the stratigraphic transition to overlying unit A, which is predominantly metaigneous rock. From a lithologic standpoint, the metasedimentary rocks of unit B closely resemble those of units E and D.

#### *Lithologic and structural details of the metasedimentary units*

#### **Units H and F: Metamorphosed pelitic, arenaceous, and calcareous rocks**

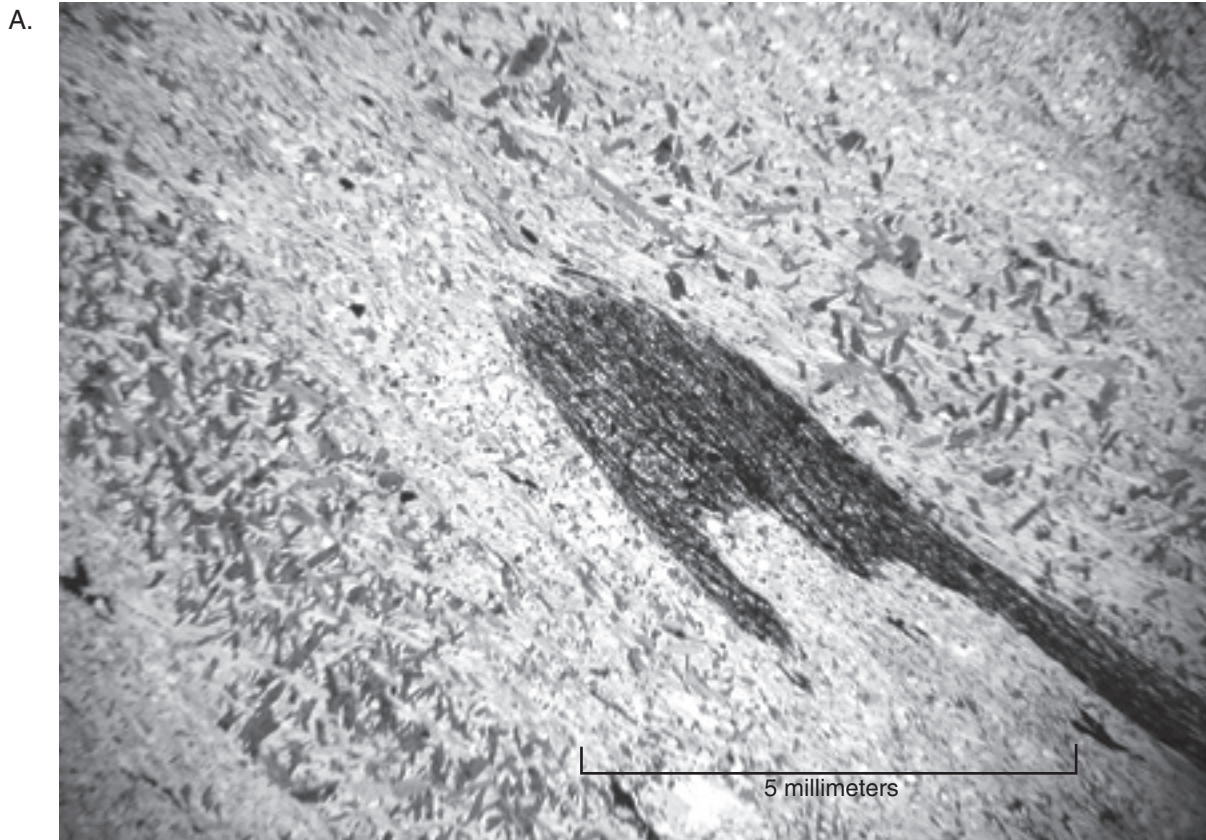
Core units H and F are very similar lithologically, and together constitute a coherent stratigraphic



sequence that is the deepest and stratigraphically oldest unit encountered in hole HB-1. Taken as a whole, the metasedimentary rocks of units H and F are strata that can be reasonably interpreted as having been original mixtures of clay, detrital quartz and feldspar, and carbonate minerals. Beds originally of pelitic or semipelitic composition are now dominated modally by the micas; beds originally of arkosic, quartz arenite, or quartz wacke composition are now quartz- and feldspar-rich schists (typically on the order of 50 to 80 percent modal quartz plus feldspar), and beds originally composed of marly material and relatively clean lime mud are now carbonate-calc-silicate-mica schist, micaceous to quartzose marble, and relatively clean dolomite

marble. Primary sedimentary structures and textures are variably preserved. Clastic textures generally have survived metamorphism to some extent in rocks that originally were various types of sandstone or granule conglomerate, but have been obliterated from rocks that originally were siltstone or shale.

Quartz-mica schist, broadly defined, is the most abundant rock type in the H to F interval (Fig. 4A), constituting about 60 percent of the section cored. Calcareous schist, composed principally of quartz, the micas, carbonate minerals, and the feldspars (Fig. 4B), amounts to about 30 percent of the section, and is compositionally transitional between the carbonate-poor quartz-mica schist and dolomitic marble. Unit H contains a higher proportion of



**Figure 4.** Photomicrographs of mica schist varieties typical of core units H and F. All images taken with partially crossed nicols.

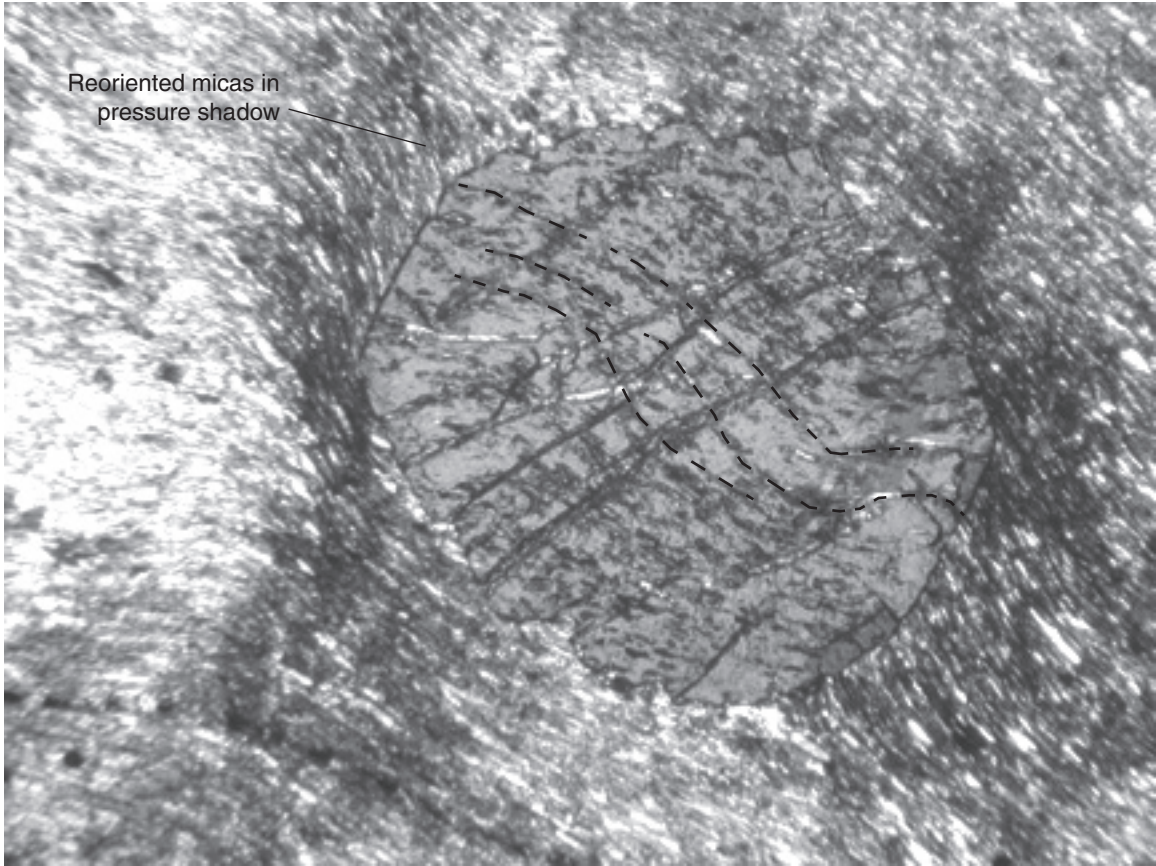
**A.** Garnet-biotite-quartz schist with thin graphitic laminae; from unit H, depth 6,838 feet. Note the rootless isoclinal fold traversed by  $S_1$  axial-plane schistosity.

**B.** Garnet-biotite-quartz schist from unit F, depth 5,146 feet. The garnet in the center (about 1.7 millimeters in diameter) contains sigmoidal inclusion trails (dashed lines).  $S_1$  micas external to the garnet are sharply reoriented in blunt asymmetric pressure shadows.

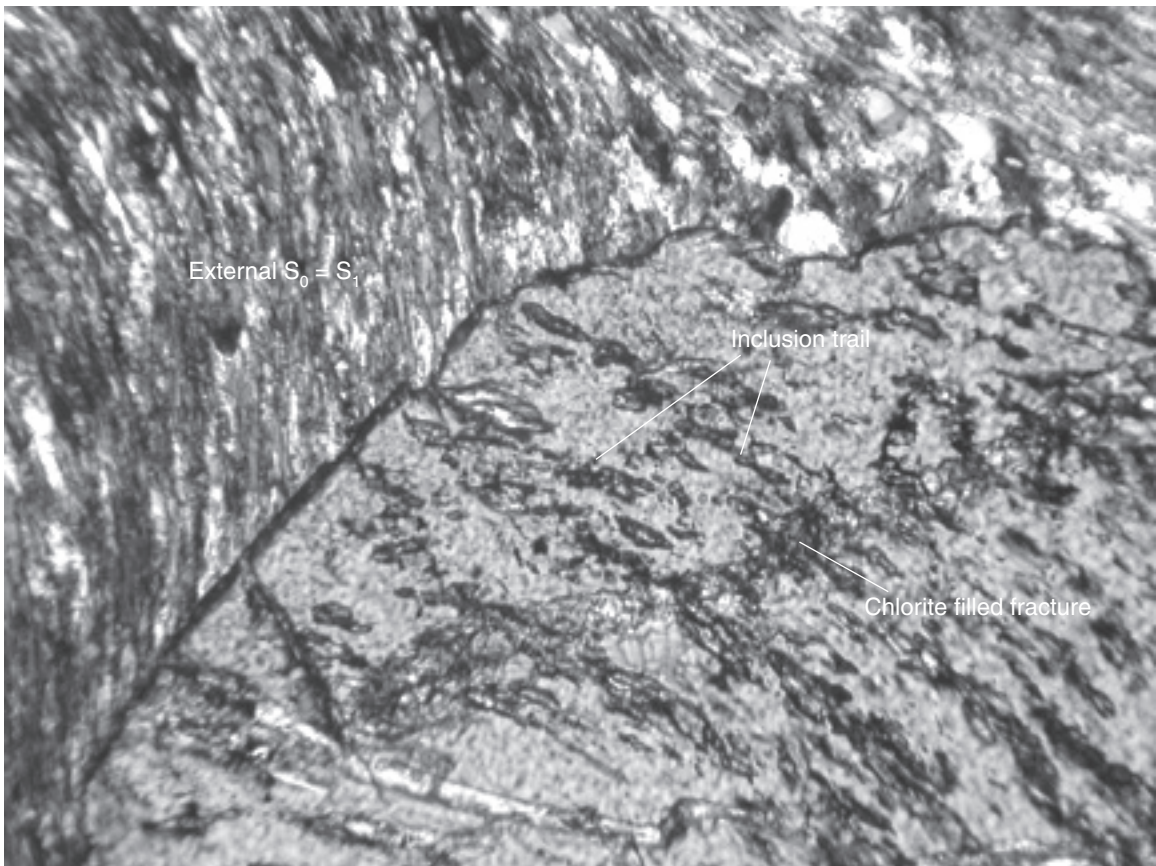
**C.** Enlarged view of the garnet margin (from Fig. 4B) showing the discordant relationship between fabric of the external rock matrix and the internal inclusion trails.



B.



C.



schists identifiable as metamorphosed quartz arenite, arkose, and related granule conglomerate than unit F, but these coarser-grained clastic rock types are represented throughout the H to F section. The major rock types (including pelitic schist, meta-arenites of various types, calcareous schist, and dolomitic marble) are interstratified on scales ranging from several centimeters to several meters and commonly display both gradational and sharp contacts with one another. Also present in the sequence are thin beds and groups of beds of tremolite schist, actinolite schist, graphite schist, and recrystallized cherty iron-formation. These relatively minor rock types are less abundant in unit H than in unit F.

Some sequences of quartz-rich meta-arenite, metagraywacke, and associated quartz-rich pelitic and semi-pelitic schists within the H to F interval contain muscovite as the predominant mica, some sections contain biotite as the predominant mica, and other sections contain both micas in roughly equal amounts. Bedding is defined by the relative proportions of quartz and the micas. Some beds, but not all, display sharp basal discontinuities and gradational tops; internally, these are size- and content-graded and typically are parallel or cross laminated in their upper micaceous parts. Local beds of microconglomerate, some containing quartz clasts and polymineralic granitic clasts as large as 15 millimeters in diameter, are fairly common.

Rocks classed as quartz-rich metagraywacke contain as much as 50 modal percent sand-size quartz, and average about 25 modal percent. The larger quartz grains are dominantly subrounded and polycrystalline, whereas smaller grains are subangular and monocrystalline. The sand-size population also includes a small fraction of granitic rock fragments (quartz and plagioclase) and monocrystalline feldspar grains. The sand-size grains are set in a matrix of very fine-grained sand- and silt-size grains of recrystallized quartz and plagioclase intergrown with the micas.

Rocks classified as metasiltstone are very fine-grained versions of the quartz wackes. They are thin- to medium-bedded and consist of various proportions of quartz and feldspar plus muscovite and rarely biotite. Commonly, the silicate minerals in the metasiltstone are patchily and irregularly replaced, wholly or in part, by secondary dolomite.

The most common type of calcareous schist in the H to F core interval is similar to the non-calcareous schist in bedding characteristics and structural development. Because carbonate minerals generally amount to 10 percent or less of the mode, bedding reflects variations in the relative abundances of silicate minerals rather than variations in carbonate

content. As the total amount of carbonate increases beyond about 10 percent, however, modal layering of carbonate species becomes evident locally. A yellowish-brown carbonate (siderite or ankerite) defines layers several centimeters thick toward the middle of unit F. Elsewhere, and more commonly, the carbonate phase is white or pale gray calcite and/or dolomite that forms discrete grains or multigrain lenses among the more abundant silicate crystals in the rock. A more carbonate-rich calcareous-schist section about 10 meters thick in the upper part of unit F is strikingly mottled in shades of orange and green. The green color is due to the presence of epidote and the orange is due to a carbonate mineral tentatively interpreted as strontium-bearing. The epidote occurs as fine-grained aggregates that comprise as much as 40 modal percent of the rock. The remaining 60 modal percent consists of nearly equal amounts of orange carbonate, muscovite, and quartz, plus minor amounts of magnetite.

Dolomite marble occurs in beds that range in thickness from a few centimeters to several meters. The rock is composed almost entirely of metamorphically recrystallized fine-grained dolomite. A lack of detrital material, except for scattered pods of recrystallized chert or very fine-grained polycrystalline quartz, implies that the pre-metamorphic protolith was a micritic dolostone.

The depth interval between 6,820 and 6,980 feet contains scattered thin to thick beds of a rock interpreted as recrystallized cherty iron-formation. The rock consists of anhedral grains of magnetite as large as 0.5 millimeter in diameter set in a matrix of recrystallized quartz. The magnetite typically occurs as disseminated grains or rarely as interlocking grains that form thin, irregular laminae oriented parallel to bedding. Pyrite is a common accessory phase, forming thin, irregular laminae oriented parallel to the principal schistosity ( $S_1$ ) and subparallel to bedding. In some beds, magnetite and pyrite collectively constitute as much as 27 percent of the modal mineralogy. Biotite (5 to 10 modal percent), graphite (3 modal percent), and garnet (2 modal percent) are minor but ubiquitous constituents. Much of the garnet occurs as scattered subhedral to anhedral grains, 0.2 to 3.0 millimeters in diameter, that have been rotated in a second foliation direction.

A meso-scale inclined to overturned fold that involves a core intercept of approximately 75 feet of strata occurs in unit F between depths 5,110 and 5,185 feet. This is the largest fold structure identified in the preliminary logging of the core. Across the folded interval, from top to bottom, bedding rotates from subhorizontal, upward-topping, through



steeply inclined to vertical, sideways-topping, to subhorizontal, upward-topping. The structure therefore is a sideways-topping inclined fold pair in which the drill core has cut the steeply inclined common limb (Fig. 5). Throughout the fold a strong schistosity ( $S_1$ ), defined by preferentially oriented biotite and muscovite and flattened quartz augen, lies nearly parallel to bedding and is folded with it; both the bedding ( $S_0$ ) and schistosity ( $S_1$ ) are transected by a second foliation ( $S_2$ ) that dips consistently about  $25^\circ$  ( $65^\circ$  to the core axis). This geometry suggests that the fold is an  $F_2$  structure. The  $S_2$  foliation in this instance is a continuous, non-domainal fabric (not a crenulation cleavage) that is defined by the preferred orientation of a second generation of metamorphic biotite. In places, the  $S_2$  fabric is enhanced by thin pods and lenses of calcite, graphitic material, and pyrite, with pyrite tending to appear in zones where the second-generation biotite has been retrograded to chlorite.

Structural geometry similar to that described above is observed on a micro scale throughout the H to F interval. A rootless  $F_2$  microfold from unit H is illustrated in Figure 4A; comparable examples are present at virtually all stratigraphic levels in the H to F section.

**Units E (metasedimentary component) and D: Metamorphosed iron-formation and pelitic rocks**

Two long intervals (a few tens of meters) and several short intervals (ten meters or less) of mineralogically, texturally, and structurally complex iron-rich metasedimentary rock are the distinctive metasedimentary component of units E and D. The iron-rich strata are interbedded with minor amounts of metapelite and significant amounts of metaigneous rocks in unit E (the volcanic portion of the latter being especially characteristic) and with various types of graphite and sulfide-bearing metapelite in unit D.

**Metamorphosed iron-rich rock**

In both units E and D, the iron-rich rock is bedded on the scale of centimeters to meters, is generally black to dark greenish-gray, and is characterized by the local presence of garnet or amphibole porphyroblasts as large as a centimeter in size (Fig. 6) in beds of appropriate bulk composition. Much less common porphyroblasts of andalusite, typically retrograded to secondary phyllosilicates, are confined to specific alumina-rich beds, and microporphyroblasts of biotite occur widely in combination with the other porphyroblastic phases. Abundantly porphyroblastic beds (garnet alone, amphibole alone, garnet + amphibole, garnet + andalusite, all assemblages

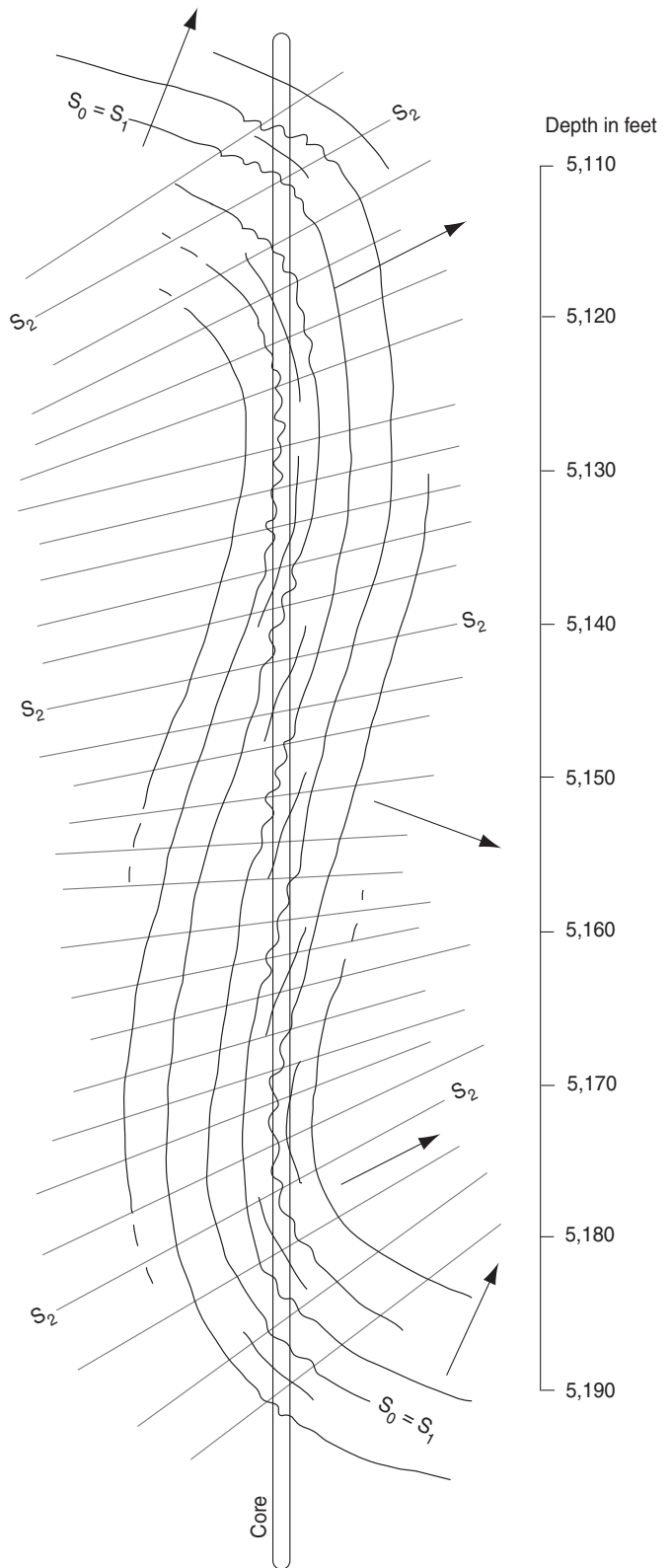
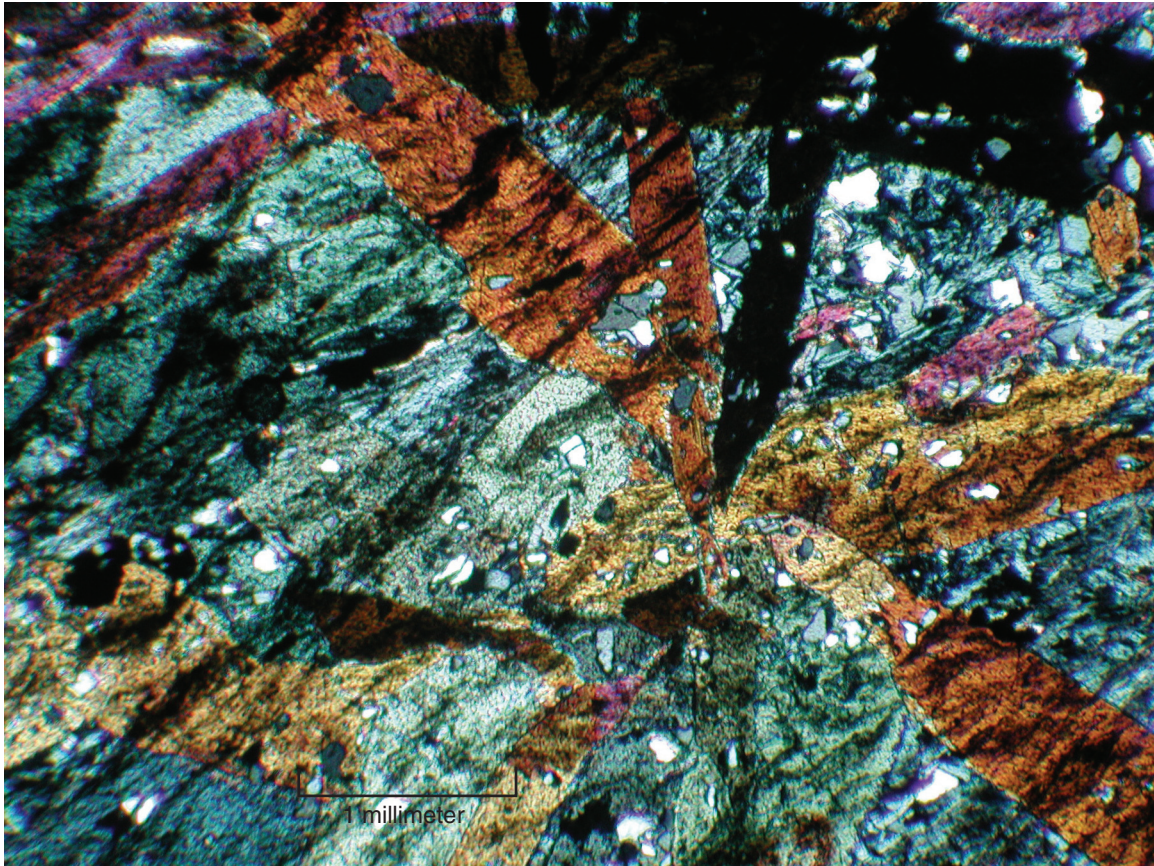


Figure 5. Sketch illustrating the structural geometry of a mesoscale  $F_2$  fold in unit F. Arrows indicate sense of stratigraphic younging.



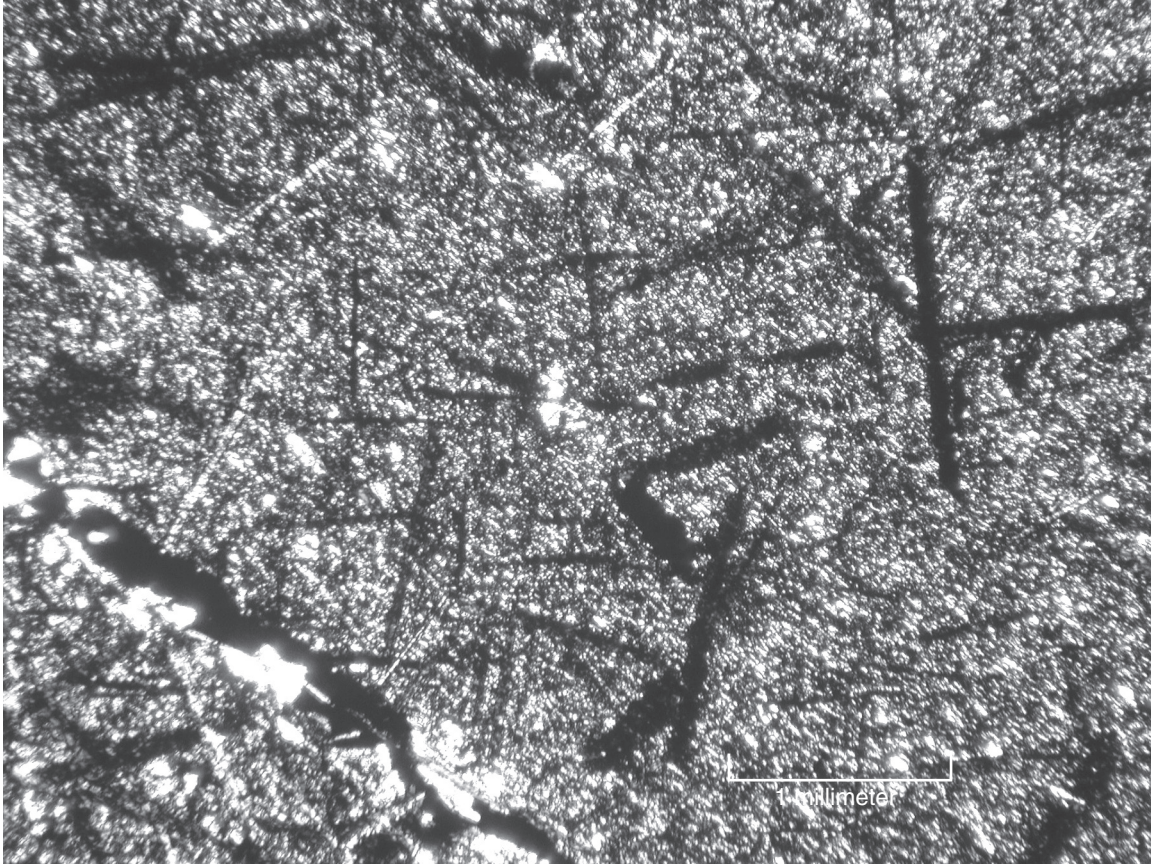
**Figure 6.** Photomicrograph with partially crossed nicols of porphyroblastic amphibole-rich iron formation at depth 4,139 feet in unit E. The randomly oriented bladed crystals of ferropargasite have grown in a finer-grained, metamorphically recrystallized, foliated rock composed principally of ferropargasite and iron-rich chlorite. A planar fabric ( $S_1?$ ) carried by opaque phases (mainly graphite and very fine-grained pyrite) was clearly imposed on the rock before recrystallization of the amphibole-rich matrix and the growth of ferropargasite porphyroblasts. In addition to the minerals and textures depicted here, this rock contains widely scattered centimeter-scale garnet porphyroblasts and very fine-grained polymineralic granules composed chiefly of graphite intergrown with quartz, albite, calcite, and pyrite. The granules are modestly flattened and rotated in the fabric plane and are tentatively regarded as primary sedimentary particles. The garnets, like the ferropargasite porphyroblasts, have grown across the fabric and are paragenetically late.

typically with biotite) are interspersed with beds or groups of beds that are porphyroblast-free.

The essentially black color of the fine- to medium-grained main mass of the rock is due to the presence of abundant graphite, iron sulfide, and iron oxide along with amphibole and biotite. The proportions of mafic silicate minerals, sulfides, oxides, and graphite vary widely and abruptly from bed to bed, but the total amount present in all beds is sufficient to impart very dark coloration to the rock as a whole. Common rock-forming minerals in addition to those listed above are carbonate species and quartz. The amount of carbonate varies strongly from bed to bed; more or less typical beds contain a

few percent of carbonate minerals, but the amount approaches 50 percent in rare layers. Less abundant minerals include plagioclase, chlorite, epidote, and muscovite. Recrystallized, poorly twinned plagioclase of approximately andesine composition is present in most layers that contain substantial quartz. Its abundance and distribution are difficult to quantify petrographically because of the optical similarity of untwinned plagioclase and quartz. Stilpnomelane (Fig. 7; Table 3) and tentatively identified greenalite are present in rare beds that retain the vestiges of primary pelletal texture and appear to have escaped the pervasive effects of lower amphibolite-grade regional metamorphism.





**Figure 7.** Photomicrograph with partially crossed nicols of porphyroblastic stilpnomelane-bearing iron-formation at depth 2,461 feet in unit D. The randomly oriented stilpnomelane blades have grown across the principal fabric ( $S_1$ ?) of a fine-grained rock composed of iron phyllosilicates, calcite, quartz, and pyrite. This rock type is interstratified with coarsely porphyroblastic garnet-amphibole iron-formation texturally and compositionally similar to the rock shown in Figure 6.

A penetrative  $S_1$  foliation, carried principally by aligned phyllosilicates, amphiboles, and graphite, and to a lesser extent by flattened lenses of quartz and carbonate, typically lies at a low angle to bedding ( $S_0$ ) throughout most of units E and D. Sulfide stringers tend to be oriented parallel to this fabric. A second planar fabric ( $S_2$ ), commonly a domainal crenulation cleavage and less commonly a continuous schistosity, transects  $S_1$  and bedding and refracts across lithologic contacts. The crenulation cleavage varies markedly from bed to bed in the strength of its development, favoring layers that are phyllosilicate- or amphibole-rich. It is marked by concentrations of opaque minerals and by aligned grains of reoriented and/or recrystallized biotite and amphibole.

The principal non-porphyroblastic minerals in the main mass of the rock typically range from 0.2 to 1.5 millimeters average in the longest dimension. Phyllosilicates and amphiboles commonly are of a

characteristic and narrow size range in a given bed, but may differ in size by a factor of ten or more from bed to bed. They are preferentially aligned in  $S_1$  and crenulated in  $S_2$ . Quartz and carbonate typically form a mosaic of polygonally recrystallized, subequant grains in beds where they are the dominant minerals present. In beds dominated modally by phyllosilicates and amphiboles, quartz and carbonate species form scattered grains and mosaic-textured ovoid to lensoid masses elongate in  $S_1$ . Like the phyllosilicates and amphiboles, the quartz and carbonate exhibit a characteristic grain size in any given layer, but differ in grain size by a factor of ten or more from layer to layer.

Porphyroblasts in the iron-rich rocks are of two textural types: 1. Relatively small and abundant crystals of biotite and green acicular amphibole (0.3 to 0.5 millimeter in length) that are oriented at steep but variable angles to the  $S_1$  fabric, and 2. Large,

**Table 3.** Electron microprobe analyses of stilpnomelane in iron-formation at depth 2,641 feet. Ten analyses from five positions within two separate acicular crystals show an essentially constant composition for the mineral. Analyses by P. McSwiggen.

Sample	1	2	3	4	5	6	7	8	9	10	mean	standard deviation
SiO <sub>2</sub>	45.537	45.709	45.765	46.393	45.633	44.655	44.728	45.071	44.976	45.049	45.35	0.55
Al <sub>2</sub> O <sub>3</sub>	6.927	6.92	6.938	6.805	7.041	6.683	6.725	6.812	6.786	6.814	6.85	0.11
TiO <sub>2</sub>	0.04	0	0	0.002	0	0	0	0	0	0	0.00	0.01
FeO	31.99	31.974	32.035	32.059	32.251	31.629	31.631	31.539	31.088	31.7	31.79	0.34
MgO	3.58	3.561	3.554	3.454	3.406	3.354	3.321	3.451	3.422	3.502	3.46	0.09
MnO	1.025	0.972	1.072	1.054	1.072	1.036	1.03	1.01	1.114	1.062	1.04	0.04
CaO	0.003	0.008	0.008	0.004	0.024	0.013	0	0.021	0.022	0	0.01	0.01
Na <sub>2</sub> O	0.8	0.85	0.859	0.913	1.03	1.275	1.399	1.156	0.958	1.113	1.04	0.20
K <sub>2</sub> O	2.063	2.28	2.279	2.029	2.166	2.486	2.752	2.322	2.292	2.429	2.31	0.21
Total	91.965	92.274	92.51	92.713	92.623	91.131	91.586	91.382	90.658	91.669	91.851	
Based on 22 oxygens												
Si	7.2367	7.2444	7.2387	7.2977	7.2184	7.2082	7.1965	7.2278	7.2537	7.2129		
Al	1.2975	1.2927	1.2935	1.2617	1.3129	1.2716	1.2754	1.2877	1.2901	1.2859		
Ti	0.0048	0	0	0.0002	0	0	0	0	0	0		
Fe	4.2517	4.2381	4.2377	4.2175	4.2666	4.2698	4.2563	4.2299	4.1933	4.2447		
Mg	0.8481	0.8413	0.8379	0.81	0.8031	0.8071	0.7966	0.8249	0.8226	0.8358		
Mn	0.138	0.1304	0.1436	0.1405	0.1437	0.1416	0.1403	0.1372	0.1522	0.1441		
Ca	0.0006	0.0014	0.0014	0.0008	0.004	0.0023	0.0001	0.0035	0.0038	0		
Na	0.2465	0.2611	0.2635	0.2784	0.3158	0.3989	0.4363	0.3595	0.2995	0.3456		
K	0.4183	0.4609	0.4598	0.4071	0.4371	0.5119	0.565	0.4751	0.4716	0.4961		
Based on 8 Si atoms												
Si	8.000	8.000	8.000	8.000	8.000	8.000	8.000	8.000	8.000	8.000		
Al	1.434	1.429	1.430	1.395	1.451	1.406	1.410	1.424	1.426	1.422		
Ti	0.005	0.000	0.000	0.000	0.000	0.000	0.000	0.000	0.000	0.000		
Fe	4.700	4.685	4.685	4.662	4.717	4.720	4.705	4.676	4.636	4.692		
Mg	0.938	0.930	0.926	0.895	0.888	0.892	0.881	0.912	0.909	0.924		
Mn	0.153	0.144	0.159	0.155	0.159	0.157	0.155	0.152	0.168	0.159		
Ca	0.001	0.002	0.002	0.001	0.004	0.003	0.000	0.004	0.004	0.000		
Na	0.272	0.289	0.291	0.308	0.349	0.441	0.482	0.397	0.331	0.382		
K	0.462	0.510	0.508	0.450	0.483	0.566	0.625	0.525	0.521	0.548		
Fe/Fe+Mg+Mn	0.812	0.813	0.812	0.816	0.818	0.818	0.820	0.815	0.811	0.812		

more or less randomly scattered crystals of garnet, andalusite, and green amphibole (5 to 15 millimeters in largest dimension). The small porphyroblasts of type 1 have grown across S<sub>1</sub> in an orientation that is approximately parallel to S<sub>2</sub> fabric in rocks that display unequivocal S<sub>2</sub> fabric elements. However, transversely aligned microporphyroblasts of this type are not limited to beds that display strong development of S<sub>2</sub>. They are common in rocks that lack crenulation fabrics, and therefore the timing

relationship between porphyroblast growth and the mechanical development of S<sub>2</sub> fabric elements is not entirely clear. Many of these porphyroblasts are thin, delicate crystals that are not bent or fractured and therefore appear to have grown in a static rather than a dynamic mechanical environment.

The large garnet and andalusite porphyroblasts of type 2 exhibit complex patterns of zonal and sector-controlled growth and are choked with inclusions of opaque minerals, quartz, biotite, and

rarely amphibole. Some large garnets are flanked by asymmetric pressure shadows enriched in quartz and contain spiral patterns of inclusions that indicate reorientation under shear nominally parallel to  $S_1$ . Others completely lack these features. Furthermore, some garnets display clear evidence of rotation in  $S_2$ , whereas others do not.

Many large amphibole porphyroblasts are blade-like crystals that are oriented subnormal to  $S_0$  and  $S_1$  and thus may record growth related to  $D_2$  dynamics. Some of these amphibole porphyroblasts are kinked sharply more or less normal to their length, however, which suggests a layer-normal compression subsequent to crystal growth. This is not easily reconciled with the layer-parallel (or nearly parallel) compression required to  $S_2$  crenulations, and is interpreted to indicate a post- $D_2$  flattening subnormal to  $S_1$ .

The garnet composition, as determined by electron microprobe analysis, is approximately 60 percent almandine, 20 percent spessartine, and 20 percent grossular (Table 4); individual porphyroblast crystals are compositionally zoned, having narrow rims that are enriched in iron and depleted in manganese and calcium relative to their homogeneous cores (Fig. 8). The amphibole porphyroblasts are an iron-rich pargasite (Fig. 9; Table 5). The pargasite porphyroblasts exhibit virtually no compositional zoning. Textural criteria strongly suggest that the garnet and pargasite crystallized in chemical equilibrium. The mineral compositions presented in Tables 4 and 5 therefore represent equilibrium pairs of garnet and pargasite from two specific iron-rich layers of slightly differing bulk composition, at depths of 4,139 and 3,149 feet. Although the iron content of these rocks is high, ( $Fe_2O_3$  around 16 to 20 weight percent), it is not as high as in other rocks in the E to D section. The bulk whole-rock composition of sample 3,149 is given in Table 9, column 8.

#### ***Metamorphosed pelitic rocks of various types***

The most common type of "normal" metasedimentary rock that is intimately interstratified with beds of iron-rich material in units E and D is composed predominantly of quartz, biotite, and graphite plus variable, small amounts of iron sulfide and oxide minerals. Garnet and andalusite form small porphyroblasts in specific layers. The rock is generally thin-bedded to laminated and possesses the physical attributes of typical phyllite and/or fine-grained schist derived from a protolith of interlayered shale, siltstone, and fine-grained graywacke. Less abundant rock types within the metasedimentary sections contain significant percentages of chlorite,

actinolite, and carbonate minerals in addition to quartz, biotite, and graphite (Appendix Fig. 1). The more mafic of these originally may have contained a component of volcanic ash admixed with epiclastic constituents; there is no textural evidence surviving that would verify this contention, but the presence of abundant mafic metavolcanic rocks in the E to D interval makes the notion tenable. Rock types that contain appreciable proportions of carbonate minerals were probably derived from limey muds.

Altogether, the attributes of the normal metasedimentary rocks in the E to D interval suggest derivation from muds deposited in relatively quiescent water somewhat distant from sources of sediment supply. The sediment consisted of epiclastic detritus augmented from time to time by inputs of volcanic material, possibly including hydrothermal products as well as volcanic ash. The contributions of chemical/hydrothermal sedimentation became proportionally greater during periods of diminished epiclastic and pyroclastic sediment supply, resulting in the deposition of an iron-rich muck composed of clays, epiclastic quartz, hydrothermal chert, carbonate minerals, iron-silicate minerals, pyrite, and graphite. Layers of this muck became the iron-rich strata described in the previous section. Indeed, there appears to be a fairly smooth geochemical gradation in iron content from rocks that contain normal pelitic amounts to those in which total iron as  $Fe_2O_3$  reaches 30 weight percent or more. This gradation is discussed more fully in the "Geochemistry of the cored bedrock" section.

The structures and metamorphic fabrics in the normal sedimentary intervals are the same as those in the iron-rich intervals. A complex history of fabric development and metamorphic mineral growth is indicated for both.

#### **Unit B: Metamorphosed pelitic rocks, many rich in carbonaceous material**

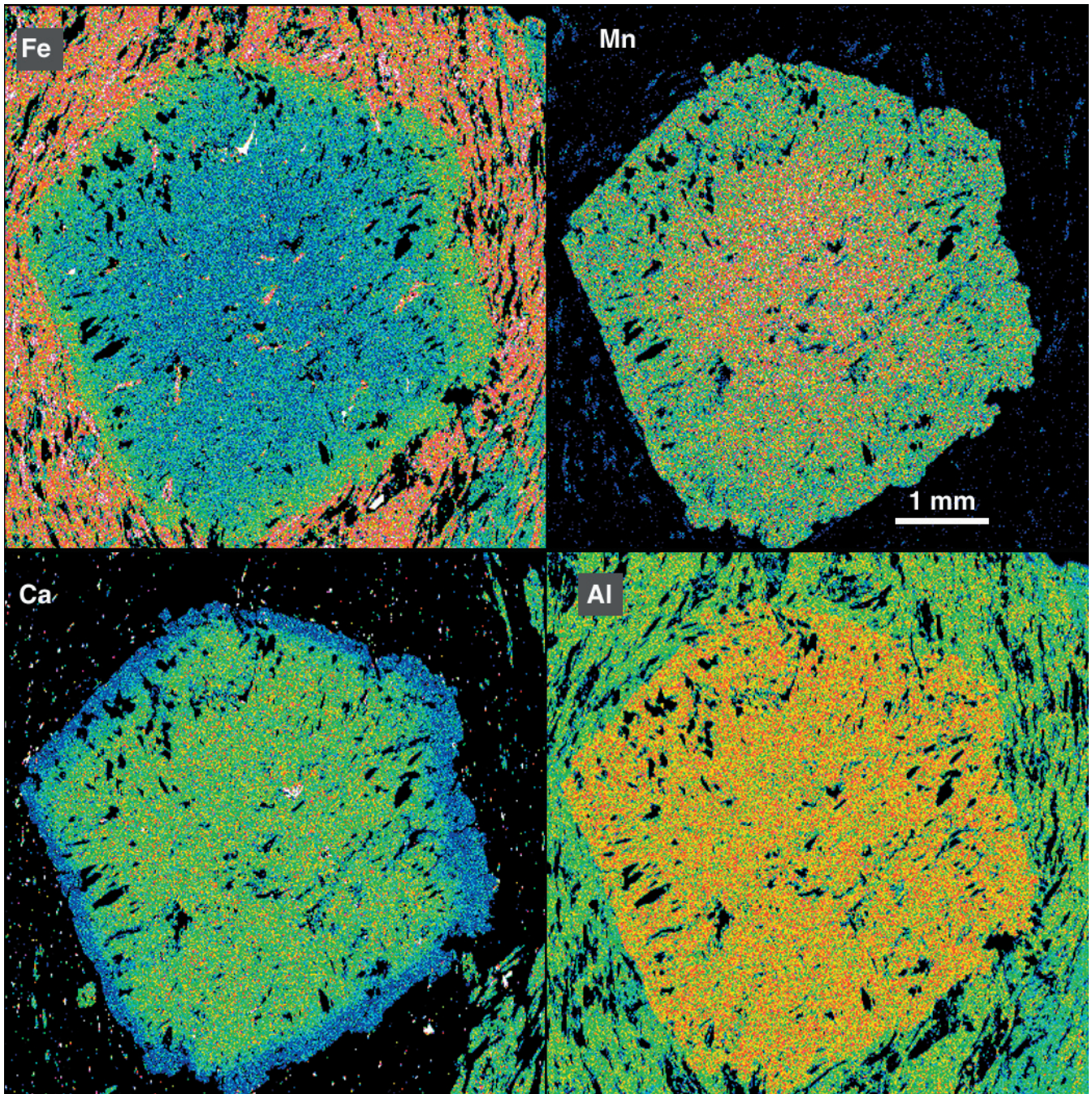
Unit B is a relatively thin interval between the depths of 1,809 and 1,993 feet that consists of interlayered graphitic phyllite, metasilstone, and quartz-mica schist. Textural and modal attributes suggest that, prior to metamorphism, the constituent rocks were carbonaceous shale, siltstone, and very fine-grained quartz wacke. Also present are beds several centimeters to several meters thick of a more massive fine-grained rock that is interpreted provisionally as a metamorphosed tuff, possibly a reworked deposit in which volcanoclastic and epiclastic components were mixed. The proportion of graphite or carbonaceous material in the rocks of this unit varies greatly, ranging from a few percent



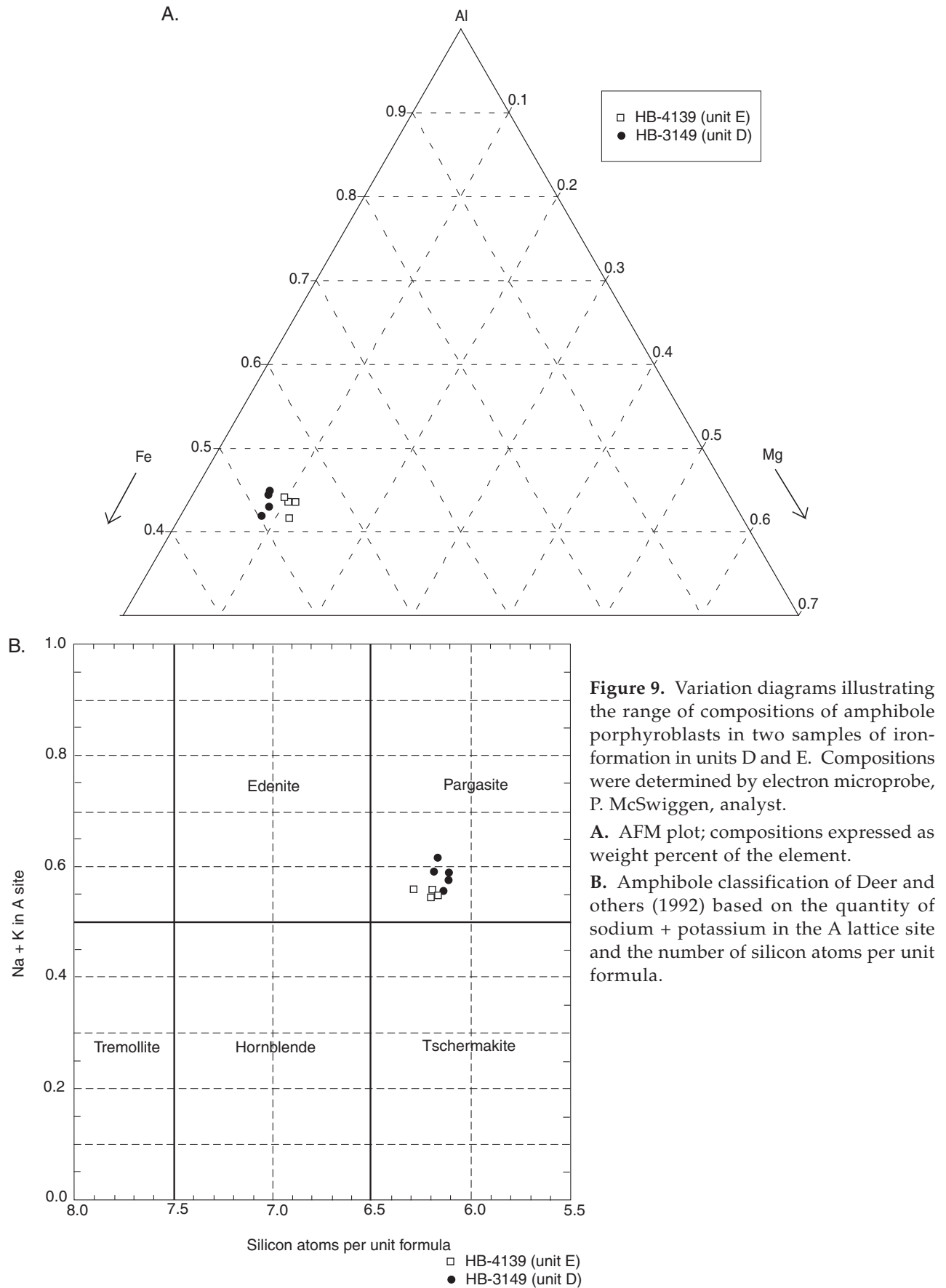
**Table 4.** Electron microprobe analyses of garnets in iron-rich rocks at depths 3,149 and 4,139 feet. The analyses are from rim, core, and intermediate positions within single garnet porphyroblasts. Element scans of garnet at depth 3,149 feet are shown in Figure 8. Data from other garnet porphyroblasts in other iron-formation beds exhibit similar compositional ranges and zoning patterns. Analyses by P. McSwiggen.

Sample	1	2	3	4	5	6	7	8	9	10	11	12	13	14	15	16	17	18
Location in grain	HB-4139 Rim	HB-4139 Rim	HB-4139 Rim	HB-4139 Mid	HB-4139 Mid	HB-4139 Core	HB-4139 Core	HB-4139 Core	HB-4139 Rim	HB-4139 Rim	HB-4139 Rim	HB-4139 Mid	HB-4139 Mid	HB-4139 Mid	HB-4139 Mid	HB-4139 Core	HB-4139 Core	HB-4149 Core
SiO <sub>2</sub>	37.40	36.95	37.28	37.09	37.09	37.25	37.10	37.10	37.01	37.19	37.06	37.32	37.47	37.41	37.19	37.28	37.21	37.24
TiO <sub>2</sub>	0.11	0.11	0.08	0.08	0.07	0.11	0.11	0.09	0.11	0.06	0.05	0.16	0.18	0.14	0.22	0.23	0.25	0.21
Al <sub>2</sub> O <sub>3</sub>	21.68	21.52	21.72	21.60	21.75	21.49	21.50	21.48	21.77	21.60	21.72	21.49	21.52	21.53	21.45	21.42	21.53	21.59
Cr <sub>2</sub> O <sub>3</sub>	0.00	0.01	0.00	0.01	0.01	0.00	0.00	0.00	0.01	0.00	0.00	0.00	0.03	0.02	0.03	0.01	0.00	0.02
FeO	26.24	26.55	27.04	26.73	26.58	26.93	26.83	26.74	29.36	29.51	28.31	23.29	23.43	24.17	23.09	22.00	22.17	22.17
MnO	8.57	8.64	8.50	8.62	8.95	8.23	8.44	8.32	6.51	6.18	6.61	6.97	7.49	6.79	7.40	8.63	8.53	8.81
MgO	0.40	0.43	0.42	0.43	0.39	0.41	0.38	0.38	0.36	0.34	0.31	0.18	0.18	0.21	0.18	0.16	0.14	0.16
CaO	7.13	7.20	6.67	7.10	6.48	7.02	6.89	7.07	6.43	6.55	7.30	11.09	11.27	11.02	11.57	11.33	11.42	10.99
Total	101.53	101.40	101.71	101.65	101.30	101.44	101.24	101.17	101.54	101.43	101.36	100.49	101.55	101.28	101.11	101.06	101.25	101.18
Si	2.977	2.956	2.970	2.960	2.966	2.974	2.970	2.971	2.958	2.973	2.962	2.978	2.967	2.969	2.958	2.965	2.956	2.960
Al tet	0.023	0.044	0.031	0.041	0.034	0.026	0.030	0.029	0.042	0.027	0.038	0.022	0.033	0.031	0.042	0.035	0.044	0.040
Total tet	3.000	3.000	3.000	3.000	3.000	3.000	3.000	3.000	3.000	3.000	3.000	3.000	3.000	3.000	3.000	3.000	3.000	3.000
Al total	2.034	2.029	2.039	2.031	2.050	2.022	2.028	2.028	2.050	2.035	2.046	2.021	2.008	2.014	2.010	2.009	2.016	2.022
Fe total	1.747	1.776	1.801	1.784	1.777	1.798	1.796	1.791	1.962	1.973	1.892	1.554	1.551	1.604	1.536	1.464	1.473	1.474
Al oct	2.011	1.985	2.008	1.991	2.016	1.997	1.998	1.999	2.008	2.009	2.008	1.999	1.975	1.983	1.968	1.974	1.971	1.982
Ti	0.007	0.006	0.005	0.005	0.004	0.007	0.007	0.006	0.006	0.004	0.003	0.009	0.011	0.008	0.013	0.014	0.015	0.012
Cr	0.000	0.001	0.000	0.000	0.000	0.000	0.000	0.000	0.001	0.000	0.000	0.000	0.002	0.001	0.002	0.001	0.000	0.001
Fe <sup>+3</sup>	0.000	0.010	0.000	0.000	0.000	0.000	0.000	0.000	0.000	0.000	0.000	0.000	0.010	0.010	0.020	0.010	0.010	0.000
Total oct	2.018	2.003	2.013	1.996	2.020	2.003	2.005	2.004	2.015	2.013	2.011	2.008	1.998	2.003	2.003	1.998	1.997	1.995
Fe <sup>+2</sup>	1.747	1.766	1.801	1.784	1.777	1.798	1.796	1.791	1.962	1.973	1.892	1.554	1.541	1.594	1.516	1.454	1.463	1.474
Mn	0.578	0.585	0.573	0.583	0.606	0.557	0.572	0.564	0.440	0.418	0.448	0.471	0.502	0.457	0.499	0.582	0.574	0.593
Mg	0.048	0.051	0.050	0.051	0.047	0.049	0.046	0.045	0.042	0.040	0.037	0.022	0.021	0.025	0.021	0.019	0.017	0.018
Ca	0.609	0.618	0.569	0.607	0.555	0.601	0.591	0.606	0.550	0.561	0.625	0.948	0.956	0.937	0.986	0.965	0.972	0.936
Total X sites	2.981	3.020	2.994	3.024	2.985	3.004	3.005	3.006	2.995	2.993	3.001	2.995	3.020	3.012	3.021	3.019	3.025	3.021
almandine	58.60	58.49	60.17	58.98	59.55	59.85	59.77	59.57	65.51	65.94	63.03	51.89	51.04	52.92	50.17	48.15	48.35	48.78
spessartine	19.39	19.38	19.15	19.27	20.30	18.53	19.04	18.76	14.70	13.98	14.92	15.72	16.63	15.16	16.50	19.26	18.97	19.62
pyrope	1.61	1.68	1.68	1.67	1.57	1.62	1.52	1.49	1.41	1.34	1.22	0.73	0.69	0.81	0.70	0.62	0.55	0.61
grossular	20.41	20.45	19.01	20.07	18.59	20.00	19.67	20.17	18.37	18.74	20.84	31.65	31.65	31.10	32.63	31.97	32.13	30.99





**Figure 8.** Electron microprobe element scans of a compositionally zoned garnet porphyroblast in iron-rich metasediment of unit D, at depth 3,149 feet. The plots show core-to-rim variations in iron, manganese, calcium, and aluminum. The pattern observed in this grain of gradual core-to-rim diminution in manganese, sharp outer rim diminution in calcium, and sharp outer-rim increase in iron is replicated in many other garnet grains in the iron-rich strata.





**Table 5.** Electron microprobe analyses of a blue-green amphibole in iron-rich rocks at depths 3,149 and 4,139 feet. Analyses from rim, core, and intermediate positions within single crystals reveal no systematic compositional zoning. Amphibole compositions in other iron-formation beds are closely similar. Analyses by P. McSwiggen.

Sample	1	2	3	4	5	6	7	8	9
	HB-4139	HB-4139	HB-4139	HB-4139	HB-3149	HB-3149	HB-3149	HB-3149	HB-3149
SiO <sub>2</sub>	40.49	39.756	40.011	40.091	39.226	39.827	39.247	39.231	39.529
Al <sub>2</sub> O <sub>3</sub>	15.487	16.765	16.463	16.51	16.911	16.286	15.842	16.983	17.012
TiO <sub>2</sub>	0.214	0.232	0.24	0.244	0.231	0.199	0.211	0.228	0.205
FeO	24.863	25.015	24.813	24.507	25.865	26.064	26.728	25.853	25.583
MgO	3.259	2.82	2.993	3.223	2.268	2.474	2.419	2.233	2.239
MnO	0.552	0.5	0.534	0.47	0.286	0.308	0.279	0.281	0.26
CaO	10.806	10.787	10.805	10.941	11.114	11.009	10.7	11.092	11.261
Na <sub>2</sub> O	1.601	1.523	1.513	1.57	1.42	1.572	1.559	1.4	1.355
K <sub>2</sub> O	0.389	0.455	0.454	0.448	0.807	0.594	0.709	0.767	0.748
Total	97.661	97.853	97.826	98.004	98.128	98.333	97.694	98.068	98.192
Based on 23 oxygens									
Si	6.285	6.163	6.197	6.190	6.106	6.181	6.164	6.107	6.133
Al tet	1.715	1.837	1.803	1.810	1.894	1.819	1.836	1.893	1.868
Total tet	8.000	8.000	8.000	8.000	8.000	8.000	8.000	8.000	8.000
Al total	2.833	3.063	3.006	3.005	3.103	2.979	2.933	3.116	3.111
Al oct	1.118	1.226	1.203	1.194	1.209	1.161	1.097	1.223	1.243
Ti	0.025	0.027	0.028	0.028	0.027	0.023	0.025	0.027	0.024
Fe	3.228	3.243	3.214	3.164	3.367	3.383	3.511	3.366	3.319
Mg	0.754	0.652	0.691	0.742	0.526	0.572	0.566	0.518	0.518
Mn	0.073	0.066	0.070	0.062	0.038	0.041	0.037	0.037	0.034
Total oct	5.197	5.213	5.207	5.190	5.167	5.180	5.236	5.171	5.139
Ca	1.797	1.792	1.793	1.810	1.854	1.831	1.801	1.850	1.872
Na	0.482	0.458	0.454	0.470	0.429	0.473	0.475	0.423	0.408
K	0.077	0.090	0.090	0.088	0.160	0.118	0.142	0.152	0.148
Total X site	2.356	2.340	2.337	2.368	2.443	2.422	2.418	2.425	2.428
Fe/Fe+Mg+Mn	0.796	0.819	0.809	0.798	0.857	0.847	0.853	0.858	0.857
Na+K	0.559	0.548	0.544	0.558	0.589	0.591	0.617	0.575	0.556

to as much as 50 percent by volume. Where graphite or carbonaceous material is a minor component, it occurs along the foliation surfaces as discontinuous, lens-shaped stringers. Where a major component, as in the uppermost 10 feet of the unit, the stringers merge across foliation planes to form irregularly shaped masses that have a greasy feel. Resistivity values measured across the entire drilled thickness of the unit range from  $0.02 \times 10^3$  to  $0.67 \times 10^3$  ohms, values an order of magnitude greater than those measured in other units of the core. These values imply that carbonaceous material is a ubiquitous component of unit B, even where it cannot readily be seen in hand specimens.

Strongly foliated, graphite-poor, biotite-muscovite-chlorite schist is interbedded with metabasalt in the

lowermost 30 feet (9 meters) of Unit B. This zone, portrayed as mixed schist in Appendix Figure 1, is transitional to the predominantly volcanic sequence of underlying unit C. As mentioned previously, the B/C contact may be tectonic to some extent. In other words, shearing between sequences of contrasting mechanical competence may have been focused in the zone of lithologic transition.

The pelitic and semipelitic rocks of unit B are laminated to very thin-bedded (bed thicknesses in the millimeter to centimeter range). Beds of metasiltstone and fine-grained quartz wacke are somewhat thicker and typically are graded. The grading is defined by silt- to very fine-grained sand-size grains of quartz that are enclosed in a matrix of quartz, muscovite, and carbonaceous material. The matrix material

is interpreted to be the metamorphic equivalent of carbonaceous mud. Minor unconformities, small-scale slump features such as over-steepened and overturned folds, and compaction features such as flame structures and clastic dikes are common.

The bedding in unit B is generally subhorizontal and essentially parallel to a strong subhorizontal schistosity. Some beds of original silt or fine-grained sand are boudinaged, implying that tectonic stretching occurred parallel to bedding and tectonic flattening perpendicular to it. In the more thoroughly recrystallized, mica-rich rocks classified as graphitic phyllite or quartz-mica schist, there are typically two well developed foliations. The earlier one ( $S_1$ ) is oriented essentially parallel to bedding ( $S_0$ ); both  $S_1$  and  $S_0$  are locally folded into tight, nearly recumbent, small-scale folds to which the second foliation ( $S_2$ ) is axial-planar (Fig. 10). In portions of the core where fold hinges are lacking (such as on the more or less straight limbs of  $F_2$  folds), the  $S_2$  foliation is inclined about  $10^\circ$  to  $30^\circ$  to  $S_1$  and  $S_0$ . Ubiquitous millimeter-scale veinlets of quartz and calcite + pyrite  $\pm$  epidote are distorted or broken by translation on surfaces parallel to  $S_2$ .

Most of the laminated to thin-bedded graphitic rocks are composed chiefly of quartz, untwinned alkali feldspar, biotite, muscovite, and graphite in varying proportions. Garnet, commonly replaced partly or totally by carbonate, is present in layers of appropriate bulk composition. Retrograde metamorphic effects are ubiquitous but unevenly developed; secondary chlorite and white mica together almost totally replace biotite in parts of unit B, but are virtually absent from other parts. Secondary carbonate and pyrite also are present widely. The carbonate replaces garnet, as mentioned above, and also forms streaky replacement veinlets parallel to  $S_1$ . The pyrite forms layer-parallel stringers and occurs with quartz and carbonate in thin, transverse veinlets.

The  $S_1$  fabric is carried mainly by fine-grained biotite (and its retrograde breakdown products),

graphite, and flattened lensoid aggregates of quartz, alkali feldspar, and carbonate. The  $S_2$  fabric is defined in different ways in different places. Most commonly it is a crenulation cleavage in which the cleavage films (actually thin zones) are occupied by graphite, fine-grained mica, and rarely pyrite. Less commonly, the  $S_2$  fabric is carried by blocky porphyroblasts of biotite that are aligned transverse to  $S_1$ .

The layer-controlled garnet porphyroblasts are strongly rotated in  $S_2$ . Straight inclusion trails of quartz, presumably marking  $S_1$ , are oriented at high angles to  $S_2$ , which is the dominant fabric in many garnet-bearing intervals (Fig. 11). Essentially symmetrical pressure shadows around the garnets are filled with quartz and carbonate.

The more coarsely-grained, crystalline layers within unit B describable as quartz-mica schist differ compositionally from the finer-grained, laminated rocks in that they contain less graphite and more muscovite. However, the attributes of the  $S_1$  and  $S_2$  fabrics are essentially the same as those in the laminated rocks.

## Metaigneous rocks

### General characteristics

Mafic volcanic and hypabyssal rocks are interlayered throughout the Hattenberger core (Fig. 3). The 1,006-foot core interval defined as **unit A** (depth 803 to 1,809 feet) is essentially all metaigneous rock, as is the 287-foot interval defined as **unit C** (depth 1,993 to 2,280 feet). Unit E contains two long intercepts of mafic metaigneous rock—a 597-foot interval between depths 3,190 and 3,787 feet in unit E, and a 829-foot interval between depths 3,950 and 4,779 feet. **Unit G**, between depths 5,620 and 6,120 feet, is a single, sill-like intrusion delineated by sharply defined chilled contacts against quartz-mica schists of units H and F. Thinner intervals of mafic rock occur elsewhere in the core, within predominantly metasedimentary sections.

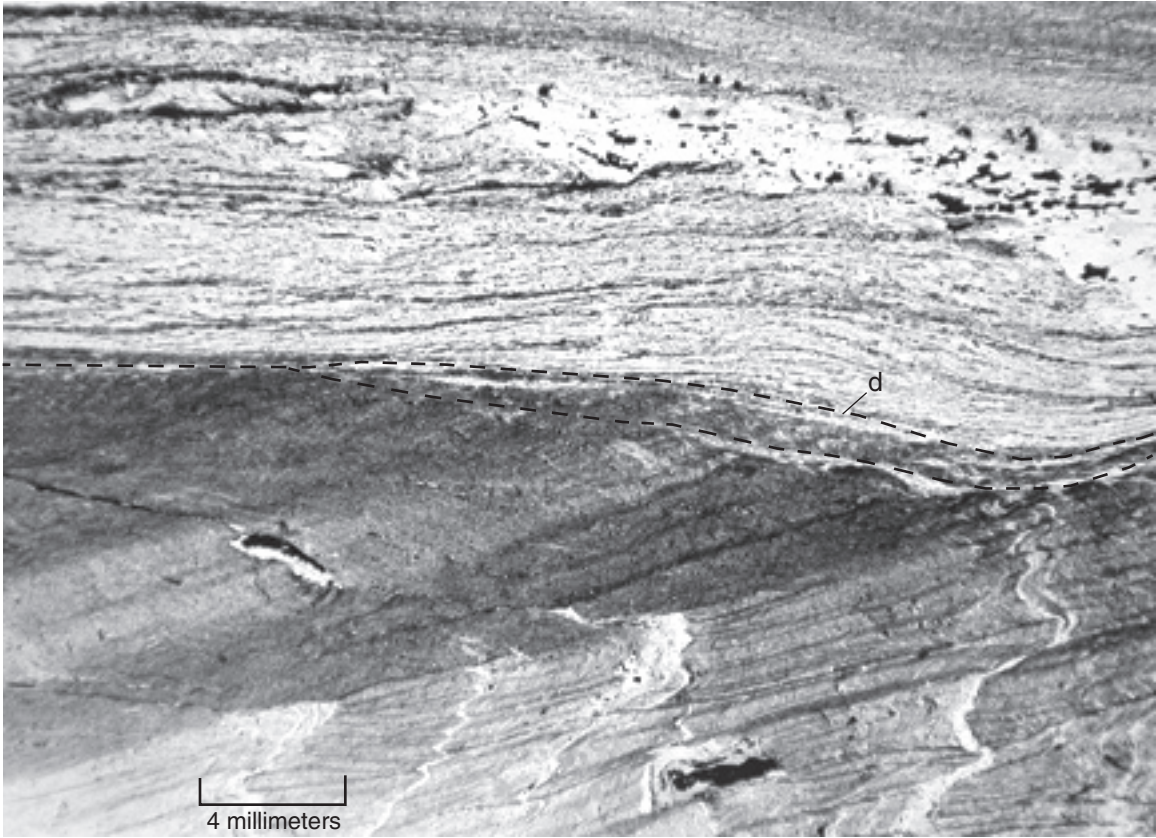
**Figure 10.** Photomicrographs illustrating the relationships among microdecollements, slaty cleavage ( $S_1$ ), and crenulation cleavage ( $S_2$ ) in graphitic mica phyllite of unit B, depth 1,832 feet.

**A.** The microdecollement surface (dashed line; d) is between laminated, quartz-rich phyllite (above) and more graphitic and micaceous, crenulated phyllite (below). Crenulation cleavage is virtually absent from the rock above the microdecollement, but is strongly developed below it.

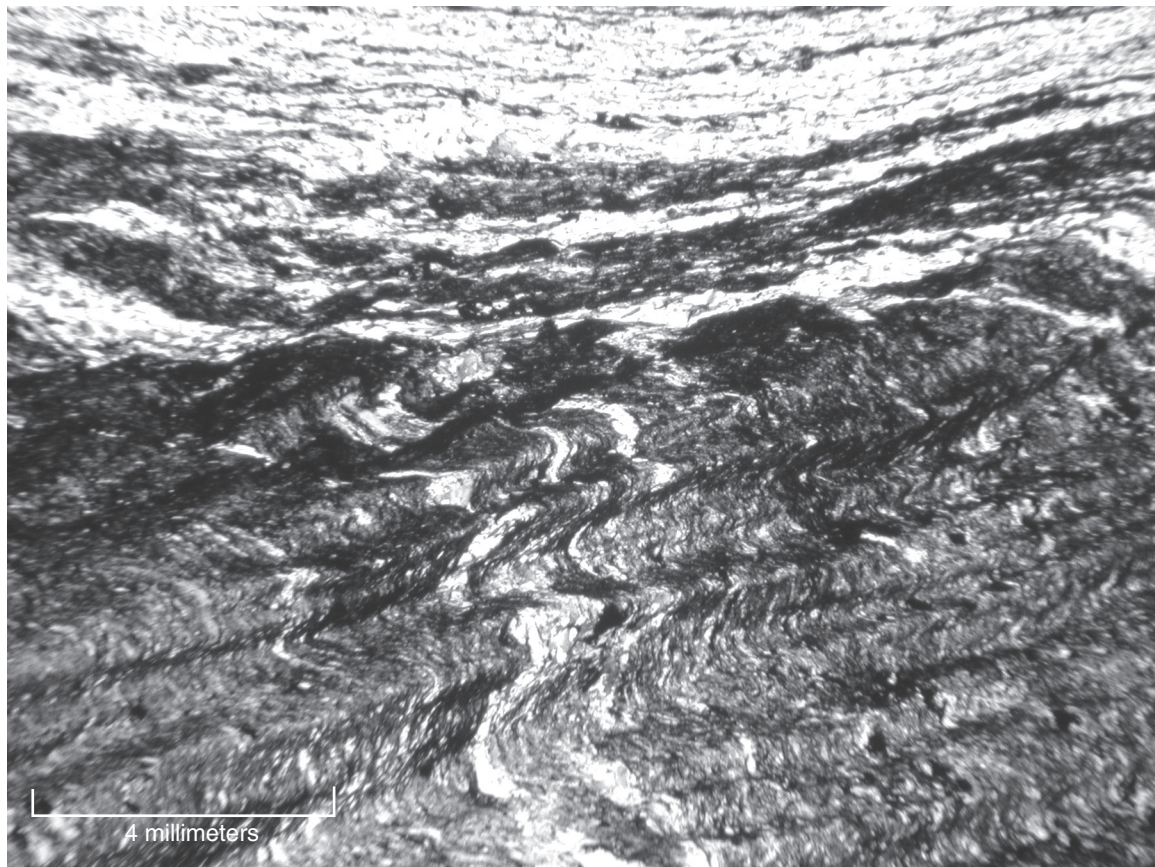
**B.** Enlarged view of cleavage relationships in the graphitic phyllite immediately below the microdecollement. Crenulated  $S_1$ , which is essentially parallel to sedimentary lamination, is inclined steeply to the right; the crenulation cleavage is inclined shallowly to the left.  $S_2 \times S_1$  fabrics of this sort are developed in rheologically soft layers throughout the core, but are particularly common in the graphitic metapelites and related rocks of units E, D, and B.



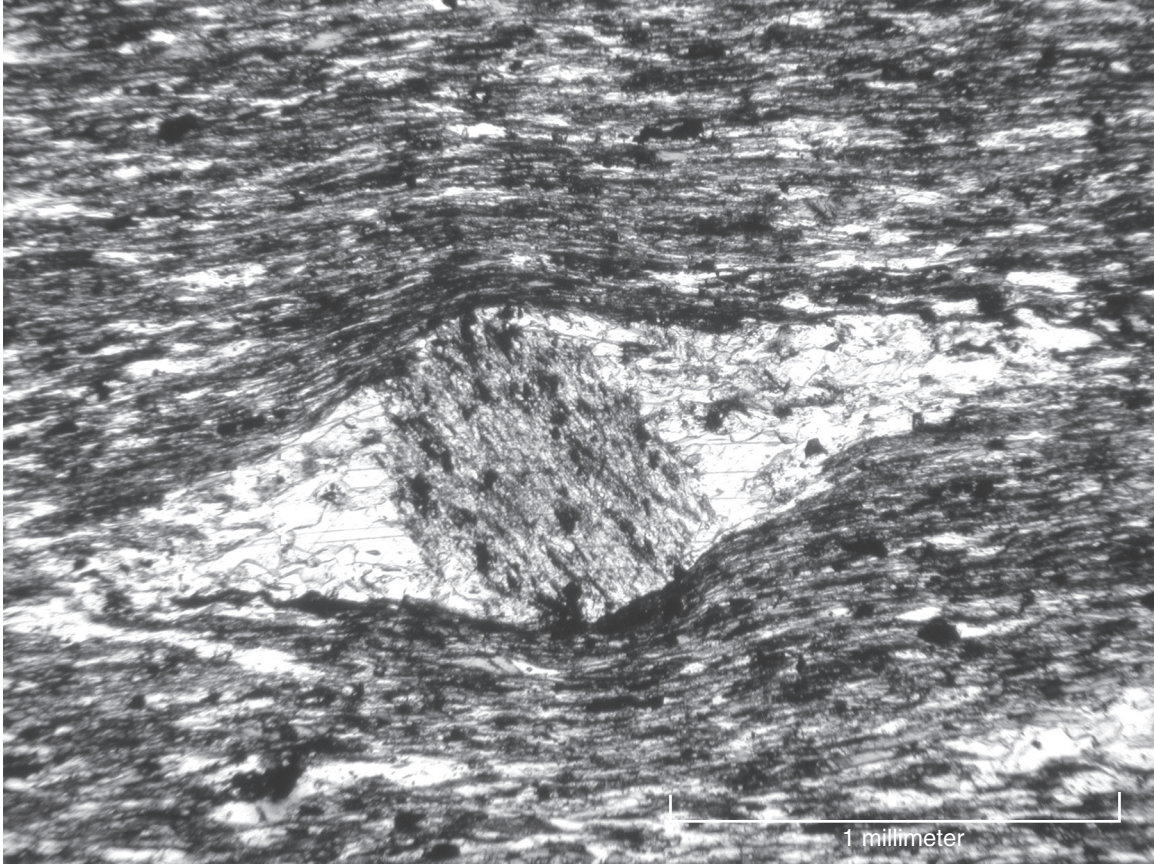
A.



B.







**Figure 11.** Photomicrograph of a tectonically rotated porphyroblast in unit B, at depth 1,839 feet. The porphyroblast is a carbonate pseudomorph of an unknown precursor mineral (cordierite or grossular?) that contains abundant inclusions of graphite, quartz, chlorite, and iron oxides. The enclosing rock is graphite-chlorite-biotite-muscovite-quartz phyllite. Inclusion trails in this porphyroblast and others in the same rock are oriented at high angles to the external foliation, which in this case is probably  $S_2$  effectively parallel to  $S_1$ . Carbonate-quartz pressure shadows ("wings") are moderately but consistently asymmetric, indicating a counterclockwise sense of porphyroblast rotation in the field of view.

As is typically the case with mafic rocks metamorphosed and deformed under conditions of the lower amphibolite facies, primary igneous textures and structures are variably preserved. In some parts of the core, originally volcanic (extrusive) rocks are readily distinguished from originally hypabyssal (intrusive) rocks, and in other parts they are not. Within clearly defined volcanic intervals, individual flow units grade upward from a massive basal portion to pillowed middle and upper portions. The pillow rocks are typically amygdaloidal. Most contacts between flow units are difficult to place precisely, but some flow tops are distinguished by variably thin units of breccia, locally derived interflow detritus, and angular clasts of chert.

Intervals in the Hattenberger core termed metadiabase may represent either the coarser-

grained interior portions of thicker flow units or separate cogenetic intrusions. Preserved textures range from diabasic (most common) to gabbroic. The rocks consist principally of blocky grains of blue-green metamorphic amphibole and variably saussuritized plagioclase set in a groundmass of a fibrous amphibole. Minor biotite and chlorite are present in some intervals; these are interpreted to be retrograde phases. Leucoxene after sphene, apatite, and Fe-Ti oxides are common accessory minerals.

The metaigneous rocks, unlike the metasedimentary portions of the core, are not pervasively foliated. Deformation fabrics are weak to absent in the most massive parts of thick flows and sills (Fig. 12A). Brittle to semiductile shear zones are relatively common in the mafic rocks, however, on scales of thickness that range from millimeters (Fig.

12B) to several meters. These range in character from zones of scaly, crenulated, chlorite or chlorite-actinolite schist to vein-filled fracture systems. The most common vein minerals within shear zones are calcite, epidote, and quartz.

Quite distinct from the metamorphosed and deformed igneous rocks of Penokean affinity are two tabular intrusions of essentially fresh diabasic gabbro that are intersected by the core not far from the contact between units E and F (Appendix Fig. 1). These intrusions have chilled margins in which there are phenocrysts of olivine set in a black, glassy groundmass; and unchilled interior portions composed of abundant anhedral to subhedral plagioclase set in an intergranular groundmass of augite, olivine, and minor amounts of Fe-Ti oxides. They probably are dikes associated with magmatic activity in the Mesoproterozoic (Keweenaw) Midcontinent rift.

#### *Lithologic and structural details of the metaigneous rocks*

##### **Unit G: Metadiabase and metagabbro**

Unit G, between depths 5,620 and 6,120 feet, is composed almost totally of massive to vaguely layered metagabbro and metadiabase. The rock is medium- to coarse-grained and commonly is equigranular in texture. Chilled margins a few feet thick define the upper and lower contacts, and imply that unit G may be a single intrusive body. Internally, the grain size of the rock varies between about 0.5 and 5.0 millimeters. The grain-size transitions generally are gradational, and impart a broad-scale, non-rhythmic, layered or streaked appearance to the core. This textural variation is interpreted as a primary igneous feature, modified to varying degrees by subsequent metamorphism and tectonism.

Tectonic deformation is manifested in the abundant, sharply walled shear zones and shear veins present throughout the drilled thickness of unit G. The shear zones range in thickness from several centimeters to several tens of centimeters and are occupied chiefly by fibrous to acicular amphibole that is aligned in a strong L-S fabric subparallel to the shear-zone walls. The shear veins span a similar thickness range and are distinguished by the presence of calcite, quartz, biotite, pyrite, and Fe-Ti oxides in addition to abundant fibrous amphibole. Some veins contain evidence of having been emplaced prior to shearing, where primary vein-type textures clearly have been modified by imposed shear fabrics. Other veins contain only highly sheared material and are in effect banded or laminated phyllonite zones in which there are interdigitated segregation bands of granular calcite, quartz, biotite, and green amphibole.

It appears that pre-existing veins were mechanically weak zones along which deformation was focused in the otherwise massive and stiff metagabbro.

The unsheared, unaltered metagabbro and metadiabase in unit G are composed predominantly of equigranular blue-green hornblende and plagioclase plus accessory Fe-Ti oxides, sphene, leucoxene, and clinozoisite. Primary igneous textures survive to a limited extent, particularly in the coarser-grained gabbroic rocks. Overall, however, primary textures have been largely obliterated by the growth of metamorphic hornblende and the concomitant saussuritization and recrystallization of plagioclase. Hairline calcite-quartz veins a millimeter or two in thickness are widespread throughout the massive rocks.

##### **Unit E: The metaigneous component of a mixed stratigraphic interval**

Metaigneous rocks make up about 75 percent of the drilled thickness of unit E, forming subunits that range for the most part between 10 and 150 feet in thickness. The interstratified metasedimentary subunits typically are between 3 and 15 feet thick. Contacts between originally igneous and sedimentary intervals commonly are gradational over thicknesses of less than 1 foot to several feet; hornblende-rich metaigneous rocks grade into biotite-rich metasedimentary rocks through intervals of mixed schist in which both hornblende and biotite are present in significant amounts. These gradational contacts in some instances are of probable tectonic origin, reflecting mechanical mixing and metasomatic processes in shear zones between relatively competent and less competent rocks. In other cases they may be stratigraphic, representing the interbedding or intermixing of mafic volcanoclastic material with epiclastic shale.

A substantial fraction of the metaigneous rock in unit E apparently was a succession of fairly thick basalt flows. Although the physical evidence is incomplete, having been obfuscated to varying degrees by the effects of metamorphism and deformation, many of the flows apparently had thick, massive, basal and medial portions and thin, pillowed to autobrecciated caps. The massive parts of flows contain small relict phenocrysts of plagioclase in a homogeneous groundmass that now is largely metamorphic amphibole; locally, the phenocrysts are aggregated into glomeroporphytic clots. Intervals of flow top or interflow pillow breccia typically are thinner than two feet (60 centimeters). On average, the breccia fragments range from 3 to 5 centimeters in apparent diameter and have quenched rims 3

to 5 millimeters thick. The interior portions of the fragments are composed chiefly of very fine-grained, grayish-green amphibole. The rims consist of admixed biotite and calcite with or without intergrown amphibole. The upper parts of some flows contain relict amygdules 0.5 to 2 millimeters in diameter. They are rimmed by biotite and filled with calcite and/or quartz, and commonly have been stretched and flattened tectonically. In general, the pillowed, vesiculated, and brecciated flow-top intervals are more pervasively foliated than the more massive flow interiors.

About half of the metaigneous rock in unit E is metadiabase (Appendix Fig. 1). Commonly, the metadiabase is massive, unfoliated to weakly foliated rock in which primary igneous textures are variably preserved. It is composed principally of blue-green metamorphic hornblende, variably recrystallized plagioclase, and biotite, plus minor quantities of Fe-Ti oxides, sphene, and secondary chlorite, epidote, and calcite. This mineral assemblage is also characteristic of the metamorphosed flows, which are distinguished from the metamorphosed diabase sills only on the basis of relict structures and textures.

#### **Unit C: Metabasalt and metadiabase**

Unit C, between the depths of 1,993 and 2,280 feet, consists of hornblende-rich metaigneous rocks that are texturally and mineralogically much like those in unit A described below. The rocks clearly identifiable as volcanic are variably porphyritic metabasalt in which both pyroxene and plagioclase were phenocryst phases. Amygdules filled by calcite, quartz, epidote, or combinations of these are locally preserved. The amygdules tend to be clustered into discrete zones of originally vesiculated rock about 30 centimeters thick that are flanked by rock that is massive and apparently was not vesiculated. The amygdules in the lower parts of the vesiculated zones are sparingly distributed, spherical, and 1 to 2 millimeters in diameter. In the upper parts they are more abundant, stretched or flattened parallel to the zone boundaries, and as long as 4 millimeters. Some amygdaloidal zones are truncated sharply on the top by irregular surfaces that are immediately overlain by very fine-grained equigranular metabasalt. These collective attributes suggest that the amygdaloidal zones are at the tops of flows and that the massive intervals above them are the basal parts of overlying flows.

Much of unit C consists of relatively featureless, massive, fine- to medium-grained, metaigneous rock that on megascopic examination would be logged as metadiabase. The microscopic igneous textures of this rock type are remarkably well preserved,

however. Most of the rock is sparsely porphyritic, and the groundmass has the felty intergranular texture typical of massive basalt. These observations, along with the previously described evidence for flow tops, strongly suggest that unit C consists chiefly if not entirely of thick metabasalt flows.

The only evidence for subaqueous extrusion of the parent volcanic rocks is a layer of equivocal pillow breccia at depth 2,220 feet. This rock contains vaguely developed ovoid structures about 3 centimeters in apparent diameter that show some indications of quenched rinds. It is situated stratigraphically above a zone of moderately amygdaloidal metabasalt, and therefore appears to be at or close to a flow top.

The uppermost and lowermost few feet of unit C contain thin intervals of laminated to thin-bedded schist. The schist consists mostly of fine-grained plagioclase, biotite, and lesser amounts of calcite, hornblende, and quartz. Biotite commonly is replaced by chlorite. It is likely that the schistose rocks have resulted from shear at and near the margins of the massive, mechanically strong unit C, but there is no conclusive textural evidence to support this assertion. There is clear evidence of shear fabric in the uppermost part of underlying unit D, as in the depth interval 2,291 to 2,300 feet.

#### **Unit A—Metabasalt and metadiabase**

Unit A, between the depths of 803 and 1,809 feet, consists dominantly of fine-grained, light grayish-green to dark greenish-gray metabasalt that for the most part lacks a visible metamorphic fabric. Much of the unit is massive to vaguely layered, but several intervals of pillow breccia, each about 0.5 to 1.0 meter thick, are present, especially in the depth interval between 1,270 and 1,500 feet. Other intervals, as near the top of the hole, are coarse-grained metadiabase.

Most of the massive to vaguely layered rock is a metamorphosed porphyritic basalt in which relict but largely replaced phenocrysts of pyroxene and plagioclase are readily apparent (Fig. 12A). Former pyroxene phenocrysts are replaced principally by pale blue-green hornblende, whereas the former plagioclase phenocrysts are replaced by aggregates of epidote, calcite, and sodic plagioclase. In much of the core, the pseudomorphing hornblende has itself been retrograded to chlorite and carbonate. In contrast, a small proportion of original plagioclase phenocrysts has escaped metamorphic recrystallization almost completely. The groundmass of the metabasalt consists primarily of prismatic blue-green hornblende together with significant but smaller amounts of granular epidote, untwinned



plagioclase, and leucoxene. In places, biotite is a significant groundmass constituent.

The metabasalt displays considerable variability in primary igneous textures and the development of metamorphic fabric. Former pyroxene phenocrysts typically range between 0.1 and 3.0 millimeters in length and make up about 10 percent of the rock volume. Locally, however, the fraction of pyroxene phenocrysts drops below 1 percent or rises to more than 40 percent. Former plagioclase phenocrysts range between 0.3 and 4.0 millimeters in length, and like the pyroxene phenocrysts, range widely in modal abundance. Although the phenocrysts for the most part are not preferentially oriented, there are several core intervals as thick as 3 meters each within which the plagioclase crystals exhibit a strong trachytic fabric. Similarly, the groundmass is for the most part a fine-grained mat in which the prismatic hornblende crystals are randomly oriented. Locally, however, the groundmass hornblendes are strongly aligned. This fabric appears to be mimicking an igneous flow fabric in some cases, and in others it is clearly a metamorphic phenomenon. In general, however, the development of unequivocal metamorphic fabric is confined to the immediate vicinity of the many brittle to semibrittle shear zones that cut the rock, and to the shear zones themselves. The shear zones are 5 to 20 centimeters thick and have abruptly gradational contacts with unshered rock. Hornblende within the shear zones is extensively replaced by biotite and calcite, and the biotite in turn is extensively replaced by chlorite.

Estimated modes of the metabasalt vary substantially. The proportion of hornblende (phenocryst pseudomorphs plus the prismatic variety in the groundmass) in unshered rock ranges between 15 and 85 volume percent, of plagioclase between 3 and 65 percent, and of biotite, calcite, and epidote between 0 and 10 percent each. Sphene, leucoxene, and pyrite are widespread trace constituents.

Intervals of fragmental rock interpreted as pillow breccia contain clasts 3 to 5 centimeters in apparent diameter that have very fine-grained chilled rinds 1 to 2 centimeters thick. The rinds are cut by radial veinlets of calcite and epidote 1 to 4 millimeters thick. The chilled rinds and slightly coarser interior portions of the clasts are composed chiefly of very fine-grained, pale green amphibole that is extensively replaced by chlorite, and subhedral plagioclase that is commonly sausseritized.

Randomly oriented vein-filled fractures are abundant throughout unit A. These are typically about 1 to 2 millimeters thick and rarely as thick as 3 centimeters. The veins contain varying proportions

of calcite, quartz, pyrite, and biotite that is partly replaced by chlorite. The pyrite content ranges from trace amounts to several percent.

The lowermost 30 feet or so of unit A consists of very fine-grained epidote amphibolite that is intercalated with beds of mica-rich graphitic slate and phyllite similar to the dominant metasedimentary rock types in unit B. The basal contact of unit A is placed at a shear zone several centimeters thick in which a pronounced crenulation cleavage has developed that is inclined approximately 10° to the shear-zone margins and to bedding within the sequences of rock above and below. This shear zone and several thinner ones in the basal part of unit A are composed chiefly of chlorite and epidote; quartz and poorly twinned sodic plagioclase occur irregularly in minor amounts. The shear zones and relatively unshered rock near them are cut by numerous, thin, quartz-pyrite veins.

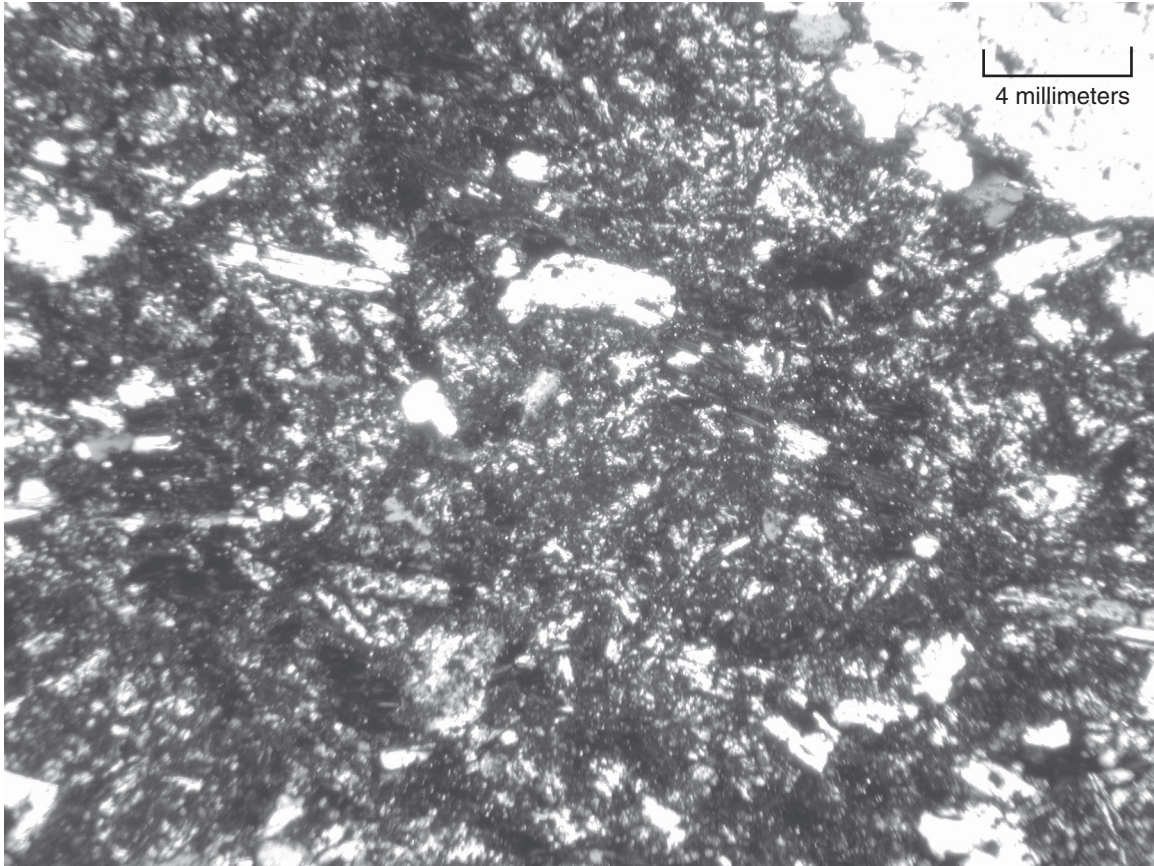
## STRATIGRAPHIC INTERPRETATION

The sequences of rock types encountered in the HB-1 core fit rationally into the framework of Paleoproterozoic stratigraphic units established in east-central Minnesota. On the basis of lithology and succession, all of the rocks in the core below unit A (except for the minor intersections of Keweenaw dikes) are assignable to formations of the Mille Lacs Group as defined by Morey (1978). Unit A also fits rationally in the Mille Lacs Group, but is here erected and named as a new stratigraphic entity not included in Morey's original group definition.

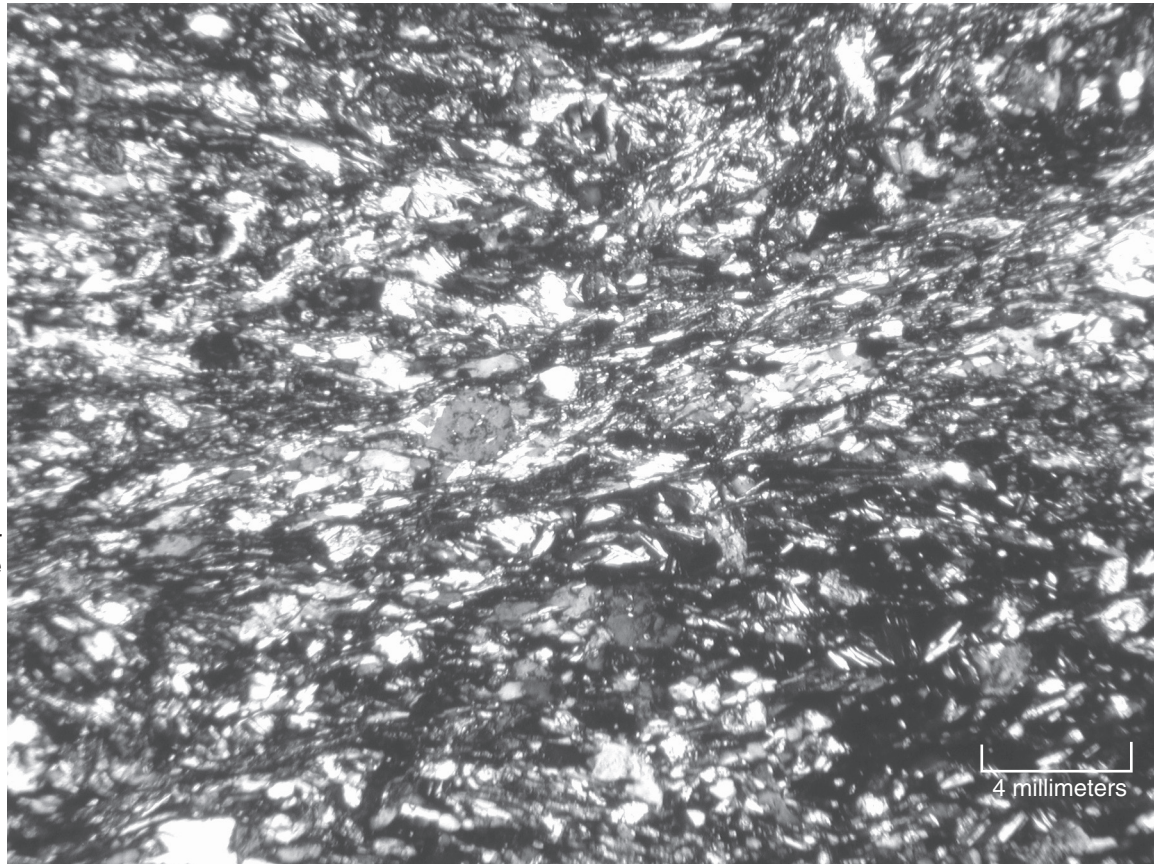
The schistose quartzite, quartz-rich mica schist, biotite-muscovite schist, calcareous mica schist, and dolomitic marble of core units H and F are comparable in all significant respects to rocks in the middle and upper parts of the **Denham Formation** as exposed at the type locality (Morey, 1978; Boerboom and Jirsa, 2001). Furthermore, the mafic sill of core unit G, although apparently a single, thick intrusion, is approximately at the same stratigraphic level as geochemically similar metamorphosed mafic flows and fragmental rocks in the type section (Boerboom and Jirsa, 2001; Southwick and others, 2001). However, it is well established from detailed mapping at the type locality that the fine-scale lithostratigraphic units of which the Denham Formation is composed tend to pinch out abruptly and intertongue with one another (Boerboom and Jirsa, 2001). Therefore, it is unlikely that subunits of the formation correlate precisely over the 12-mile (20-kilometer) distance between the Denham Formation type locality and the Hattenberger drill hole (Fig. 1), even though the



A.



B.



Shear zone

Shear zone

formation as a whole apparently extends that far in the subsurface.

The lithologic attributes of core units E, D, C, and B correspond well to the described attributes of the **Glen Township Formation** in its drilling-defined type section: it "...consists predominantly of interbedded pyrite- and pyrrhotite-rich carbonaceous slate, recrystallized cherty iron-formation, metabasalt, highly altered diabase, and lesser amounts of quartzite, quartz-rich siltstone, argillite, and calcareous rocks of limestone affinity." (Morey, 1978, p. 20). The iron-bearing minerals in the iron-formation and iron-rich carbonaceous slate of units E and D are very fine-grained iron sulfide and somewhat coarser-grained iron silicate phases, including stilpnomelane, Fe pargasite, Fe biotite, and garnet, whereas the predominant iron-bearing phases in iron-rich rocks in the type Glen Township Formation cores are sulfides. This difference is attributable to a combination of differences in the primary sedimentary facies and the grade of metamorphism between the two localities. The volcanic and hypabyssal rocks within units E and D are very similar petrographically to those in the Glen Township Formation at and near the type locality, and this general similarity is borne out in their geochemical compositions (Southwick and others, 2001; see further discussion below).

The metaigneous rocks of unit A, between depth 1,809 and the top of coring at depth 803 feet, could logically be included in the Glen Township Formation, inasmuch as the rocks are essentially identical to the metaigneous components of subjacent units E and C. On the other hand, the metaigneous succession of unit A is more than 1,000 feet thick, and rocks very similar to unit A are first bedrock over a considerable area of east-central Minnesota (Fig. 2). Therefore, we see merit in treating unit A as a distinct formation, and propose the informal name **Kettle River formation** for the succession of mafic volcanic and hypabyssal rocks it contains. The reference stratotype for the Kettle River formation is the core from Hattenberger Number 1, unit A, as described more fully in the "Unit A—Metabasalt and metadiabase" section of this report and portrayed in Appendix Figure 1. The core material is stored at the offices of the Minnesota Geological Survey.

Metagraywacke is not represented abundantly in the Hattenberger core. Most of the metasedimentary rocks in units E, D, and B were derived from fine-grained, very thin-bedded to laminated protoliths such as mudstone, shale, and iron-rich chemical sediments. Thin intervals of rhythmically interbedded metashale and fine-grained metagraywacke are present locally but are only minor constituents of the total section drilled. The metasedimentary rocks of units H and F are mainly quartz-rich schists of various kinds that are interbedded with calcareous schist and marble. The protolithic section from which these rocks formed was a sequence of fine- to medium-grained lithic sandstone, siltstone, dolomitic siltstone, and dolostone that may have been deposited in a shallow marine environment in which the current regime was locally or occasionally conducive to the deposition of graded beds. Occasional storm events may have produced currents of sufficient strength to transport and deposit thin beds of fine-grained conglomerate. The diagnostic rhythmites of classical graywacke-mudstone turbidites are not present in either the H to F or the E to D to B interval of the Hattenberger core.

It would appear, therefore, that the substantial thickness of rhythmically bedded metagraywacke that crops out north of the Denham Formation in Pine County (Figs. 1, 2) is not represented in the Hattenberger drill core. There are several possible explanations for this, including non-deposition of the graywacke facies at Kettle River or thrusting out of the graywacke interval during tectonism. In any case, the contact between units F and E is a critical horizon, representing either an abrupt change in depositional facies from marine shelf to a quiescent deep-water environment that was affected periodically by mafic volcanism, a cryptic but regionally significant zone of thrusting, or a combination of these.

## GEOCHEMISTRY OF THE CORED BEDROCK

### Introduction

Fifty-five samples were selected from the Hattenberger core for chemical analysis. Forty-three of these were chosen to be representative of the major

**Figure 12.** Photomicrographs illustrating typical textures and fabrics in metabasalt.

**A.** Well preserved igneous texture in metabasalt within a thick, relatively massive flow unit in unit A, depth 1,782 feet. Relict microphenocrysts of plagioclase and pyroxene (the latter pseudomorphed by green hornblende) are readily identifiable. Tectonic fabric is essentially lacking.

**B.** Sheared, partially recrystallized metabasalt at depth 1,761 feet in unit A. Small-scale ductile shear zones are well developed and the bulk of the rock displays a penetrative foliation.



rock types encountered in the core; they lack veining, shearing, or other obvious evidence of metasomatic alteration, and thus represent protolith compositions as nearly as possible. The remaining 12 samples were selected to investigate the geochemical attributes of atypical materials such as veins, mylonitic and other varieties of sheared rock, and minor rock types of uncertain origin and history. All of the analyzed rocks are metamorphic and contain mineral assemblages indicative of development under conditions of the upper greenschist or lower amphibolite facies.

The chemical analyses were performed by Activation Laboratories, Limited (ACTLABS) of Ancaster, Ontario at the "exploration" level of precision and accuracy. Major-element concentrations were obtained by ICP methods following fusion. Associated minor and trace element concentrations were analyzed by INAA methods following fusion. The laboratory furnished data on 50 chemical species as well as analyses of total carbon, organic carbon, graphitic carbon, carbon dioxide, and total sulfur in a selected number of samples. To provide completeness for the record, all analytical results are tabulated in Appendix Table 1. Because Appendix Table 1 is complete, it contains both meaningful data for rock classification and petrogenetic interpretation and other data of marginal value for those purposes. Marginal data are those reported for trace elements at or below detection limits or those for trace elements that have no known bearing on the petrogenesis of the rock types encountered by the Hattenberger core.

To aid in comprehending the geochemical characteristics of the rocks in the core, the data in Appendix Table 1 have been reorganized into seven condensed tables that contain only values for chemical species of petrogenetic significance. These tables, numbered 6 through 12 in the main text of this report, also include descriptive statistics and petrochemical ratios of various kinds that are relevant to the petrogenetic interpretation of the rocks. The data contained in tables 6 through 12 are the basis of the discussion and diagrams that follow.

### **Metamorphosed clastic sedimentary rocks of the Denham Formation**

Five chemical analyses of typical metaclastic rocks in the Denham Formation portion of the core are presented in Table 6. It is evident from simple inspection of the data that the rocks are strongly enriched in  $K_2O$  relative to  $Na_2O$ , and that  $K_2O$  and  $Al_2O_3$  vary sympathetically. The variation in  $SiO_2$  content is wide, extending from about 49 to about 90 weight percent; the sympathetic variation of  $K_2O$

and  $Al_2O_3$  holds across that span.  $CaO$  contents are low across the range of  $SiO_2$  variation;  $Fe_2O_3$  and  $MgO$  vary sympathetically, reflecting variable biotite content in the present rocks and variable inputs of mafic constituents to the original sediment. The abundances of selected major and trace elements normalized against the composition of the North American shale composite (NASC; Fig. 13A) show considerable scatter within a range of about one order of magnitude depletion relative to the NASC standard. Within that range, the more siliceous and thus more arenaceous rock types are generally more depleted in trace elements across the board than the less siliceous and thus more argillaceous rock types. The NASC-normalized rare earth element plots (Fig. 13B) have flat to weakly negative slopes and fall in a broad band approximately between 2 times enrichment and 0.1 times depletion relative to the standard. These data also show a systematic diminution in rare earth element abundance with increasing  $SiO_2$  content, suggesting that the primary rare earth signature was contributed from the micaceous, original, argillaceous components of the rock and that the admixing of detrital quartz served mainly to dilute it.

If metamorphism was isochemical (difficult to establish or refute in rocks of this type), the inferred protolithic assemblage of sedimentary strata spanned a range of quartz-rich, K-rich compositions. It possibly consisted of rocks that were various mixtures of detrital quartz, muscovite, and clay minerals, plus minor amounts of unspecified mafic components. This fits with observations in outcrop at the type locality of the Denham Formation (Boerboom and Jirsa, 2001), which indicate that the basal part of the formation was derived in large part from saprolitic residuum developed on the nonconformably subjacent McGrath Gneiss. The lowest strata are quartz-sericite schists of various kinds, some of which contain relict sand-size clasts of K-feldspar and the micas, and interbeds of granule and pebble metaconglomerate in which lithic clasts of gneiss are identifiable. The metaclastic part of the Denham Formation section cored in HB-1 is interpreted as a diverse package of submature sandstones plus compositionally related finer- and coarser-grained sedimentary rocks that were derived mainly from weathered McGrath Gneiss, as at the type locality. The section cored may have been deposited some distance seaward from the source of detrital sediment, however, and therefore was finer-grained on average, prior to metamorphism, than the rocks at the type locality of the Denham Formation.



**Table 6.** Chemical analyses of schistose metaclastic rocks from the Denham Formation (core units H and F). Major-element oxides reported in weight percent; minor and trace elements in parts per million.

Code no	hbgr 41	hbgr 42	hbgr 45	hbgr 48	hbgr 54
Subunit	F	F	F	F	H
Sample	5118	5181	5411	5606	7046
SiO <sub>2</sub>	84.93	90.60	49.12	56.49	57.59
TiO <sub>2</sub>	0.09	0.03	1.48	0.84	0.67
Al <sub>2</sub> O <sub>3</sub>	3.94	2.23	19.96	19.92	21.79
Fe <sub>2</sub> O <sub>3</sub>	6.02	2.91	11.91	7.54	7.64
FeO					
MnO	0.18	0.08	0.05	0.03	0.06
MgO	0.91	0.42	2.91	3.49	2.24
CaO	1.25	0.96	2.38	1.19	0.21
Na <sub>2</sub> O	0.38	0.01	0.13	3.09	0.66
K <sub>2</sub> O	1.02	1.00	8.44	5.66	5.33
P <sub>2</sub> O <sub>5</sub>	0.99	0.19	0.31	0.13	0.07
CO <sub>2</sub>					
C/tot					
S/tot					
H <sub>2</sub> O					
LOI	0.65	0.93	3.50	2.08	3.77
sum	100.36	99.36	100.20	100.44	100.03
FeO <sup>t</sup>	5.42	2.62	10.72	6.79	6.88
Rb	27	22	155	134	159
Sr	54	34	31	90	61
Ba	95	137	897	910	632
Sc	2.5	1	21	14	19
Nb					
Hf	1.7	1.2	7.2	6.9	2.5
Ta	<1	<1	1	2	<1
Zr	56	39	260	253	90
Y	7	2	40	31	18
Cr	34	16	100	127	154
Ni	13.0	9.0	46.0	57.0	52.0
Cu	12.0	28.0	2.0	5.0	22.0
Zn	28.0	8.0	94.0	41.0	83.0
V	13.0	6.0	86.0	78.0	96.0
Cs	3	0.5	2.7	3.2	3.3
Th	2.5	1.4	12.9	13.5	11.2
La	10	4.1	73.6	54.5	47.4
Ce	28	11	148	113	95
Nd	11	6	67	53	39
Sm	1.4	0.5	10.4	7.8	5.8
Eu	0.4	0.1	2.9	1.7	1.4
Gd					
Tb	<0.5	<0.5	1.5	1.1	<0.5
Yb	0.4	0.2	3.1	2.6	1.5
Lu	0.06	<0.05	0.49	0.37	0.22

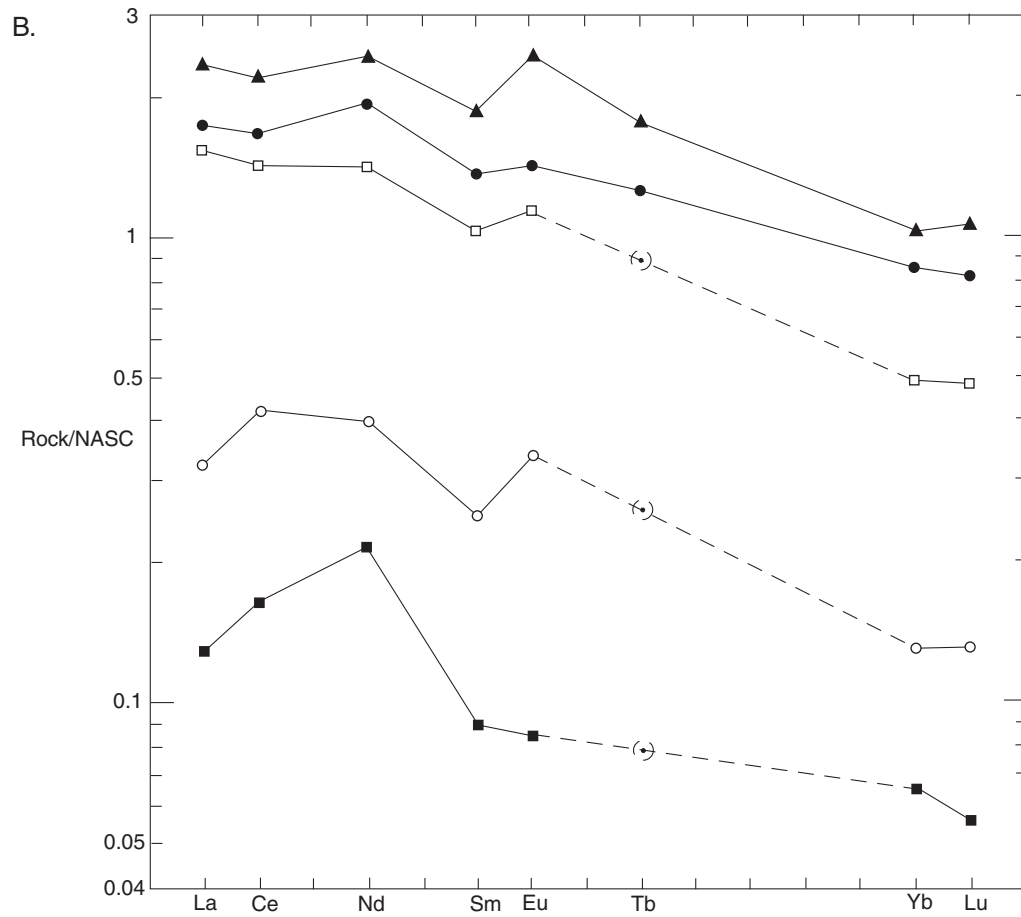
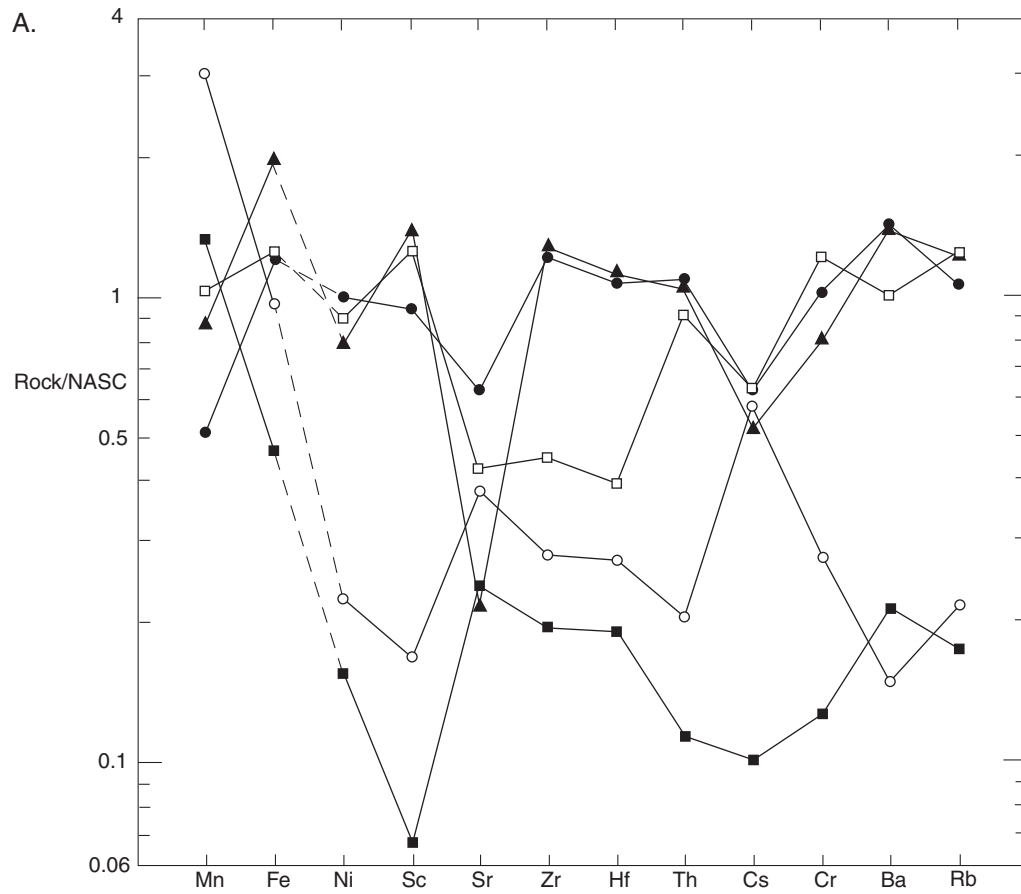
5118: Micaceous quartzite

5181: Micaceous quartzite

5411: Biotite-muscovite-quartz phyllite

5606: Biotite-muscovite-quartz schist

7046: Biotite-muscovite-quartz phyllite



### Metamorphosed limey mudrock and dolostone of the Denham Formation

Table 7 contains six chemical analyses of calcareous schist and marble from unit F, here interpreted as the upper part of the Denham Formation. The calcareous schist, which consists chiefly of phyllosilicates, quartz, and carbonate minerals in varying proportions, contains appreciable amounts of  $\text{SiO}_2$ ,  $\text{Al}_2\text{O}_3$ , and the alkalis, whereas the phyllosilicate-poor marble contains much less of these components. Dolomite is the chief mineral in the marble, as reflected in the high content of CaO and MgO in the chemical analyses, and also is the dominant carbonate species in the calcareous schist. The modal and geochemical compositions indicate that the rocks of the calcareous schist-marble suite originally were dolomitic shale, shaly dolostone, and sandy or silty dolostone. None of the analyzed samples is a pure carbonate rock devoid of a silicate component.

It is evident from direct inspection of the data in Table 7 that the abundances of major, trace, and rare earth elements in this suite of rocks vary widely and erratically from sample to sample. This is consistent with an origin of the rocks from a mixed sedimentary protolith in which the principal constituents were detrital clay, quartz-rich sand or silt, and chemically or biochemically precipitated dolomite. The varying elemental abundances simply reflect the relative proportions of these original sedimentary components. The detrital components probably were materials compositionally similar to the range of metaclastic rock types that make up most of the Denham Formation section, as described and discussed in the preceding section.

### Metamorphosed iron-rich strata of the Glen Township Formation

Table 8 contains eight analyses of strongly iron-enriched strata (greater than 20 weight percent total  $\text{Fe}_2\text{O}_3$ ) from core units D and E, here interpreted as part of the Glen Township Formation. The analyzed rocks are composed principally of silica ( $43.49 \pm 9.22$  weight percent) and iron (total iron as  $\text{Fe}_2\text{O}_3 = 29.27 \pm 5.25$  weight percent), proportions similar to

those in chemically precipitated Precambrian iron-formations in many districts (James, 1992). They also contain relatively high amounts of  $\text{Al}_2\text{O}_3$  ( $9.50 \pm 3.12$  percent),  $\text{K}_2\text{O} + \text{Na}_2\text{O}$  ( $1.34 \pm 0.88$  percent), and zirconium ( $189 \pm 58$  parts per million), constituents that indicate the original presence of a significant clastic component in the analyzed rocks. The NASC-normalized elemental abundance profiles of the iron-rich rocks show that manganese is enriched to an even greater degree than iron, relative to the standard, and that the abundances of a selected suite of trace elements are slightly depleted on average (Fig. 14A). The normalized rare earth element profiles have flat to slightly negative slopes and cluster rather closely around the NASC values (Fig. 14B). Together, the elemental abundance patterns for the iron-rich rocks are comparable to the normalized patterns for the interstratified clastic metasedimentary rocks that are not anomalously enriched in iron (Fig. 15; see discussion in the following section). This suggests that the clastic component of the iron-rich strata probably was mud comparable to that from which the associated "normal" metasedimentary rocks were derived.

Further geochemical evidence that the iron-rich rocks were originally a mixture of a clastic component (mud) and a chemically precipitated, probably hydrothermal component is presented in Figures 16 and 17. Figure 16, modified from Marchig and others (1982) and Wonder and others (1988), ascribes pelagic, diagenetic, and hydrothermal origins to iron-formations on the basis of  $\text{Y}/\text{P}_2\text{O}_5$  and  $\text{Zr}/\text{Cr}$  ratios. The Hattenberger iron-rich rocks plot dominantly in the pelagic field, well away from the restricted hydrothermal field. The hydrothermal field on this diagram is based on data from modern hydrothermal systems and iron-rich rocks in geologic settings reasonably interpreted as hydrothermal in origin. Average compositions of the Biwabik Iron Formation (Morey, 1992), unoxidized Trommald Iron Formation in the Gloria drill hole (Melcher and others, 1996), and the Homestake Iron Formation (Kath, 1990) plot within it. The plotted position of an average graphite schist from east-central Minnesota, based

**Figure 13.** NASC—normalized elemental abundance plots for five metaclastic rocks of the Denham Formation. Values reported as less than the analytical detection limit are arbitrarily assigned values equal to the detection limit for plotting purposes.

**A.** Manganese, iron, and a suite of trace elements. Plotting order of elements selected to reduce "noise" in the diagram.

**B.** Rare earth elements. Plots for quartz-rich rocks are indicated by heavy lines. Denham Formation data are from Table 6; NASC composition is from Gromet and others (1984).

**Table 7.** Chemical analyses of calcareous schist and marble from the Denham Formation (core units H and F). Major-element oxides reported in weight percent; minor and trace elements in parts per million.

Code no	hbgr 37	hbgr 38	hbgr 39	hbgr 43	hbgr 44	hbgr 46
Subunit	F	F	F	F	F	F
Sample	4845	4934	5067	5256	5284	5532
SiO <sub>2</sub>	70.17	13.26	56.55	8.64	9.96	77.88
TiO <sub>2</sub>	0.19	<0.01	0.55	<0.01	0.02	0.09
Al <sub>2</sub> O <sub>3</sub>	6.82	0.30	13.76	0.25	0.43	1.61
Fe <sub>2</sub> O <sub>3</sub>	2.52	1.46	4.26	1.57	2.52	1.07
FeO						
MnO	0.03	0.08	0.03	0.10	0.10	0.07
MgO	6.92	17.66	3.68	18.60	18.07	1.98
CaO	7.88	27.88	5.22	27.07	30.67	9.56
Na <sub>2</sub> O	2.24	<0.01	0.29	0.02	<0.01	0.01
K <sub>2</sub> O	1.00	0.02	7.69	0.10	0.02	0.88
P <sub>2</sub> O <sub>5</sub>	0.03	<0.01	0.07	<0.01	<0.01	0.05
CO <sub>2</sub>		39.42		43.79	35.74	
C/tot		10.76		11.98	9.83	
S/tot		0.06		0.03	0.03	
H <sub>2</sub> O						
LOI	2.65	38.38	6.38	42.48	37.54	7.55
sum	100.46	99.04	98.48	98.84	99.34	100.75
FeO <sup>t</sup>	2.27	1.31	3.83	1.41	2.27	0.96
Rb	22	<10	98	<10	<10	17
Sr	76	44	53	28	25	21
Ba	246	1	437	4	<1	194
Sc	4.5	0.3	11	0.4	0.4	1.3
Nb						
Hf	0.7	<0.5	2.4	<0.5	<0.5	<0.5
Ta	<1	<1	<1	<1	<1	<1
Zr	27	3	95	2	6	13
Y	4	7	22	2	4	5
Cr	46	5	94	2	3	13
Ni	36.0	6.0	61.0	8.0	4.0	11
Cu	3.0	2.0	27.0	3.0	2.0	5
Zn	20.0	7.0	108.0	70.0	136.0	25
V	27.0	2.0	91.0	2.0	2.0	6
Cs	<0.5	<0.5	3.8	<0.5	<0.5	0.7
Th	2.4	0.6	8.1	<0.5	<0.5	1.1
La	6.6	4.4	28.3	1.5	3.7	4.4
Ce	13	6	52	<3	5	10
Nd	<5	<5	25	<5	<5	5
Sm	1	0.6	4.1	0.2	0.4	0.7
Eu	0.3	0.1	1	<0.1	0.1	0.1
Gd						
Tb	<0.5	<0.5	<0.5	<0.5	<0.5	<0.5
Yb	0.4	0.3	1.5	<0.1	0.1	0.5
Lu	0.06	<0.05	0.25	<0.05	<0.05	0.07

4845: Fine-grained carbonate-biotite-quartz-muscovite schist

4934: Dolomite marble; minor quartz, muscovite

5067: Laminated muscovite-biotite-quartz-carbonate schist

5256: Dolomite marble; minor quartz, muscovite, Fe-oxide

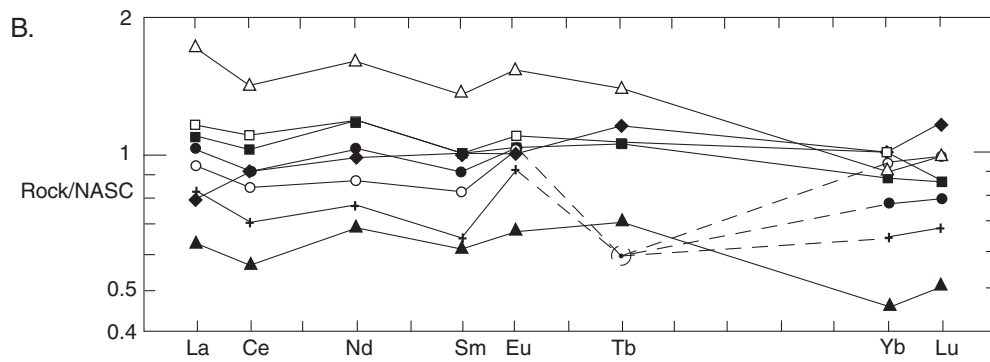
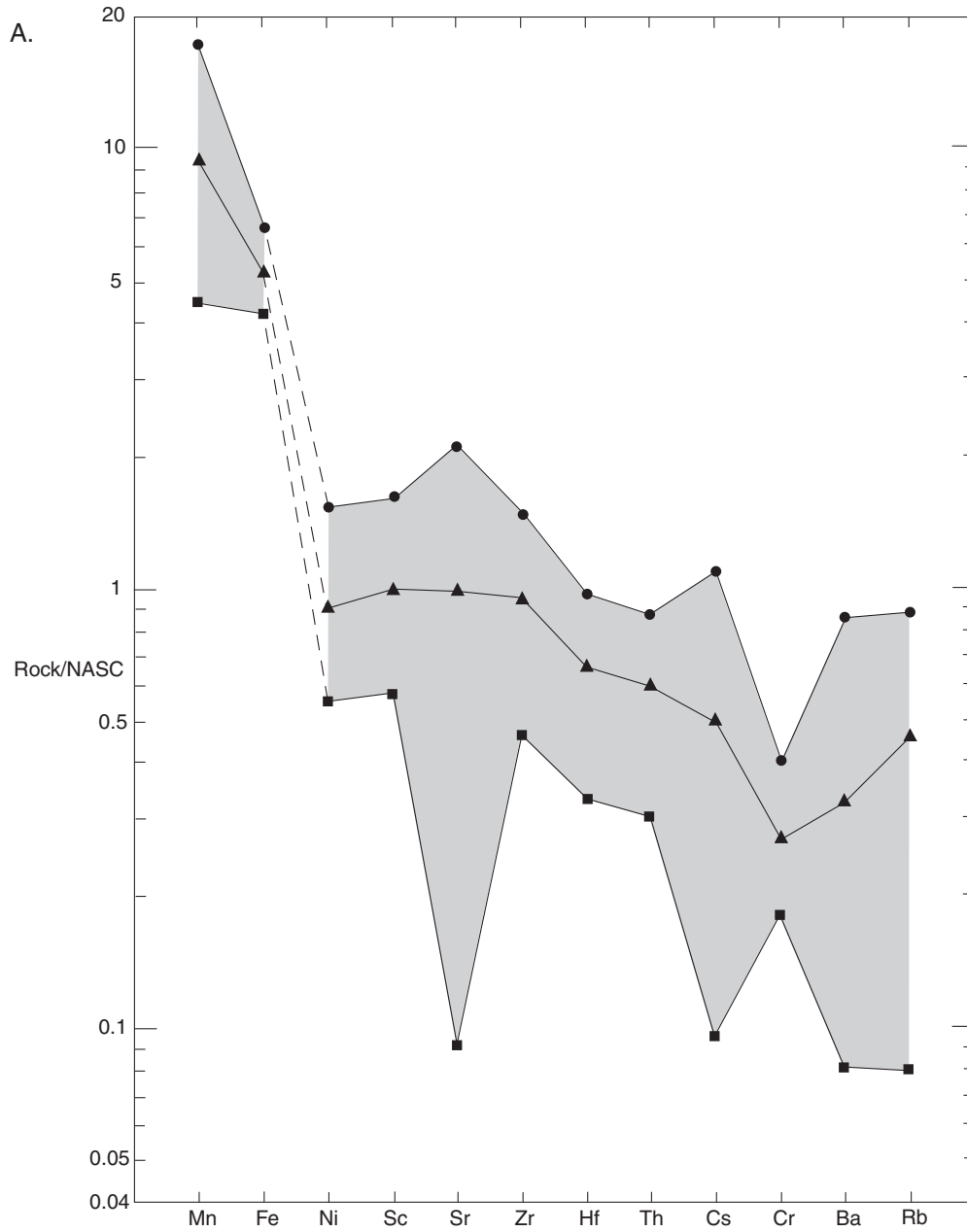
5284: Dolomite marble; rare scapolite (?) phenocrysts, heavily altered

5532: Carbonate-biotite-muscovite-quartz schist

**Table 8.** Chemical analyses of metamorphosed iron-rich sedimentary rocks (iron-formation and closely allied rock types) from the Glen Township Formation (core units E and D). Major-element oxides reported in weight percent; minor and trace elements in parts per million.

Code no	hbgr 16	hbgr 17	hbgr 18	hbgr 19	hbgr 20	hbgr 21	hbgr 28	hbgr 31		
Subunit	D	D	D	D	D	D	E	E		
Sample	2431	2437	2456	2461	2495	2544	3485	3938	mean	std dev
SiO <sub>2</sub>	48.27	45.05	60.51	33.52	37.63	36.99	50.17	35.79	43.49	9.22
TiO <sub>2</sub>	1.03	1.01	0.48	1.18	0.97	2.19	1.31	1.02	1.15	0.48
Al <sub>2</sub> O <sub>3</sub>	10.68	9.24	5.05	9.51	8.36	15.60	6.84	10.72	9.50	3.12
Fe <sub>2</sub> O <sub>3</sub>	24.51	26.54	20.74	31.19	30.54	30.53	32.24	37.88	29.27	5.25
FeO										
MnO	0.29	0.58	0.36	0.87	0.70	0.39	0.25	0.56	0.50	0.22
MgO	3.08	3.09	1.62	3.09	2.38	3.26	2.37	3.22	2.76	0.58
CaO	2.67	3.35	2.65	5.90	6.15	0.36	2.16	2.01	3.16	1.97
Na <sub>2</sub> O	0.09	0.06	0.02	0.18	0.09	1.46	0.23	0.41	0.32	0.48
K <sub>2</sub> O	1.89	0.38	0.23	1.06	0.25	1.25	0.47	2.65	1.02	0.88
P <sub>2</sub> O <sub>5</sub>	0.10	0.10	0.06	0.13	0.09	0.23	0.09	0.10	0.11	0.05
CO <sub>2</sub>					4.5					
C/tot					2.88					
S/tot					4.33					
H <sub>2</sub> O										
LOI	6.40	9.39	6.23	11.78	11.11	6.73	4.20	6.19	7.75	2.68
sum	99.05	98.82	97.97	98.39	98.31	98.99	100.33	100.59	99.04	
FeO <sup>t</sup>	22.06	23.89	18.67	28.07	27.49	27.48	29.02	34.09	26.34	
Rb	69	32	<10	50	<10	63	22	111	57.83	31.59
Sr	95	134	94	228	302	61	13	216	142.88	97.28
Ba	396	52	54	189	61	174	193	552	208.88	179.31
Sc	17	16	8.7	15	15	24	11	12	14.84	4.64
Nb										
Hf	5.3	4.1	2.1	4.3	3.8	6.1	3.4	4.3	4.18	1.20
Ta	3	2	<1	2	<1	2	2	2	2.17	0.41
Zr	255	181	93	184	168	278	151	205	189.38	58.21
Y	31	34	20	33	25	42	21	39	30.63	8.05
Cr	31	32	23	31	35	50	35	30	33.38	7.69
Ni	46.0	36.0	57.0	37.0	69.0	32.0	89.0	51.0	52.13	19.28
Cu	60.0	92.0	187.0	175.0	147.0	6.0	681.0	395.0	217.88	220.17
Zn	89.0	77.0	48.0	96.0	76.0	124.0	54.0	128.0	86.50	29.19
V	160.0	148.0	82.0	123.0	129.0	186.0	103.0	151.0	135.25	33.09
Cs	3.3	1.2	1.2	3.1	<0.5	2.2	1.3	5.8	2.59	1.67
Th	9.3	7.4	3.7	6.9	6.7	10.8	5.4	8.5	7.34	2.23
As	<2	<2	<2	<2	<2	<2				
Au	0.007	<0.005	0.006	0.020	<0.005	<0.005				
La	29.6	34.7	19.9	37.1	32.8	54.1	25.7	24.7	32.33	10.47
Ce	56	68	38	75	62	96	47	63	63.13	17.68
Nd	24	33	19	33	28	44	21	27	28.63	8.02
Sm	4.6	5.6	3.4	5.3	5.1	7.8	3.6	5.2	5.08	1.36
Eu	1.2	1.2	0.8	1.3	1.2	1.8	1.1	1.1	1.21	0.28
Gd										
Tb	<0.5	0.9	0.6	0.9	<0.5	1.2	<0.5	1.0	0.92	0.22
Yb	2.9	2.7	1.4	2.9	2.3	2.8	2.0	3.0	2.50	0.56
Lu	0.44	0.39	0.23	0.39	0.36	0.44	0.31	0.54	0.39	0.09

Note: All analyzed rocks are combinations of graphite, chlorite, Fe silicates including stilpnomelane, Fe sulfides, and Fe oxides. 3485 also contains Fe pargasite; 2544 also contains garnet; 3938 also contains both Fe pargasite and garnet.



on 29 analyses tabulated by McSwiggen and Morey (1989), is included on Figure 16 as an additional reference point.

Figure 17, based on logic developed and explained in detail by Lottermoser and Ashley (1996), shows the compositions of Hattenberger iron-rich rocks and interstratified "normal" pelitic rocks (Table 6) in terms of their  $TiO_2/FeO_t$  and  $Al_2O_3/(Al_2O_3 + FeO_t + MnO)$  ratios. Also shown for reference on the diagram are compositions of the Biwabik, Trommald, and Homestake Iron Formations, typical silicate and sulfide iron-formations as reported by James (1992), typical graphite schist from east-central Minnesota, the North American shale composite (NASC; Gromet and others, 1984), and an average Canadian-Shield Proterozoic shale (Cameron and Garrels, 1980). The iron-rich rocks plot along a trend between the pelitic rocks and chemically precipitated iron-formation as represented by the Biwabik Iron Formation, a position strongly suggesting that the Hattenberger iron-rich rocks originally were mixtures of clastic and chemically precipitated components. Furthermore, the Hattenberger pelitic rocks cluster strongly around the NASC and Proterozoic shale compositions, indicating that these rocks are not particularly anomalous in their geochemistry.

### **Metamorphosed carbonaceous mudstone and allied rocks of the Glen Township Formation**

Table 9 contains 11 analyses of assorted "normal" metapelitic rocks from core units B, D, and E that are interpreted to have consisted originally of fine-grained epiclastic detritus mixed with various proportions of carbonaceous material, iron-rich chemical sediment, and volcanic ash. Four of these analyses (columns 8 through 11) are of rock types that contain variable amounts of porphyroblastic pargasite or garnet and have iron contents expressed as  $Fe_2O_3$  in the 13 to 20 weight-percent range. These rocks are considered to be lean or transitional iron-formation.

The geochemical compositions of these metapelites, including the transitional iron-rich rocks, are similar to ordinary shale (Fig. 15A). On average, manganese is enriched about three times and iron about two times above NASC values, which suggests

that some hydrothermally generated manganese-iron material was admixed with predominantly epiclastic material in the original sediment. Trace-element abundances hover around NASC values, on average showing modest depletions relative to the standard (Fig. 15A). Normalized barium and chromium abundances are dispersed over three orders of magnitude, probably reflecting minor variability in the proportions of mafic and feldspathic detritus in the original muds. Beds interpreted as former volcanic ash make up a small fraction of the stratigraphic section dominated by metapelitic rocks in core units B, D, and E (Appendix Fig. 1), and it is therefore likely that volcanic ash and other volcanic debris constituted a variable small fraction of the sediment in beds that consisted mainly of non-volcanic epiclastic material. Rocks that contain more than about 4 weight percent MgO may be derived from protoliths that included some proportion of mafic volcanic material, although this cannot be a universal indicator of provenance in the absence of textural verification. Analyzed rocks from depths 1,845 and 1,862 feet (Table 9, columns 2 and 4) do contain petrographic evidence of volcanoclastic parentage, and the composition of sample 1,862 is reasonably close to that of a basaltic rock.

NASC-normalized rare earth element patterns are virtually flat and show modest REE depletion relative to the standard (Fig. 15B). Some sample profiles exhibit a weakly positive europium anomaly that again suggests minor variations in the content of feldspars in the parent sedimentary mix.

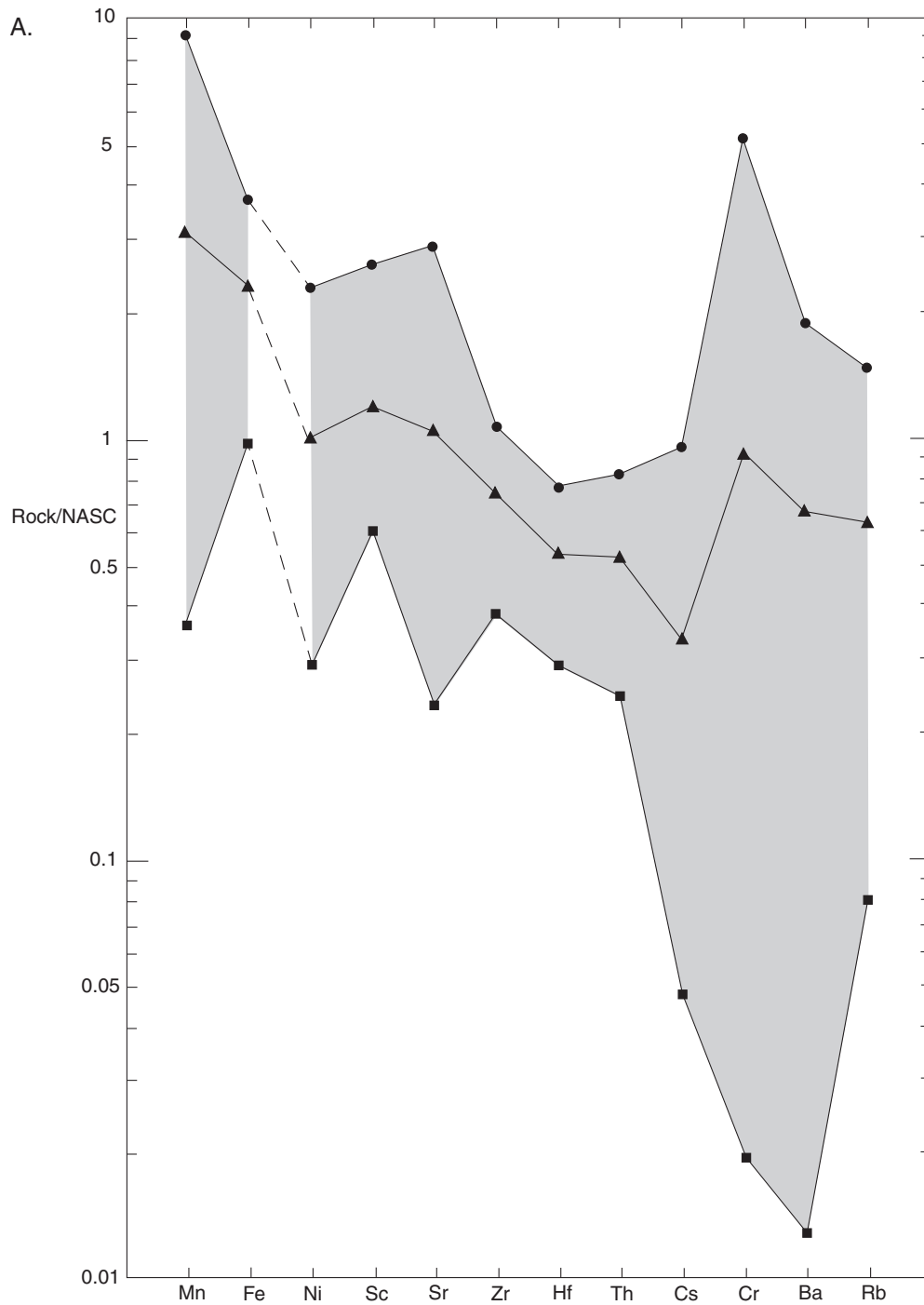
### **Metamorphosed mafic igneous rocks—Kettle River formation and others**

Representative geochemical data for the metamorphosed mafic igneous rocks cut by the Hattenberger core are presented in Tables 10 and 11, which contain data for low-K and high-K analyses, respectively. The division of the total dataset into these two subgroups is based on a simple plot of  $K_2O$  vs.  $SiO_2$  (Fig. 18), which clearly shows a clustering of analyses in terms of  $K_2O$  content. Moreover, all analyses in the high-K subgroup are for samples within unit E, which suggests that this composition may have

**Figure 14.** NASC—normalized elemental abundance plots for iron-rich rocks (iron-formation) of the Glen Township Formation. Values reported as less than the analytical detection limit are arbitrarily assigned values equal to the detection limit for plotting purposes.

**A.** Manganese, iron, and a suite of trace elements for three samples. Plotting order of elements selected to reduce "noise" in the diagram.

**B.** Rare earth elements for eight samples. Glen Township Formation data are from Table 8; NASC composition is from Gromet and others (1984).

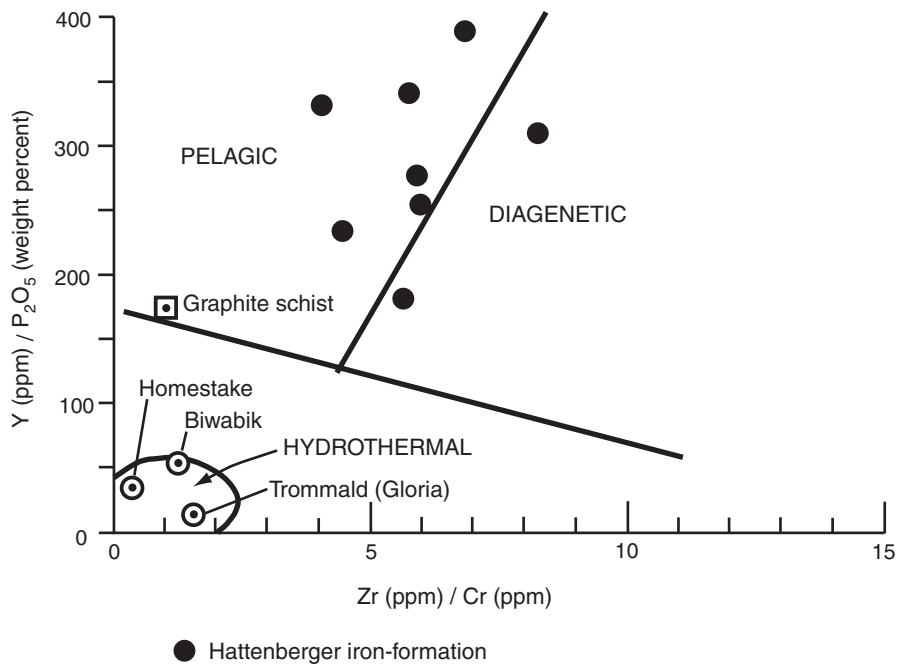
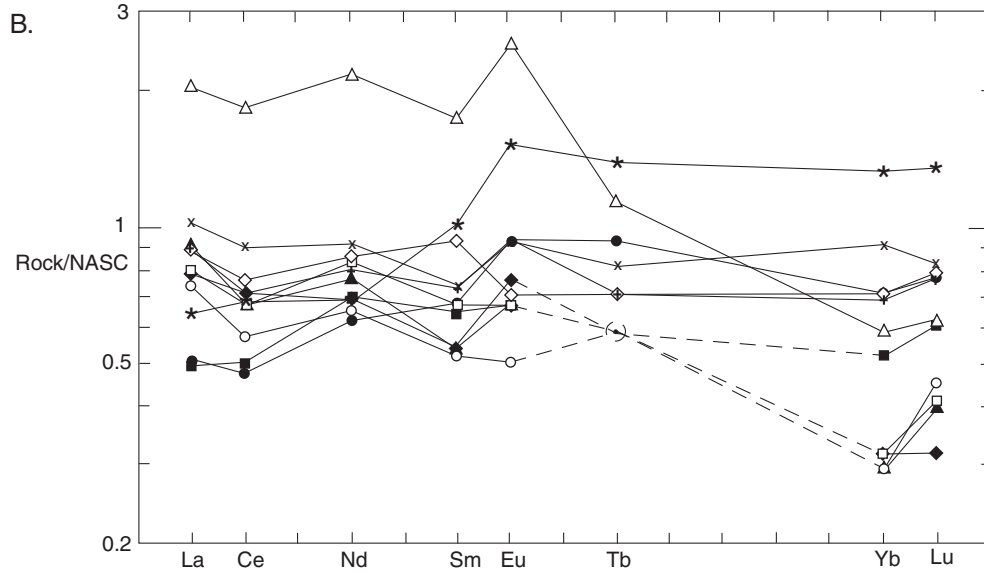


**Figure 15.** NASC—normalized elemental abundance plots for "normal" metapelitic rocks of the Glen Township Formation. Values reported as less than the analytical detection limit are arbitrarily assigned values equal to the detection limit for plotting purposes.

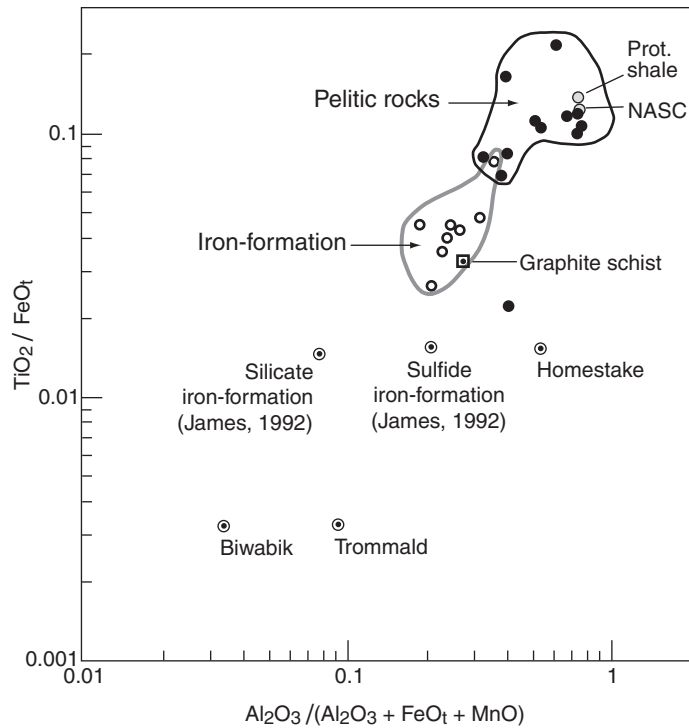
**A.** Manganese, iron, and a suite of trace elements for three samples. Plotting order of elements selected to reduce "noise" in the diagram.

**B.** *On facing page.* Rare earth elements for ten samples. Glen Township Formation data are from Table 9; NASC composition is from Gromet and others (1984).





**Figure 16.** Geochemical discrimination diagram for the depositional environments of iron-formation, modified from Marchig and others (1982) and Wonder and others (1988). Data for HB-1 iron-rich rocks (Glen Township Formation) are plotted; see text for details.



**Figure 17.** Major-element ratio diagram showing the compositions of iron-rich and "normal" metasedimentary rocks of the Glen Township Formation and several reference compositions. Data are from Tables 8 and 9. See text for details.

stratigraphic significance. Small, nonsystematic variations in the alkali contents of metabasaltic rocks commonly are viewed as metasomatic or metamorphic effects (for example Jolly, 1980; Grunsky and others, 1992). The observed variations in  $K_2O$  in the Hattenberger samples are interpreted to suggest that during regional metamorphism,  $K_2O$  migrated from  $K_2O$ -rich pelitic rocks into nearby basaltic rocks more effectively in unit E, where pelitic, mafic volcanic, and mafic hypabyssal rocks are intimately interstratified on the scale of meters to tens of meters, than it did in other parts of the drilled section where volcanic and sedimentary rock units are more coarsely interstratified.

The fundamental similarity among all of the Hattenberger metaigneous rocks is illustrated by the tight clustering of data points in the Fe-tholeiite field of the Jensen plot (Fig. 19; Jensen, 1976). The Jensen plot classifies volcanic rocks in terms of cation proportions of magnesium, iron, titanium, and aluminum and is designed to minimize the impact of alkali mobility in the classification process. Further evidence of geochemical coherence is presented in the spider diagram of Figure 20 and the chondrite-normalized rare earth element plot of Figure 21. The analyses cluster tightly across the elemental spectrum of the spider plot except for considerable dispersal in barium and potassium (both ascribable to metasomatic/metamorphic mobility) and an

anomalous positive excursion for lead, which is a poorly understood but seemingly characteristic geochemical feature of Penokean metabasaltic rocks in east-central Minnesota (Southwick and others, 2001). Overall, the large-ion lithophile elements (LILE) are significantly enriched relative to the normalizing composition of ocean-island basalt and the plots have generally concave shapes. The rare earth element plots exhibit moderately negative slopes; the light rare earth elements (LREE) are enriched about 100 times and the heavy rare earth elements (HREE) about 10 times chondrite abundances. These patterns are characteristic of tholeiitic rocks from a variety of tectonic settings. Elevated values of the large-ion lithophile elements and lead are consistent with a petrogenesis that involved continental crust.

Plots of the HB-1 analyses in the Pearce-Cann diagram (Fig. 22A; Pearce and Cann, 1973), which assigns tectonic settings to volcanic rocks on the basis of their contents of titanium, zirconium, and yttrium, cluster in the "within-plate" and "ocean-floor" fields. Plots of the data into the major-element discrimination diagram of Pearce and others (1977; Fig. 22B) yield putative tectonic settings that are mainly in the "continental" field but overlap slightly into the "ocean island" and "orogenic" fields. Altogether, the analytical data and associated plots in Figures 18 through 22 are broadly consistent with results obtained from other volcanic components in the

**Table 9.** Chemical analyses of metamorphosed carbonaceous mudstone, transitional iron-rich rocks, and related pelites from the Glen Township Formation (core units E, D, and B). The rocks presently are phyllite and fine-grained micaceous schist. Major-element oxides reported in weight percent; minor and trace elements in parts per million.

Code no	hbgr 5	hbgr 6	hbgr 7	hbgr 8	hbgr 9	hbgr 10	hbgr 14	hbgr 26	hbgr 27	hbgr 32	hbgr 33
Subunit	B	B	B	B	B	B	D	D	E	E	E
Sample	1818	1845	1855	1862	1870	1947	2334	3149	3277	4016	4134
SiO <sub>2</sub>	48.94	46.16	59.07	46.96	58.15	58.89	52.73	51.34	47.1	47.19	60.65
TiO <sub>2</sub>	0.36	1.29	0.53	1.41	0.69	0.58	2.02	1.52	2.78	1.01	0.99
Al <sub>2</sub> O <sub>3</sub>	11.11	15.85	17.20	14.82	18.93	18.61	15.96	9.21	11.66	8.34	9.27
Fe <sub>2</sub> O <sub>3</sub>	18.01	14.00	5.59	14.29	6.36	6.82	10.48	20.69	18.86	13.6	16.45
FeO											
MnO	0.07	0.12	0.06	0.16	0.02	0.03	0.13	0.5	0.27	0.19	0.33
MgO	1.32	4.35	2.08	8.11	1.62	1.90	2.50	2.22	4.61	2.46	2.25
CaO	3.84	3.77	2.43	3.01	0.55	0.87	2.22	5.89	9.42	10.81	6.61
Na <sub>2</sub> O	1.03	2.63	1.88	1.86	0.52	4.27	6.07	0.09	0.95	1.04	0.89
K <sub>2</sub> O	3.00	3.81	3.73	0.96	6.17	2.97	1.15	0.1	1.4	3.19	0.85
P <sub>2</sub> O <sub>5</sub>	0.02	0.14	0.02	0.20	0.20	0.03	0.48	0.11	0.28	0.06	0.09
CO <sub>2</sub>	3.76									10.12	
C/tot	3.33									4.12	
S/tot	8.11									1.57	
H <sub>2</sub> O											
LOI	9.87	5.74	5.09	6.39	4.85	3.68	4.54	6.83	1.7	10.89	2.57
sum	97.61	97.90	97.70	98.22	98.10	98.66	98.33	98.53	99.1	98.81	100.93
FeO <sup>i</sup>	16.21	12.60	5.03	12.86	5.72	6.14	9.43	18.62	16.97	12.24	14.81
Rb	72	186	96	58	139	89	36	<10	54	87	22
Sr	72	123	90	74	33	131	408	120	149	342	97
Ba	389	214	496	28	340	682	534	8	548	1199	236
Sc	9.1	25	11	29	13	10	22	15	39	13	14
Nb											
Hf	1.8	2.7	3.3	2.6	3.1	3.7	3.4	4	4	3.9	4.1
Ta	<1	2	<1	<1	<1	1	1	2	1	1	2
Zr	77	118	134	112	132	148	216	181	179	162	176
Y	13	20	12	26	15	11	30	27	46	23	26
Cr	647	110	86	37	100	100	52	45	24	26	26
Ni	133.0	69.0	62.0	71.0	73.0	70.0	39.0	34	49	26	17
Cu	185.0	149.0	31.0	44.0	103.0	216.0	29.0	30	387	108	24
Zn	10.0	368.0	110.0	127.0	75.0	58.0	112.0	77	137	58	62
V	167.0	192.0	125.0	221.0	191.0	189.0	170.0	109	328	106	129
Cs	1.8	4.9	<0.5	1.9	1.6	1	1.1	<0.5	2.2	2.6	1
Th	5.8	4.2	9.7	3	9.2	10.1	6.3	5.5	3.1	6.7	7
La	23.1	15.1	28.8	15.6	24.8	27.3	63.1	24.3	20.1	27.5	1.7
Ce	38	33	46	32	45	48	123	47	45	53	60
Nd	18	19	21	17	23	19	60	22	19	24	25
Sm	2.9	3.6	3	3.8	3.7	3.1	9.8	4.1	5.8	4.3	4.2
Eu	0.6	0.8	0.8	1.1	0.8	0.9	3	1.1	1.8	1.1	1.1
Gd											
Tb	<0.5	<0.5	<0.5	0.8	<0.5	<0.5	1.0	0.6	1.2	0.6	0.7
Yb	0.9	1.6	0.9	2.2	1.0	1.0	1.8	2.1	4.1	2.2	2.8
Lu	0.21	0.28	0.18	0.35	0.19	0.15	0.28	0.35	0.62	0.36	0.38

1818: Graphite-biotite-quartz-muscovite schist/phyllite

1845: Biotite-chlorite-graphite-quartz schist/phyllite with scattered clots of carbonate-epidote-opaques

1855: Graphite-carbonate-biotite-quartz-muscovite-chlorite schist/phyllite

1862: Graphite-carbonate-biotite-quartz-muscovite-chlorite schist/phyllite

1870: Graphite-biotite-quartz-muscovite schist/phyllite; minor chlorite

1947: Graphite-biotite-quartz-muscovite schist/phyllite; minor chlorite

2334: Graphite-biotite-quartz-muscovite schist/phyllite

3149: Garnet-pargasite-graphite-chlorite schist; transitional to metamorphosed iron-formation

3277: Biotite-plagioclase-graphite-pargasite schist; transitional to iron-formation

4016: Interlaminated biotite-quartz and biotite-carbonate schist with transverse pargasite porphyroblasts; transitional to iron-formation

4134: Quartz-muscovite-biotite-chlorite-carbonate schist with transverse pargasite porphyroblasts; transitional to iron-formation

**Table 10.** Chemical analyses of low-K metamorphosed mafic volcanic rocks and closely associated hypabyssal rocks from throughout the Hattenberger core (Core units G, E, C, and A). Rocks in this group contain less than 0.6 weight-percent K<sub>2</sub>O. Major-element oxides reported in weight percent; minor and trace elements in parts per million.

Code no	hbgr 1	hbgr 2	hbgr 3	hbgr 11	hbgr 12	hbgr 13	hbgr 30	hbgr 49	mean	std dev
Subunit	A	A	A	C	C	C	E	G		
Sample	1126	1416	1682	2010	2192	2263	3818	5652		
Rock type	mgb	mb	mdb	mb	mdb	mb	prob. mdb	mgb	n = 8	
SiO <sub>2</sub>	50.08	44.92	48.46	47.78	47.88	44.93	50.74	47.04	47.73	2.12
TiO <sub>2</sub>	1.60	1.56	1.51	1.57	1.37	1.15	2.16	1.66	1.57	0.29
Al <sub>2</sub> O <sub>3</sub>	16.37	16.78	14.78	13.53	14.43	13.25	14.43	15.30	14.86	1.25
Fe <sub>2</sub> O <sub>3</sub>	11.10	11.01	12.85	12.51	12.81	10.97	15.45	14.04	12.59	1.59
FeO										
MnO	0.15	0.17	0.19	0.18	0.21	0.17	0.21	0.21	0.19	0.02
MgO	4.96	4.18	6.41	4.87	6.42	6.10	5.02	6.68	5.58	0.93
CaO	9.93	13.08	10.72	10.79	12.44	9.05	6.77	9.72	10.31	1.97
Na <sub>2</sub> O	3.64	3.26	2.87	3.25	2.22	2.66	3.75	2.66	3.04	0.53
K <sub>2</sub> O	0.27	0.42	0.37	0.24	0.44	0.55	0.49	0.23	0.38	0.12
P <sub>2</sub> O <sub>5</sub>	0.19	0.18	0.16	0.23	0.25	0.20	0.39	0.13	0.22	0.08
CO <sub>2</sub>										
C/tot										
S/tot										
H <sub>2</sub> O										
LOI	1.64	5.12	1.01	5.28	1.29	8.74	1.33	2.89	3.41	2.75
sum	99.97	100.69	99.33	100.21	99.75	97.81	100.75	100.60	99.88	
FeOt	9.99	9.91	11.57	11.26	11.53	9.87	13.91	12.64	11.33	
Mg# (atomic)	46.97	42.94	49.72	43.56	49.84	52.43	39.18	48.54	46.76	
Rb	<10	<10	<10	<10	<10	<10	<10	<10	<10	
Sr	250	348	249	148	561	312	262	199	291	125
Ba	98	187	169	46	237	398	191	61	173	113
Sc	26	26	38	28	33	27	27	33	30	4
Nb										
Hf	2.6	2.2	2.4	1.9	2	1.8	237	2.1	32	83
Ta	2	<1	<1	<1	<1	<1	2	<1	2	0
Zr	116	99	85	99	91	80	143	96	101	20
Y	28	25	25	21	23	18	29	24	24	4
Cr	130	146	290	32	145	140	32	210	141	85
Ni	79.0	59.0	77.0	33.0	67.0	76.0	23.0	143.0	70	36
Cu	263.0	222.0	210.0	130.0	146.0	31.0	88.0	242.0	167	81
Zn	70.0	98.0	118.0	95.0	88.0	72.0	97.0	98.0	92	16
V	184.0	174.0	228.0	225.0	241.0	200.0	280.0	205.0	217	34
Cs	<0.5	0.9	<0.5	<0.5	0.6	<0.5	0.9	<0.5	0.8	0
Th	2.4	1.4	1.5	1.6	1.5	1.6	3	1.7	1.8	1
La	13.2	10.6	10.1	12.6	16.1	14.9	25.1	10.3	14.11	4.95
Ce	30	20	25	27	37	30	52	23	30.50	10.10
Nd	17	14	12	14	19	20	21	14	16.38	3.34
Sm	3.7	2.9	3.1	3.3	3.9	3.4	5.3	3.2	3.60	0.76
Eu	1.2	0.9	1.1	0.9	1.4	1	1.5	1	1.13	0.23
Gd										
Tb	0.7	<0.5	0.7	<0.5	0.6	<0.5	0.6	<0.5	0.65	0.06
Yb	2.2	2.0	2.2	1.5	2.0	1.5	2.0	2.2	1.95	0.29
Lu	0.37	0.27	0.31	0.23	0.28	0.25	0.28	0.34	0.29	0.05

Note: All analyzed samples consist dominantly of the mineral assemblage blue-green hornblende+plagioclase+Fe-Ti oxides +sphene+clinozoisite; chlorite, biotite, quartz, and calcite are present in variable small amounts. Mgb, mb, and mdb indicate metagabbro, metabasalt, and metadiabase, respectively.

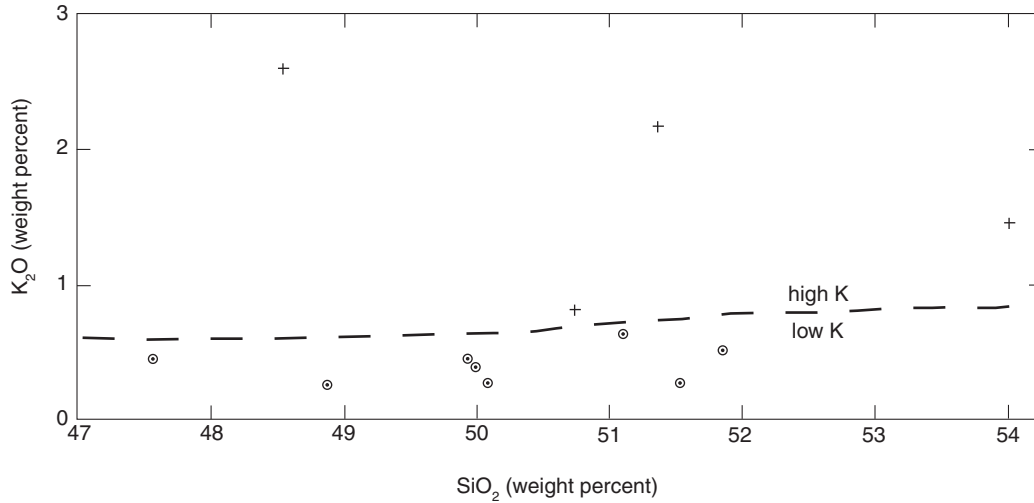


**Table 11.** Chemical analyses of high-K metamorphosed mafic volcanic rocks and closely associated hypabyssal rocks from the Glen Township Formation (core unit E). Rocks in this group contain more than 0.6 weight-percent K<sub>2</sub>O. Major-element oxides reported in weight percent; minor and trace elements in parts per million.

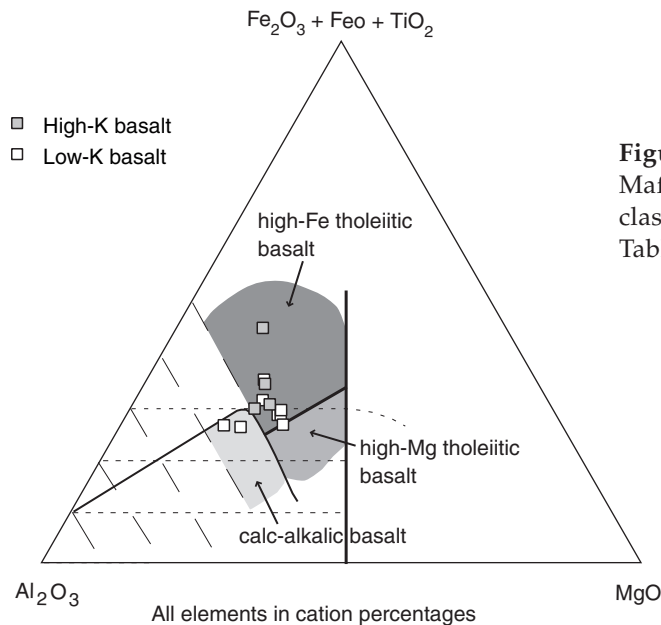
Code no	hbgr 29	hbgr 34	hbgr 35	hbgr 36	mean	std. dev
Subunit	E	E	E	E		
Sample	3623	4332	4411	4652		
Rock type	mb	mb-int	mb-int	mb-int	n = 4	
SiO <sub>2</sub>	45.87	52.83	49.04	47.33	48.77	3.00
TiO <sub>2</sub>	2.35	1.83	2.10	1.98	2.07	0.22
Al <sub>2</sub> O <sub>3</sub>	14.26	14.63	13.35	13.46	13.93	0.62
Fe <sub>2</sub> O <sub>3</sub>	22.41	12.02	13.77	11.92	15.03	4.99
FeO						
MnO	0.25	0.17	0.26	0.22	0.23	0.04
MgO	4.12	4.92	4.74	5.24	4.76	0.47
CaO	4.16	7.75	9.71	7.57	7.30	2.31
Na <sub>2</sub> O	0.68	3.08	3.90	3.40	2.77	1.43
K <sub>2</sub> O	2.54	1.43	0.77	1.98	1.68	0.76
P <sub>2</sub> O <sub>5</sub>	0.14	0.38	0.40	0.21	0.28	0.13
CO <sub>2</sub>						
C/tot						
S/tot						
H <sub>2</sub> O						
LOI	1.89	1.35	2.29	7.04	3.14	2.63
sum	98.72	100.36	100.33	100.36	99.94	
FeO <sup>t</sup>	20.17	10.82	12.39	10.73	13.53	
Mg# (atomic)	26.71	44.80	40.56	46.57	38.54	
Rb	80	28	18	42	42	27.18
Sr	272	626	322	202	356	186.93
Ba	1276	548	268	634	682	426.02
Sc	25	23	28	28	26	2.45
Nb						
Hf	7	3.7	3.9	3.5	5	1.66
Ta	2	2	1	<1	2	0.58
Zr	314	201	142	129	197	84.37
Y	38	41	28	25	33	7.70
Cr	54	24	39	39	39	12.25
Ni	45.0	18.0	22.0	23.0	27	12.19
Cu	3.0	25.0	9.0	7.0	11	9.66
Zn	49.0	96.0	114.0	36.0	74	37.21
V	206.0	226.0	274.0	265.0	243	32.16
Cs	2.3	<0.5	0.6	1.8	1.6	0.87
Th	10	5.1	4.1	3.1	5.6	3.06
La	39.9	40.9	30.2	20.2	32.80	9.69
Ce	78	74	68	48	67.00	13.32
Nd	34	34	35	23	31.50	5.69
Sm	6.3	6.8	6.5	5.2	6.20	0.70
Eu	2.1	2.3	1.9	1.4	1.93	0.39
Gd						
Tb	0.9	1.0	<0.5	1.0	0.97	0.06
Yb	3.4	2.7	2.5	2.2	2.70	0.51
Lu	0.53	0.36	0.36	0.3	0.39	0.10

Note: All analyzed samples consist dominantly of the mineral assemblage blue-green hornblende+plagioclase+biotite+Fe-Ti oxides+sphene+clinozoisite; chlorite, quartz, and calcite are present in variable small amounts.

Mb and mb-int indicate metabasalt and metabasalt/meta-andesite, respectively.



**Figure 18.**  $K_2O$ - $SiO_2$  variation diagram for mafic metaigneous rocks. The analyses break into high-K and low-K clusters at about 0.6 weight percent  $K_2O$ . Major-element data from Tables 10 and 11 were recalculated volatile-free and with total iron as FeO to obtain the plotted  $K_2O$  and  $SiO_2$  values.



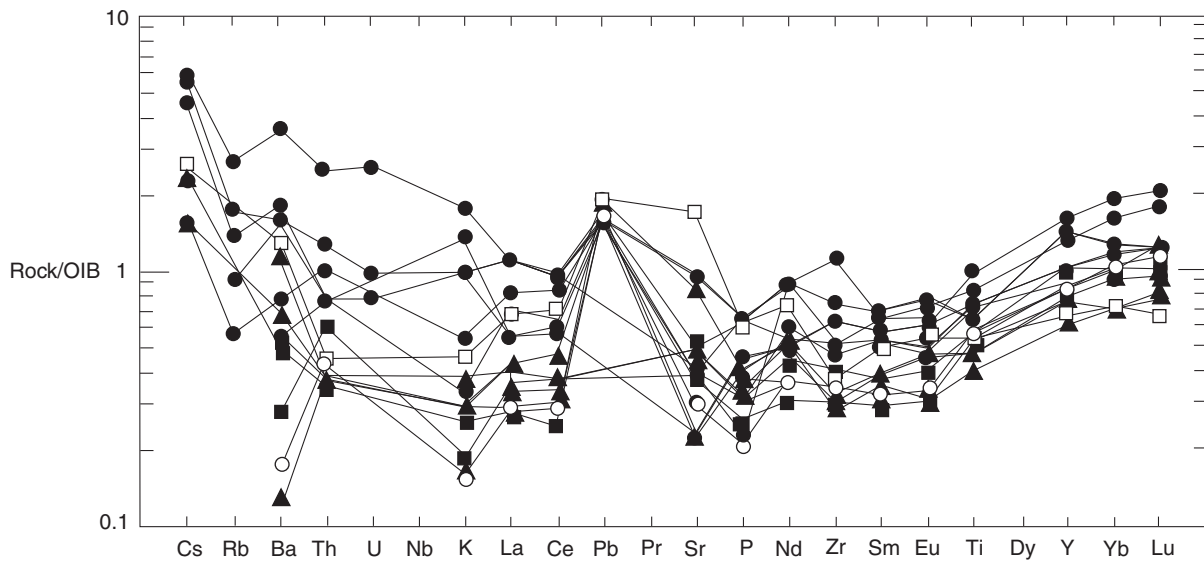
**Figure 19.** Mg—Fe + Ti—Al cation plot (Jensen, 1976). Mafic metaigneous rocks of the Kettle River formation classify mainly in the iron tholeiite field. Data are from Tables 10 and 11.

Penokean fold-and-thrust belt as developed in east-central Minnesota (Fig. 23; also Southwick and others, 2001).

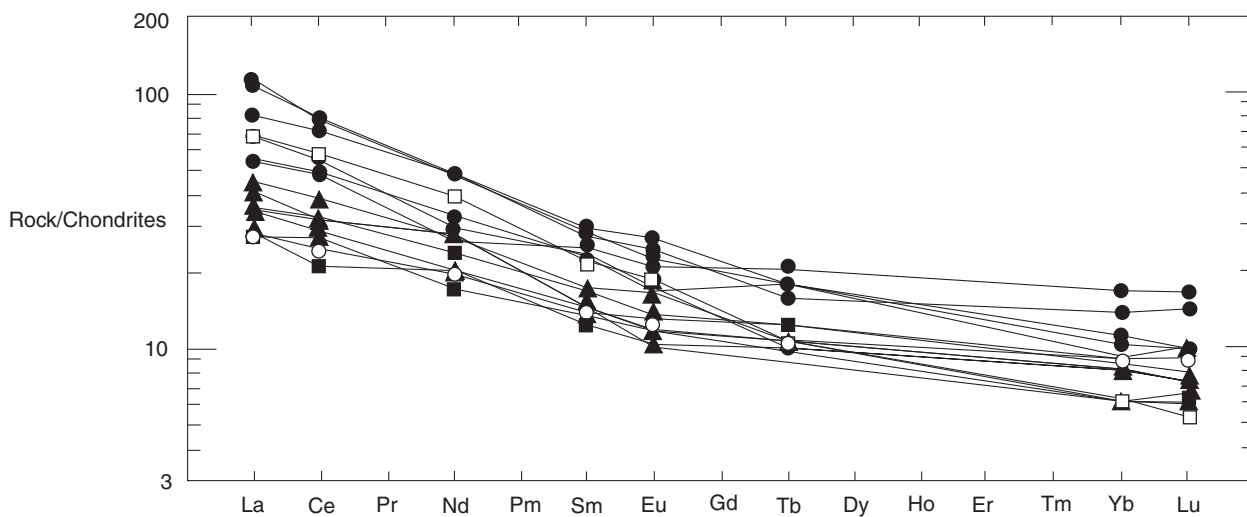
#### Miscellaneous veins, sheared rocks, and minor intrusions

Table 12 contains geochemical data for rocks in HB-1 that have experienced obvious alteration or

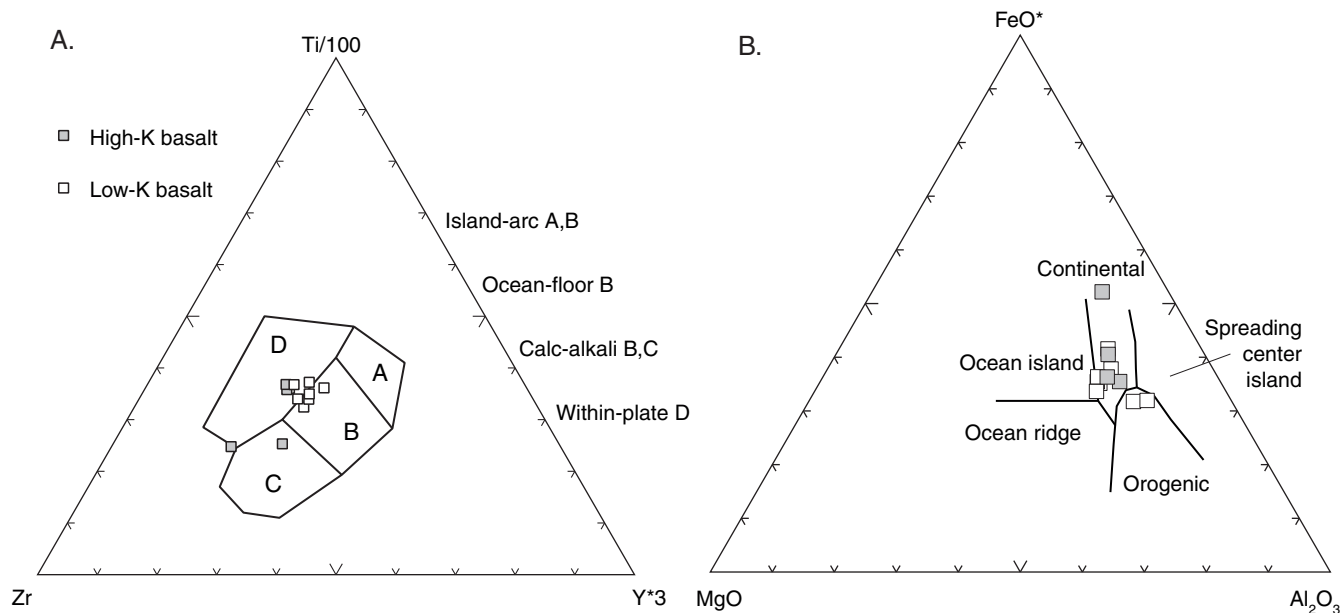
are otherwise not typical of the major rock units cut in the drilling. The rock types for which data are presented are described in footnotes to the table. The assorted veins, shear zones, and metasomatized rocks were sampled and analyzed to test for the presence of base metals, precious metals, and associated "pathfinder" elements. No anomalous concentrations were found.



**Figure 20.** Spider plot of minor and trace elements in 12 mafic metaigneous rocks normalized against ocean island basalt (OIB). OIB values are from Sun and McDonough (1989). Data are from Tables 10 and 11.



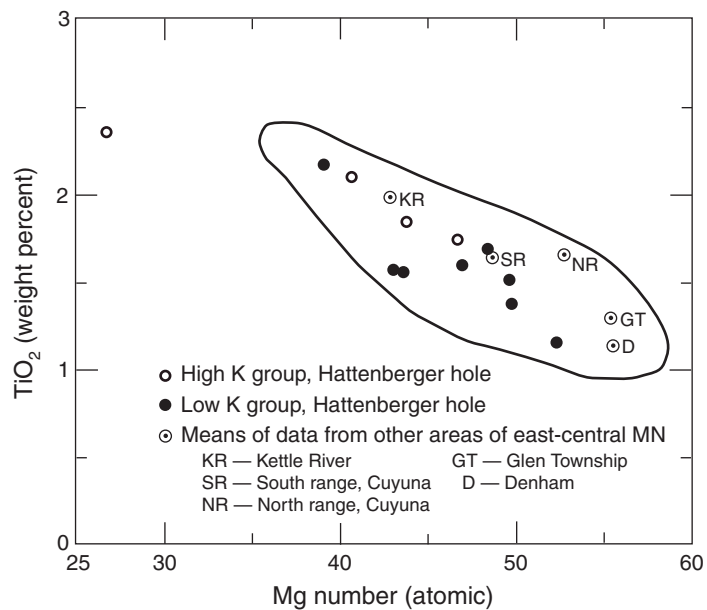
**Figure 21.** Rare earth element plot of data from 12 samples of metaigneous rocks normalized against chondrite. Chondrite values are from Taylor and McLennan (1985). Data are from Tables 10 and 11.



**Figure 22.** Discrimination diagrams for assigning putative tectonic environments of origin for mafic metaigneous rocks of the Kettle River formation and other stratigraphic levels in HB-1.

**A.** The Y—Ti—Zr diagram of Pearce and Cann (1973).

**B.** The AFM plot of Pearce and others (1977). Data are from Tables 10 and 11.



**Figure 23.** Scattergram plot of TiO<sub>2</sub> vs. Mg number for mafic metaigneous rocks of east-central Minnesota. Low-K and high-K analyses from HB-1 (Tables 10 and 11) fall within the field occupied by data from outcrop and drill-core samples from other areas. The field boundary and the average compositions of mafic rocks from other areas are based on data in Southwick and others (2001).



**Table 12.** Chemical analyses of altered, veined, or sheared rocks and rocks of uncertain or atypical protolith from throughout the Hattenberger core. Major-element oxides reported in weight percent; minor and trace elements in parts per million.

Code no	hbgr 4	hbgr 15	hbgr 22	hbgr 23	hbgr 24	hbgr 25	hbgr 40	hbgr 47	hbgr 50	hbgr 51	hbgr 52	hbgr 55
Subunit	A	D	D	D	D	D	F	F	G	G	H	H
Sample no	1793	2429	2666	2984	3010	3047	5115	5549	5831	6120	6812	7317
SiO <sub>2</sub>	85.40	39.12	23.33	41.03	51.52	47.21	56.33	55.25	33.05	50.84	18.04	71.60
TiO <sub>2</sub>	0.04	1.13	1.65	2.26	1.91	1.52	0.62	0.97	0.56	0.77	0.14	0.11
Al <sub>2</sub> O <sub>3</sub>	3.89	13.10	16.72	14.80	15.80	14.71	18.79	18.22	9.72	16.77	3.65	2.81
Fe <sub>2</sub> O <sub>3</sub>	4.12	10.72	42.47	15.55	10.25	12.30	11.76	10.97	5.34	5.35	46.18	6.40
FeO												
MnO	0.02	0.21	1.05	0.15	0.11	0.20	0.11	0.04	0.17	0.14	0.34	0.15
MgO	0.09	4.03	4.43	4.35	3.18	5.71	2.28	2.40	13.10	2.88	3.46	1.13
CaO	3.07	13.15	1.10	7.15	5.01	12.70	0.27	3.73	18.30	9.54	11.34	8.51
Na <sub>2</sub> O	1.52	3.78	0.09	2.30	3.80	1.01	2.25	5.24	0.07	6.33	0.08	0.23
K <sub>2</sub> O	0.06	0.32	0.39	4.16	2.52	0.67	5.67	2.47	4.80	0.84	0.47	1.25
P <sub>2</sub> O <sub>5</sub>	<0.01	0.21	<0.01	0.62	0.51	0.37	0.10	0.10	0.06	0.05	0.89	0.02
CO <sub>2</sub>		11.72									9.13	
C/tot		3.29									2.61	
S/tot		0.03									20.55	
H <sub>2</sub> O												
LOI	2.74	12.04	6.71	5.24	4.34	3.57	2.44	1.40	14.43	6.90	13.14	8.72
SUM	100.96	87.84	97.99	97.68	99.01	99.96	100.62	100.79	99.60	100.41	97.73	100.97
FeO <sup>†</sup>	3.71	9.65	38.22	14.00	9.23	11.07	10.58	9.87	4.81	4.82	41.56	5.76
Rb	11	<10	<10	61	62	<10	162	57	100	<10	33	22
Sr	165	732	83	537	576	1132	62	89	57	193	88	113
Ba	72	99	46	2538	1540	456	503	1458	947	258	36	278
Sc	0.6	24	24	29	26	29	14	20	8.4	111	5.7	2.4
Nb												
Hf	<0.5	1.2	5.5	4	3.7	2.2	2.8	4.8	3.3	6.1	0.6	<0.5
Ta	<1	1	2	2	<1	<1	<1	2	<1	<1	<1	<1
Zr	3	61	255	175	172	101	107	199	131	285	38	19
Y	<1	14	56	28	33	19	7	37	13	25	18	18
Cr	14	47	58	17	31	40	87	78	59	95	25	26
Ni	82.0	76.0	52.0	51.0	34.0	43.0	28.0	58.0	35.0	46.0	286.0	114.0
Cu	1057.0	102.0	111.0	85.0	40.0	162.0	4.0	2.0	8.0	9.0	170.0	115.0
Zn	21.0	59.0	121.0	171.0	139.0	89.0	87.0	28.0	137.0	46.0	44.0	52.0
V	3.0	213.0	228.0	317.0	309.0	224.0	85.0	44.0	34.0	55.0	23.0	16.0
Cs	<0.5	<0.5	2.4	1.6	1.8	1	9.3	1.5	4.4	2.1	1	0.8
Th	<0.5	1	9.3	3.5	3.7	1.8	11	10	8.2	11	1.1	1.1
La	0.5	9.3	39.5	52.3	51.8	24.9	27.6	101	28.5	11.1	7.1	4.8
Ce	<3	20	80	92	99	55	45	176	57	25	19	11
Nd	<5	9	36	48	56	28	18	74	25	15	7	<5
Sm	0.1	2.5	6.2	8.1	8.9	5	3	11	3.4	3.9	1.4	1.3
Eu		0.9	1.6	2.1	2.2	1.6	0.6	2.6	0.7	0.6	0.6	0.5
Gd												
Tb	<0.5	<0.5	1.2	1.0	0.9	0.6	<0.5	1.2	<0.5	0.9	<0.5	<0.5
Yb	<0.1	0.9	5.0	2.0	2.5	1.5	0.8	2.3	1.4	2.1	1.3	1.5
Lu	<0.05	0.17	0.76	0.35	0.37	0.2	0.14	0.37	0.2	0.35	0.21	0.24

1793: Chlorite-epidote-plagioclase schist with quartz-calcite-pyrite veins

2429: Sheared and carbonate-altered metabasaltic rock

2666: Garnet-chlorite-opaque phase segregation in chlorite schist

2984: Lamprophyre (?) approximately of latite composition

3010: Biotite-rich laminated schist, possibly sheared lamprophyre or latite tuff. Similar geochemically to 2984

3047: Sheared and mildly carbonate-altered metabasaltic rock

5115: Sulfide veinlet plus mineralogically zoned silicate wallrock

5549: Quartz-biotite-muscovite phyllonite or mylonite

5831: Calcite-biotite-epidote-quartz alteration zone in mafic rock

6120: Banded biotite-quartz-plagioclase-hornblende mylonite in mafic rock

6812: Calcite-biotite-quartz schist with pyrite veinlets

7317: Calcite-quartz vein with inclusions of biotite schist wallrock

# COMPOSITION OF THE WATER AND GAS PRODUCED FROM THE HATTENBERGER WELL

## Introduction

The Minnesota Geological Survey learned of the flammable nature of the gas in the Hattenberger well in fall of 1976, a few months before the general public learned of it from the reports on the Hattenberger bathroom explosion. Local visitors to the farm, among them State Senator Florian Chmielewski of Sturgeon Lake, were shown a clear blue flame that burned at the kitchen sink when Mr. Hattenberger ignited the colorless, odorless gas escaping from the water taps after gas pressure had built up in the pipes. On the urging of Senator Chmielewski, Minnesota Geological Survey staff under the supervision of Dr. Calvin Alexander (Department of Geology and Geophysics, University of Minnesota) collected samples of both gas and well water for analysis. Samples were taken on several visits over a span of several weeks.

## Geochemical attributes of the well water

Cation concentrations in a water sample taken from the 803-foot well in 1976 were analyzed by Union Carbide Corporation, Oak Ridge, Tennessee under the supervision of Todd R. Butz. Subsequently, Donald Siegl, then a graduate student at the University of Minnesota, independently determined anion concentrations in different samples of water from the 803-foot well and a nearby shallow well. Despite having been determined on different samples in different laboratories, the cation-anion results agree well in terms of charge balance, and the combined determinations reported in Table 13, column 1 therefore appear to be credible.

The analyzed Hattenberger well water differs considerably in metal content from that of average ground water in east-central Minnesota (Table 13, columns 2 and 3). It contains elevated calcium, magnesium, and sodium, as well as anomalously large amounts of boron, barium, lithium, copper, nickel, and zinc. Many other trace elements also are present in concentrations somewhat higher than average for typical ground water in east-central Minnesota. Interestingly, arsenic and uranium concentrations are lower than average, implying that conditions in the ground-water system tapped by the Hattenberger well were somewhat reducing.

Isotopic data from well-water and surface-water samples collected on and near the Hattenberger property in 1976 (Table 14) are reasonably consistent with the isotopic patterns observed in gas-water

mixtures collected from glacial-drift wells elsewhere in the central United States. These isotopic data are detailed in the "Discussion of the water and gas compositions" section below.

## Geochemical attributes of the dissolved gas

Analytical results from the gas samples collected in 1976 are summarized in Table 15. Although the results are only semi-quantitative at best, they show that approximately 25 percent of the gas volume analyzed was methane. Almost no ethane or other higher-number hydrocarbon ( $\text{CH}_4/\text{C}_2\text{H}_6 = 1488$ ) was detected in the analyzed sample, precluding the possibility that the gas originated from a leaking natural gas pipeline or storage site.

Between May and July, 1978, the Rocky Mountain Energy Company conducted a survey of dissolved helium and light hydrocarbon levels in ground water and surface water in Carlton County as part of a regional search for unconformity-related uranium deposits (Morey and Lively, 1980; Morey, 1981). Some 312 samples were collected and analyzed. Table 16 shows that two water samples from the Hattenberger farm—one from the 803-foot well and the other from a nearby shallow well—contained two to three orders of magnitude more helium and methane than the average of the sample population.

## Discussion of the water and gas compositions

Analyses by the Minnesota Department of Health of a water sample taken from the original shallow Hattenberger well in 1971 (or earlier) reported 5.4 parts per million of chloride (Minnesota Geological Survey, unpub. data), whereas water from the 803-foot well contained 2,065 parts per million chloride, a value 382 times more salty (Table 13, column 1). The archival 1971 analysis of the shallow well water also reports about half the calcium, magnesium, and sodium values reported in Table 10 for water from the 803-foot well. Nonetheless, both waters are a sodium-magnesium-calcium chloride brine. The well water from the 803-foot well contains total dissolved solids of 0.11 millequivalents/liter and thus is saltier than fresh surface water, but only 0.1 to 0.2 times as salty as typical saline formation waters in supracratonic basins of Phanerozoic age (Clayton and others, 1966), or the brines encountered in deep fractures in Precambrian rocks at several places in the Canadian Shield (Frape and others, 1984; Frape and Fritz, 1987; Bottomley and others, 1999). The water in the 803-foot well has the geochemical attributes of a mixture of fresh and saline "formation" water.

**Table 13.** Chemical analyses of ground water from the Hattenberger water well (depth 803 feet) and from wells in the surrounding vicinity of east-central Minnesota. The regional data are summarized as average compositions and associated standard deviations. No data were reported for either potassium or bicarbonate ion in the Hattenberger water analysis. Values reported in parts per billion (ppb) unless otherwise noted.

	1	2 (mean)	2 (std dev)	3 (mean)	3 (std dev)
As	<0.5	1.6	2.5	2.25	2.8
Se	<0.2	0.3	1.3	0.3	1.4
Ag	7	3	1	3	1
Al	36	26	2	32	2
B	835	28	2	35	2
Ba	313	55	2	61	2
Be	<1	2	2	2	2
Ca (ppm)	153.3	50.3	1.7	43.8	1.7
Co	7	3	2	3	2
Cr	<10	6	1	6	2
Cu	107	11	3	10	3
Fe	118	353	8	24	6
K (ppm)		1.6	2.2	9	1.4
Li	112	7	2	6	2
Mg (ppm)	140.4	19	1.9	17.5	2
Mn	143	62	6	53	6
Mo	23	7	2	7	2
Na (ppm)	845	7	1.9	7	2.1
Nb	17				
Ni	45	6	1	7	2
P	<80	93	2	100	2
Sc	1	1	2	1	2
Ti	7	3	2	3	2
U	<0.2	0.51	3.15	0.68	3.6
V	36	7	2	7	2
Y	5	1	2	1	2
Zn	316	130	4	104	4
Cl (ppm)	2065.5	30	2	23	2
SO <sub>4</sub> (ppm)	<5				
HCO <sub>3</sub> (ppm)		100.6	1.7	99.7	1.8
No. of anal.	1	101		223	

1. Ground water from Hattenberger water well, depth 803 feet.
2. Ground water from wells finished in ground-moraine deposits of the Superior lobe, east-central Minnesota (Morey and Lively, 1980, p. 61).
3. Ground water from wells finished in slaty metasedimentary rocks, east-central Minnesota (Morey and Lively, 1980, p. 74).

Analyses performed by Union Carbide Corporation, except for anion determinations, column 1



**Table 14.** Isotopic analyses of gas and water from the 803-foot Hattenberger well and Silver Creek. Analyses by Geochron Laboratories Division, Krueger Enterprises, Incorporated.

Sample	$\delta^{13}\text{C}$ , permil PDB	$\delta^{18}\text{O}$ , permil SMOW	$\delta \text{D}$ , permil SMOW
Gas, D <sup>(1)</sup>	-65.3		
Gas, E <sup>(2)</sup>	-59.7		
Water, Silver Creek <sup>(3)</sup>		-10.0 <sup>(4)</sup> -9.9 <sup>(4)</sup>	-73 ± 2
Water, Hattenberger well		-12.1	-79 ± 2

- (1) Sample D, Hattenberger well; see Table 11.  
(2) Sample E, Hattenberger well; see Table 11.  
(3) Sample from nearby Silver Creek collected in June, 1978.  
(4) Duplicate preparations and analyses.

Permil PDB: parts per thousand relative to Peedee Formation belemnite standard  
Permil SMOW: parts per thousand relative to standard mean ocean water

**Table 15.** Analyses of the gas phase emanating from the Hattenberger water well (all data in percent).

Sample	A(1)	A(2)	A(3)	B(2)	C(2)	D(2)	E(2)	Natural gas	Air
Methane	25.0	35.0	21.1	62.0	9.8	57.7	2.7	88.16	<0.0001
Ethane	<0.02	<0.0001	<0.001	<0.0001	<0.0001	<0.0001	<0.0001	4.23	<0.0001
Propane	—	<0.001	n.m.	<0.0001	<0.0001	<0.0001	<0.0001	0.70	<0.001
N <sub>2</sub>	56.5	n.m.	59.9	n.m.	n.m.	n.m.	n.m.	5.83	78.08
O <sub>2</sub>	15.4	n.m.	17.6	n.m.	n.m.	n.m.	n.m.	0.02	20.95
CO <sub>2</sub>	<0.7	n.m.	0.5	n.m.	n.m.	n.m.	n.m.	0.7	0.033
Ar	1.9	n.m.	0.7	n.m.	n.m.	n.m.	n.m.	—	0.934
He	n.m.	n.m.	0.5	n.m.	n.m.	n.m.	n.m.	0.12	0.005

n.m. = not measured

#### Sampling protocols

- A, B samples collected in glass bulbs from kitchen faucet.  
C samples collected in glass bottle with rubber top from kitchen faucet.  
D, E samples collected in aluminum tubes; D from pressure tank in basement; E directly from well casing in front yard.

#### Analytical method

- (1) Mass spectrographic analysis, Department of Chemistry, University of Minnesota.  
(2) Gas chromatographic analyses, Minnegasco Research Center.  
(3) Mass spectrographic analysis, Department of Geology and Geophysics, University of Minnesota.

**Table 16.** Abundance of helium and light hydrocarbons dissolved in water from the Hattenberger well. Analyses by the Geochemical Laboratories of Chemical Projects Limited, Toronto, Ontario.

Sample depth (feet)	Helium <sup>(1)</sup>	Methane <sup>(2)</sup>	Ethane	Ethene	Propane
803	15,412.7	13,207	0.0	0.0	0.0
19	14,542.1	722,119	96.0	0.0	0.0
Background	9.4	70 - 104	0.0	0.0	0.0

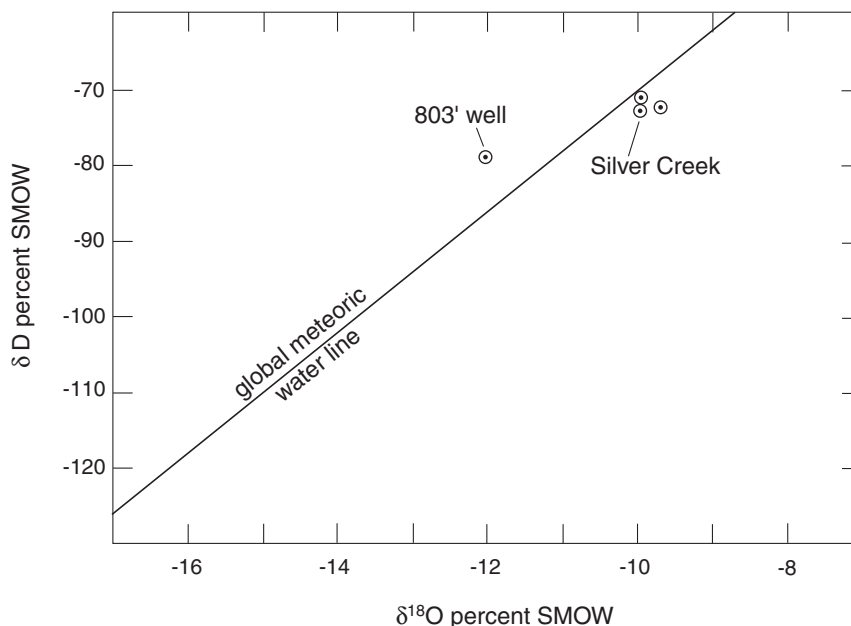
(1) Calculated concentration of helium dissolved in the sample water. Expressed as cm<sup>3</sup> He at NTP/cm<sup>3</sup> H<sub>2</sub>O x 108.

(2) Concentrations of hydrocarbons dissolved in the sample water. Expressed as cm<sup>3</sup> gas at NTP/cm<sup>3</sup> H<sub>2</sub>O x 108. Not necessarily indicative of the in situ levels if bacteriological or other mechanisms which generate light hydrocarbons continued to operate after the samples have been sealed in the container.

Water samples from the 803-foot well and from Silver Creek, a small stream near the Hattenberger property (Table 14), contain proportions of oxygen-18 (reported as  $\delta^{18}\text{O}$ ) and deuterium (reported as  $\delta\text{D}$ ) that fall near the "meteoric water line" in a plot of these isotopes at values appropriate for recent meteoric water for the northeastern Minnesota region (Fig. 24). For example, water from Lake Superior has a  $\delta\text{D}$  value of approximately -75. Furthermore, the isotopic compositions of both samples plot well away from those obtained from saline formation waters in several Phanerozoic basins (Clayton and others, 1966) or brines in fractured rocks of the Canadian Shield (Bottomley and others, 2002). Isotopically,

therefore, the Hattenberger well water appears to be of meteoric origin.

The origin of the methane in the Hattenberger well is problematic. Methane is encountered with some frequency in deep mines in the Canadian Shield and other cratonic areas, as at the Goldcorp-Red Lake Mine in northwestern Ontario (Goldcorp staff, unpub. data, 2002). The origin of the gas in deeply fractured crystalline rocks has been much debated in the literature, without clear resolution, and the occurrence of methane in the deep well in Carlton County is yet another example of a puzzling phenomenon widely observed in stable cratonic areas.



**Figure 24.** Stable isotope abundances in water from the 803-foot Hattenberger well and Silver Creek. The data for both fall very close to the global meteoric water line.

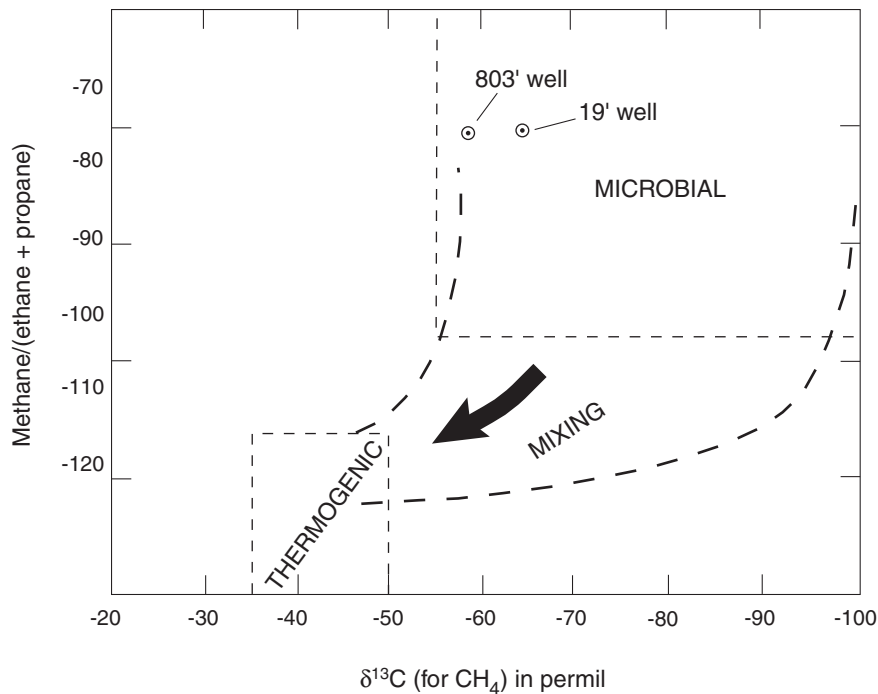
Natural processes that form methane are divided into three types: biogenic, in which gas is expelled from microorganisms during the digestion of organic compounds; thermogenic, in which gas is formed as organic matter decomposes under elevated heat and pressure; and abiogenic, in which gas is formed by reactions of deep crustal gases with minerals or by seepage of hydrocarbon- and carbon-rich primordial gases from the earth's interior (Howell and others, 1993). Much of the methane found in large natural gas accumulations is interpreted as either biogenic or thermogenic in origin.

Biogenetically produced gas can be distinguished from thermogenetically produced gas by the use of stable isotopic values and ratios of methane to higher-number hydrocarbons. Biogenetically produced methane is enriched in carbon 12, depleted in deuterium (reported as  $\delta D$ ), and contains only trace amounts of higher-number hydrocarbons (for example methane/ethane + propane >1,000). In contrast, thermogenetically produced methane is depleted in carbon 12 and has an abundance of higher-number hydrocarbons (for example methane/ethane

+ propane <100). By those criteria, methane from the Hattenberger well is biogenic in origin (Fig. 25).

Biogenic methane forms where methane-producing microorganisms operate on decomposed organic matter in near-surface environments marked by a near-total lack of oxygen and where temperatures do not exceed 97° C (207° F). Biogenic methane may form by two dominant metabolic processes. In recent environments, one process simply involves the reduction of carbon dioxide. Another set of processes involves first the fermentation of acetate, which leads to carbon dioxide, which is ultimately reduced to methane. Because the methane generated in the subsurface is less dense than the rocks in which it is produced, it diffuses slowly upward through small, interconnected pore spaces and fractures. Eventually, it can reach the earth's surface and dissipate into the atmosphere. In places, however, diffusion is impeded by impermeable rock layers, and gas will be trapped in structures where it will accumulate.

The presence of abundant helium in the Hattenberger well lacks a ready explanation. Helium is generated in rocks by the radioactive decay of



**Figure 25.** Fields of hydrocarbon ratio vs. carbon isotope ratio ( $\delta^{13}C$ ) for methane-dominated natural gas of microbial, thermogenic, and mixed origin. The gas composition from the Hattenberger well falls in the microbial field. Diagram modified from Bernard and others (1976).

uranium and thorium, but typically at concentrations too low to create a fracture porosity or hold it open. Helium in general is strongly associated with hydrocarbon deposits, but there is no known chemical or biological cause for that association because the helium is chemically inert. However, the association can be explained by the fact that during outgassing, the more abundant hydrocarbons serve as a carrier that accumulates and moves helium from one place to another. Therefore, the amount of helium at any one place can be related to variations in the concentration of the parent radioactive elements and to variations in the length of the pathways along which the helium has been swept by the flow of other gases. Because the elemental abundances of thorium and uranium in the Glen Township–Moose Lake structural panel are not atypically high (Morey and Lively, 1980), the helium in the Hattenberger well must have been swept from a large volume of rock or moved over very long pathways.

An unoriginal hypothesis to account for the chemical and isotopic attributes of the Hattenberger water–gas mixture is as follows. Recent meteoric waters circulate over a relatively large area and possibly to a relatively great depth through a three-dimensional web of open fractures in Paleoproterozoic (for example Penokean) and Mesoproterozoic (for example Keweenawan) bedrock. The meteoric water either mixes with concentrated saline formation waters, or more probably, reacts with the country rocks to produce a dilute saline solution. If that water passes into a strictly anaerobic environment that lacks even a few parts per million of oxygen, methane could form via the metabolic reaction  $\text{CO}_2 + 4\text{H}_2 = \text{CH}_4 + 2\text{H}_2\text{O}$  mediated by methane-producing microorganisms. The presence of methane at several apparently isolated stratigraphic levels in the 803-foot well and the deep core hole implies that the water–gas mixture evolved under conditions not necessarily related to any specific rocks observed in the Hattenberger well. Further, the presence of elevated helium values in the 803-foot well implies a gas-generating scenario that involved a wide geographic area.

If interactions of meteoric waters with Keweenawan sedimentary strata had anything to do with generating the saline water of the Hattenberger well, which seems plausible on the basis of observations elsewhere (Tipping and Allen, 1997) but remains unproven in the Hattenberger case, ground waters geochemically similar to the Hattenberger composition might be expected elsewhere near the sub-Keweenawan unconformity in east-central Minnesota (Fig. 1). These waters might also contain dissolved

methane-helium mixtures if they circulated through strongly reducing environments in sub-Keweenawan rocks. No such corroborative occurrences have been reported, perhaps because very few wells have been drilled into fractured, graphitic bedrock near the sub-Keweenawan unconformity. As a rule, potable water can be found at shallow levels throughout most of east-central Minnesota without drilling deeply into bedrock. Generally, therefore, there is little incentive to invade hydrogeologically inhospitable but scientifically interesting deeper environments in the search for water, and as a consequence new data that could illuminate the anomalous findings at the Hattenberger site have been slow to emerge.

## CONCLUSIONS

Our conclusions are framed as responses to the geologic questions posed in the introductory section of this report.

1. *What does the core reveal about the stratigraphic, structural, and metamorphic evolution of the Moose Lake–Glen Township panel, or more broadly, of the Minnesota segment of the Penokean orogen?*

The Hattenberger core is interpreted to contain long, vertical intercepts of the Denham Formation (lower part of the core; units H and F, between depth 4,780 feet and the end of drilling at depth 7,440 feet), and the Glen Township Formation (middle part of the core; units E, D, C, and B, between depths 4,780 and 1,809 feet). The metaigneous rocks of unit A, between depth 1,809 and the top of coring at depth 803 feet, are defined in this report as the Kettle River formation (informal name; definition subject to refinement).

The Denham Formation at the Hattenberger locality has a minimum apparent thickness of about 2,160 feet (the drilled thickness of core units H and F uncorrected for dip). The base of the Denham Formation was not reached in the drilling. The Glen Township Formation has an apparent thickness of 2,971 feet, the drilled thickness of the core units E, D, C, and B uncorrected for dip. The Kettle River formation is at least 1,000 feet thick.

This succession of stratified rocks, apparently without major tectonic inversion or repetition, records depositional conditions that changed with time from a continental-shelf, marginal marine setting (Denham Formation) to a deeper water, rift-basin setting (Glen Township Formation) in which magmatic activity became increasingly vigorous (the Kettle River). The stratigraphic succession and the geochemical attributes of the metavolcanic rocks both point to a



depositional scenario dominated by tectonic extension. Whether this was a full-scale continental stretching antecedent to breakup (Schulz and others, 1993) or some smaller-scale episode of extension, as within back-arc or intra-arc settings (Southwick and others, 2001), is debatable; however, there is little doubt that the tectonic environment during the depositional stage was one of extension.

The deformational structures and fabrics displayed in the rocks cut by the Hattenberger core clearly indicate tectonic shortening, flattening, and bulk shear. Micro- and mesoscale folds in metasedimentary rocks involve primary bedding and a first schistosity ( $S_1$ ) that is parallel or nearly parallel to bedding. These folds tend toward overturned or recumbent geometry, and in rheologically weak rocks are commonly flattened and stretched into rootless forms. The early folds are transected and refolded by a strong crenulation cleavage ( $S_2$ ) that crosses bedding and  $S_1$  at angles ranging from orthogonal to nearly parallel. In portions of the core,  $S_2$  is a continuous schistosity rather than a domainal structure. The crenulation cleavage is best developed in rheologically weak rock types, and tends to refract across layers of differing competency. Altogether, the sequence of fold structures and associated fabrics is consistent with the "nappe" geometry first described in east-central Minnesota by Holst (1984). This type of geometry implies a deformational regime in which subhorizontal shearing and subvertical flattening are dominant; it does not necessarily indicate that large-scale stratigraphic inversion (such as the production of fold nappes) actually occurred. Indeed, the Hattenberger core section is fundamentally upright.

The rheologically strong rock units in the core, mainly the thick metaigneous layers, seemingly acted as nearly undeformable plates during tectonism. Their deformation is confined to relatively narrow shear zones at unit contacts and at spaced interior locations. The massive layers appear to have moved differentially and transmitted bulk shear to interbedded layers of weaker rock. The weak layers, principally thin-bedded graphitic schists and associated metapelitic rocks, responded by developing small and mesoscale folds as well as cleavages on various orientations, approximately mimicking the development of secondary cleavages within ductile shear zones during progressive simple shear (Platt, 1984). This general situation appears to have pertained particularly to unit B, a relatively thin, weak layer sandwiched between massive metavolcanic layers in the transition zone between the Glen Township Formation and Kettle River formation.

Altogether, the deformational style exhibited by both the strong and weak rock units is consistent with a tectonic regime dominated by subhorizontal shear and subvertical flattening—the fold-and-thrust belt environment.

The observed timing relationships between fabric development and the growth of metamorphic minerals are different in different parts of the core and are not easily incorporated in a general deformational model for the entire drilled section. Whether this means that tectonic stacking has brought together panels of rock that followed slightly different pressure-temperature-time paths in their metamorphic evolution, or that the metamorphic-deformational environment within the deforming rock volume sampled by coring was heterogeneous in space and time on the 1 to 100 meter scale, is an interesting question for future investigation. Tobisch and Paterson (1988) provided a useful conceptual framework in which a future structural analysis of the Hattenberger core might be conducted. In deformed belts of diverse ages, including the Penokean, the deforming rock masses represented a broad range of material properties and the main stage of deformation was progressive and continuous in space and time rather than punctuated. In that situation, Tobisch and Paterson suggested, the common practice of correlating structural "events" from place to place, even over short distances, may lead to simplistic and erroneous conclusions. Detailed structural analysis of relationships preserved in the Hattenberger core could contribute valuable insights on the structural and metamorphic evolution of the Penokean orogen in east-central Minnesota.

*2. What are the implications, if any, of the core-hole findings for mineral exploration strategies in east-central Minnesota?*

There are no direct indications of economic minerals or mineralizing systems in the core. Nevertheless, the rock types, rock sequences, and structures are similar to those present in the vicinity of other highly productive mining camps, such as the Homestake district of western South Dakota (Kath, 1990; Caddey and others, 1991), the Mount Isa district in Queensland (Perkins, 1998; Painter and others, 1999), and the Broken Hill district of New South Wales and South Australia (Ashley and others, 1998, and references therein). The economic mineralization in these deposits is hosted by highly deformed iron-formation, calc-silicate rock, and interstratified volcanic rocks, which suggests that the geologic environment of east-central Minnesota is potentially favorable for hosting similar deposit types.

In east-central Minnesota, the "missing link" for economic mineralization of the general types represented by the mining areas mentioned above is a hydrothermal system capable of depositing and distributing metals within the favorable host environment. However, the mineralogical evidence of hydrothermal activity in the Cuyuna mining district (McSwiggen and others, 1994; Melcher and others, 1996) and the presence of barren massive sulfide deposits in the Glen Township area (Han, 1968) indicate that hydrothermal systems of poorly constrained scale and type did operate in the Penokean fold-and-thrust terrane. Thus, in our opinion, the poorly exposed area from the Hattenberger drill site westward to the North range of the Cuyuna district (Fig. 1) has potential for harboring undiscovered hydrothermal regimes and a variety of ore-deposit types. The area remains significantly under-explored.

3. *What is the origin of the emanating gas? Are rock–fluid interactions involved, and if so, to what extent?*

Our tentative conclusions on this point have been presented above in the "Discussion of the water and gas compositions" section, and will not be repeated here in full. In brief, the data available are consistent with an origin for the water–gas mixture that involves deep and areally broad circulation of meteoric waters through fractures in Proterozoic bedrock; increasing salinity of the meteoric water through mixing with saline formation water or reaction with host rocks; movement of the saline water into local anaerobic environments, perhaps within graphitic units of bedrock; and the generation of methane in those environments by the metabolic activity of anaerobic microorganisms.

It is important to recognize that these conclusions concerning the genesis of fluids are based on data acquired before core hole HB-1 was drilled. They would be substantiated (or refuted and revised) by modern analytical work that involves the collection and detailed characterization of fluid samples from different stratigraphic levels in the well bore, and concomitant detailed characterization of the rock composition and structural condition in core intervals where gas flow is noted. In that regard, the depth intervals 2,400 to 2,500 and 2,600 to 2,700 feet, both noted by the core driller as horizons where gas emanations were particularly common (Appendix Fig. 1), would be promising places for further research. These zones are within core unit D of the Glen Township Formation, in a sequence of very graphitic, sulfidic iron-formation and graphitic schist.

## REFERENCES

- Ashley, P.M., Lottermoser, B.G., and Westaway, J.M., 1998, Iron-formations and epigenetic ironstones in the Palaeoproterozoic Willyama Supergroup, Olary Domain, South Australia: *Mineralogy and Petrology*, v. 64, p. 187-218.
- Bernard, B.B., Brooks, J.M., and Sackett, W.M., 1976, Natural gas seepage in the Gulf of Mexico: *Earth and Planetary Science Letters*, v. 31, no. 1, p. 45-54.
- Boerboom, T.J., and Jirsa, M.A., 2001, Stratigraphy of the Paleoproterozoic Denham Formation—A continental margin assemblage of basalt, arkose, and dolomite [abs.]: Institute on Lake Superior Geology, 47th Annual Meeting, Madison, Wis., Proceedings, v. 47, Program and Abstracts, pt. 1, p. 6-7.
- Boerboom, T.J., Southwick, D.L., and Severson, M.J., 1999a, Bedrock geology of the Aitkin 30 x 60 minute quadrangle, east-central Minnesota: Minnesota Geological Survey Miscellaneous Map M-99, scale 1:100,000.
- 1999b, Bedrock geology of the Mille Lacs Lake 30 x 60 minute quadrangle, east-central Minnesota: Minnesota Geological Survey Miscellaneous Map M-100, scale 1:100,000.
- Bottomley, D.J., Katz, A., Chan, L.H., Starinsky, A., Douglas, M., Clark, I.D., and Raven, K.G., 1999, The origin and evolution of Canadian Shield brines: Evaporation or freezing of seawater? New lithium isotope and geochemical evidence from the Slave craton: *Chemical Geology*, v. 155, no. 7, p. 295-320.
- Bottomley, D.J., Renaud, R., Kotzer, T., and Clark, I.D., 2002, Iodine-129 constraints on residence times of deep marine brines in the Canadian Shield: *Geology*, v. 30, p. 587-590.
- Caddey, S.W., Bachman, R.L., Campbell, T.J., Reid, R.R., and Otto, R.P., 1991, The Homestake gold mine, an early Proterozoic iron-formation-hosted gold deposit, Lawrence County, South Dakota: U.S. Geological Survey Bulletin 1857-J, p. J1-J67.
- Cameron, E.M., and Garrels, R.M., 1980, Geochemical compositions of some Precambrian shales from the Canadian Shield: *Chemical Geology*, v. 28, p. 181-197.
- Clayton, R.N., Friedman, I., Graf, D.L., Mayeda, T.K., Meents, W.F., and Shimp, N.F., 1966, The origin of saline formation waters—Part 1, isotopic composition: *Journal of Geophysical Research*, v. 71, no. 16, p. 3869-3882.

- Deer, W.A., Howie, R.A., and Zussman, J., 1992, An introduction to the rock-forming minerals (2d ed.): New York, Wiley, 696 p.
- Frape, S.K., and Fritz, P., 1987, Geochemical trends for groundwaters from the Canadian Shield, *in* Fritz, P., and Frape, S.K., eds., Saline water and gases in crystalline rocks: Geological Association of Canada Special Paper 33, p. 211-223.
- Frape, S.K., Fritz, P., and McNutt, R.H., 1984, The role of water-rock interactions in the chemical evolution of groundwaters from the Canadian Shield: *Geochimica et Cosmochimica Acta*, v. 48, p. 1617-1627.
- Gromet, L.P., Dymek, R.F., Haskin, L.A., and Korotev, R.L., 1984, The "North American shale composite": Its compilation, major and trace element characteristics: *Geochimica et Cosmochimica Acta*, v. 48, no. 12, p. 2469-2482.
- Grunsky, E.C., Easton, R.M., Thurston, P.C., and Jensen, L.S., 1992, Characterization and statistical classification of Archean volcanic rocks of the Superior Province using major-element geochemistry, *in* Thurston, P.C., Williams, H.R., Sutcliffe, R.H., and Stott, G.M., eds., *Geology of Ontario: Ontario Geological Survey Special Volume 4*, pt. 2, p. 1397-1438.
- Han, T.M., 1968, Ore mineral relations in the Cuyuna sulfide deposit, Minnesota: *Mineralum Deposita*, v. 3, p. 109-134.
- Holst, T.B., 1984, Evidence for nappe development during the early Proterozoic Penokean orogeny, Minnesota: *Geology*, v. 12, p. 135-138.
- Howell, D.G., Wiese, K., Fanelli, M., Zink, L.L., and Cole, F., eds., 1993, The future of energy gases: U.S. Geological Survey Professional Paper 1570, 890 p.
- James, H.L., 1992, Precambrian iron-formations: Nature, origin, and mineralogic evolution from sedimentation to metamorphism, *in* Wolf, K.H., and Chilingarian, G.V., eds., *Diagenesis III: Amsterdam, Elsevier, Developments in sedimentology*, v. 47, p. 543-589.
- Jensen, L.A., 1976, A new cation plot for classifying subalkalic volcanic rocks: Ontario Division of Mines Miscellaneous Paper 66, 22 p.
- Jolly, W.T., 1980, Development and degradation of Archean lavas, Abitibi area, Canada, in light of major element geochemistry: *Journal of Petrology*, v. 21, no. 2, p. 323-363.
- Kath, R.L., 1990, Mineralogy and petrology of the Homestake Iron Formation and adjacent pelitic rocks, Lead, South Dakota: Conditions and assemblages of metamorphism, P-T paths, fluid evolution, and gold mineralization: Rapid City, S. Dak., South Dakota School of Mines and Technology, Ph.D. dissertation, 228 p.
- Lottermoser, B.G., and Ashley, P.M., 1996, Geochemistry and exploration significance of ironstones and barite-rich rocks in the Proterozoic Willyama Supergroup, Olary Block, South Australia: *Journal of Geochemical Exploration*, v. 57, p. 57-73.
- Marchig, V., Gundlach, H., Moller, P., and Schley, F., 1982, Some geochemical indicators for discrimination between diagenetic and hydrothermal metalliferous sediments: *Marine Geology*, v. 50, p. 241-256.
- McSwiggen, P.L., 1987, Geology and geophysics of the Denham-Mahtowa area, east-central Minnesota: Minnesota Geological Survey Miscellaneous Map M-63, scale 1:48,000.
- McSwiggen, P.L., and Morey, G.B., 1989, Geology and geochemical attributes of graphitic rocks in east-central Minnesota, *in* McSwiggen, P.L., and Morey, G.B., Graphite in early Proterozoic rocks of east-central Minnesota: Minnesota Geological Survey Information Circular 28, p. 1-57.
- McSwiggen, P.L., Morey, G.B., and Cleland, J.M., 1994, Occurrence and genetic implications of hyalophane in manganese-rich iron-formation, Cuyuna Iron Range, Minnesota, U.S.A.: *Mineralogical Magazine*, v. 58, p. 387-399.
- Melcher, F., Morey, G.B., McSwiggen, P.L., Cleland, J.M., and Brink, S.E., 1996, Hydrothermal systems in manganese-rich iron-formation of the Cuyuna North range, Minnesota: Geochemical and mineralogical study of the Gloria drill core: Minnesota Geological Survey Report of Investigations 46, 59 p.
- Morey, G.B., 1978, Lower and Middle Precambrian stratigraphic nomenclature for east-central Minnesota: Minnesota Geological Survey Report of Investigations 21, 52 p.
- 1981, Geologic terranes of Minnesota and their uranium potential: Minnesota Geological Survey Information Circular 19, 40 p.
- 1992, Chemical composition of the eastern Biwabik Iron Formation (Early Proterozoic), Mesabi range, eastern Minnesota: *Economic Geology*, v. 87, p. 1649-1658.
- Morey, G.B., and Lively, R.S., 1980, Detailed geochemical survey for east-central Minnesota: Geology and geochemistry of selected uranium targets: Grand Junction, Colo., U.S. Department of Energy Open-File Report GJBX-60 (80), 178 P.

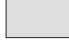




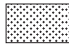

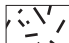
- Painter, M.G.M., Golding, S.D., Hannan, K.W., and Neudert, M.K., 1999, Sedimentologic, petrographic, and sulfur isotope constraints on fine-grained pyrite formation at Mount Isa Mine and environs, northwest Queensland, Australia: *Economic Geology*, v. 94, no. 6, p. 883-912.
- Pearce, J.A., and Cann, J.R., 1973, Tectonic setting of basic volcanic rocks determined using trace element analyses: *Earth and Planetary Science Letters*, v. 19, p. 290-300.
- Pearce, T.H., Gorman, B.E., and Birkett, T.C., 1977, The relationship between major element chemistry and tectonic environment of basic and intermediate volcanic rocks: *Earth and Planetary Science Letters*, v. 36, no. 1, p. 121-132.
- Perkins, W.G., 1998, Timing of formation of Proterozoic stratiform fine-grained pyrite: Post-diagenetic cleavage replacement at Mount Isa?: *Economic Geology*, v. 93, no. 8, p. 1153-1164.
- Platt, J.P., 1984, Secondary cleavages in ductile shear zones: *Journal of Structural Geology*, v. 6, no. 4, p. 439-442.
- Schulz, K.J., Sims, P.K., and Morey, G.B., 1993, Tectonic synthesis, *in* Sims, P.K., ed., *The Lake Superior region and Trans-Hudson orogen*, chapter 2 of Reed, J.C., Jr., Bickford, M.E., Houston, R.S., Link, P.K., Rankin, D.W., Sims, P.K., and VanSchmus, W.R., eds., *Precambrian: Conterminous U.S.: Boulder, Colo., Geological Society of America, The geology of North America*, v. C-2, p. 60-64.
- Southwick, D.L., Boerboom, T.J., McSwiggen, P.L., 2001, Geochemical characterization of Paleoproterozoic volcanic and hypabyssal igneous rocks, east-central Minnesota: *Minnesota Geological Survey Report of Investigations 57*, 33 p.
- Southwick, D.L., and Morey, G.B., 1991, Tectonic imbrication and foredeep development in the Penokean orogen, east-central Minnesota: An interpretation based on regional geophysics and the results of test-drillings, *in* Sims, P.K., and Carter, L.M.H., eds., *Contributions to Precambrian geology of Lake Superior region: U.S. Geological Survey Bulletin 1904-C*, p. C1-C17.
- Southwick, D.L., Morey, G.B., and McSwiggen, P.L., 1988, Geologic map (scale 1:250,000) of the Penokean orogen, central and eastern Minnesota, and accompanying text: *Minnesota Geological Survey Report of Investigations 37*, 25 p.
- Sun, S.S., and McDonough, W.F., 1989, Chemical and isotopic systematics of oceanic basalts: Implications for mantle composition and processes, *in* Saunders, A.D., and Norry, M.J., eds., *Magmatism in the ocean basins: Geological Society (London) Special Publication 42*, p. 313-345.
- Taylor, S.R., and McClelland, S.M., 1985, *The continental crust: Its composition and evolution: Oxford, Blackwell Scientific*, 328 p.
- Tipping, R., and Allen, D., 1997, Hydrogeology of saline- and boron-bearing ground waters in the North Shore Volcanic Group, Minnesota [abs.]: *Institute on Lake Superior Geology, 43rd Annual Meeting, Sudbury, Ontario, Proceedings*, v. 43, Program and Abstracts, pt. 1, p. 61-62.
- Tobisch, O.T., and Paterson, S.R., 1988, Analysis and interpretation of composite foliations in areas of progressive deformation: *Journal of Structural Geology*, v. 10, no. 7, p. 745-754.
- Wonder, J.D., Spry, P.G., and Windom, K.E., 1988, Geochemistry and origin of manganese-rich rocks related to iron-formation and sulfide deposits, western Georgia: *Economic Geology*, v. 83, no. 5, p. 1070-1081.

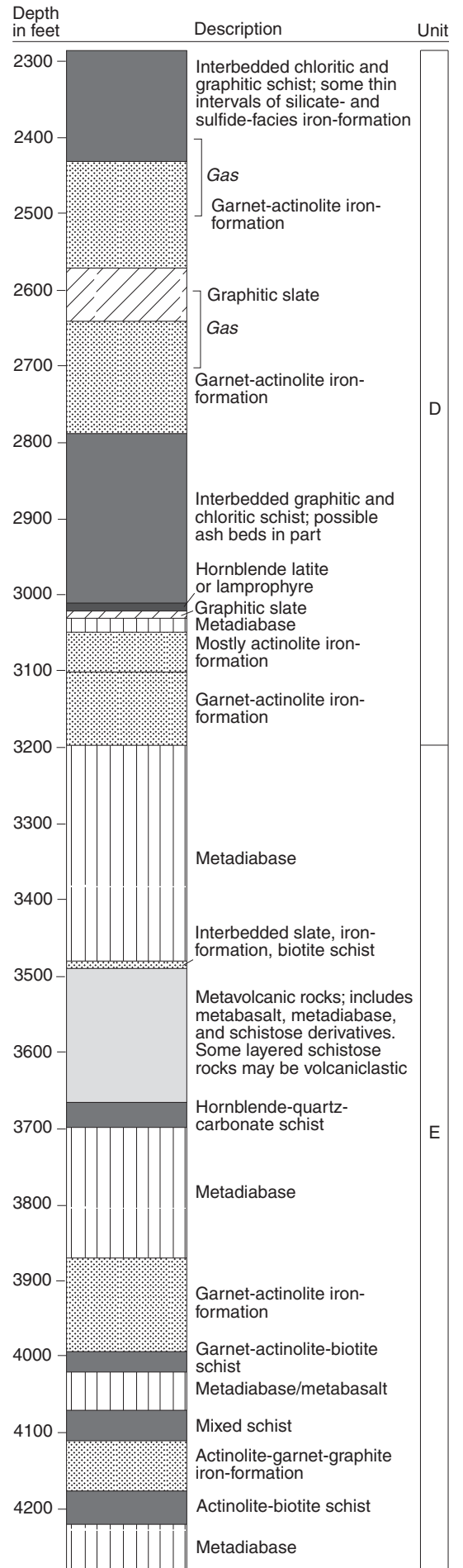
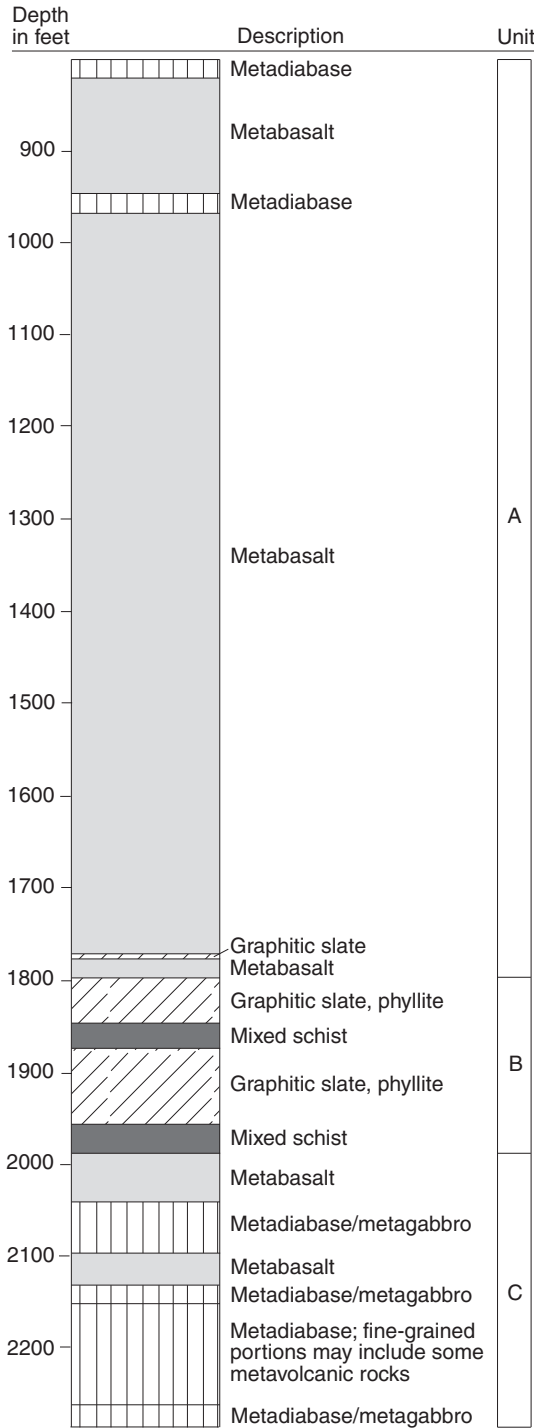
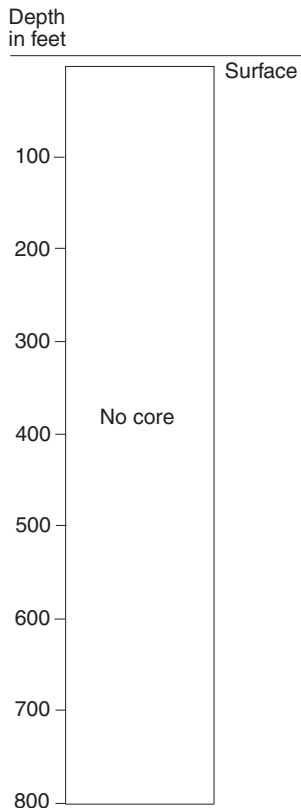


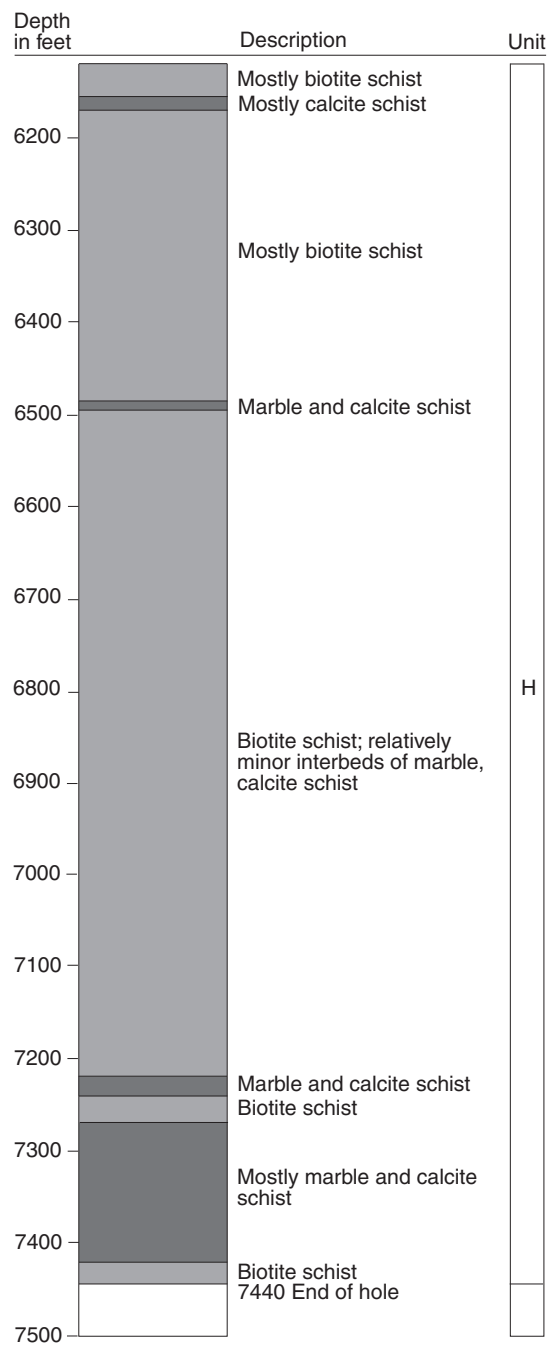
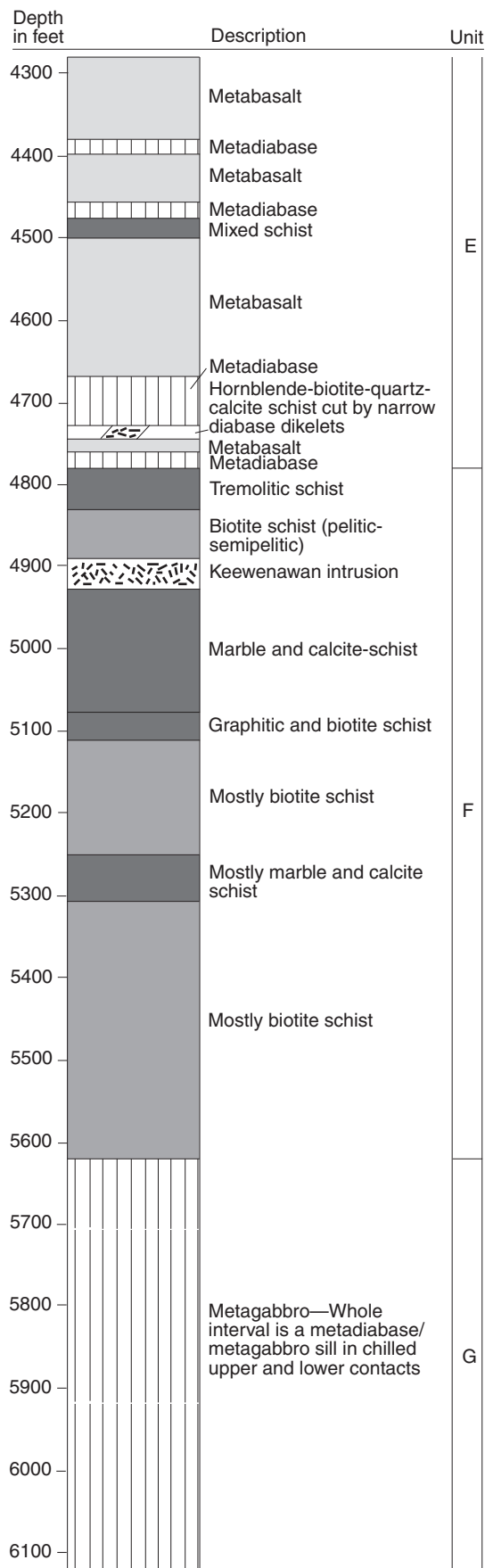
# APPENDIX

**Appendix Figure 1.** Simplified graphitic log of the Hattenberger core.

## EXPLANATION

-  Metabasalt
-  Biotite schist
-  Mixed schist
-  Slate
-  Metadiabase/metagabbro
-  Iron-formation
-  Latite
-  Keewenawan intrusion





**Appendix Table 1.** Geochemical analyses of 55 rock samples from the Hattenbeger core. Values in weight percent.

Code number	Sample number	SiO <sub>2</sub>	Al <sub>2</sub> O <sub>3</sub>	Fe <sub>2</sub> O <sub>3</sub>	MnO	MgO	CaO	Na <sub>2</sub> O	K <sub>2</sub> O	TiO <sub>2</sub>	P <sub>2</sub> O <sub>5</sub>	LOI	total %	C/total	S/total	Organic C	C as granite	CO <sub>2</sub>
hbgr 1	1126	50.08	16.37	11.10	0.15	4.96	9.93	3.64	0.27	1.60	0.19	1.64	99.97					
hbgr 2	1416	44.92	16.78	11.01	0.17	4.18	13.08	3.26	0.42	1.56	0.18	5.12	100.69					
hbgr 3	1682	48.46	14.78	12.85	0.19	6.41	10.72	2.87	0.37	1.51	0.16	1.01	99.33					
hbgr 4	1793	85.40	3.89	4.12	0.02	0.09	3.07	1.52	0.06	0.04	<0.01	2.74	100.96					
hbgr 5	1818	48.94	11.11	18.01	0.07	1.32	3.84	1.03	3.00	0.36	0.02	9.87	97.61	3.33	8.11	2.17	0.13	3.76
hbgr 6	1845	46.16	15.85	14.00	0.12	4.35	3.77	2.63	3.81	1.29	0.14	5.74	97.90					
hbgr 7	1855	59.07	17.20	5.59	0.06	2.08	2.43	1.88	3.73	0.53	0.02	5.09	97.70					
hbgr 8	1862	46.96	14.82	14.29	0.16	8.11	3.01	1.86	0.96	1.41	0.20	6.39	98.22					
hbgr 9	1870	58.15	18.93	6.36	0.02	1.62	0.55	0.52	6.17	0.69	0.20	4.85	98.10					
hbgr 10	1947	58.89	18.61	6.82	0.03	1.90	0.87	4.27	2.97	0.58	0.03	3.68	98.66					
hbgr 11	2010	47.78	13.53	12.51	0.18	4.87	10.79	3.25	0.24	1.57	0.23	5.28	100.21					
hbgr 12	2192	47.88	14.43	12.81	0.21	6.42	12.44	2.22	0.44	1.37	0.25	1.29	99.75					
hbgr 13	2263	44.93	13.25	10.97	0.17	6.10	9.05	2.66	0.55	1.15	0.20	8.74	97.81					
hbgr 14	2334	52.73	15.96	10.48	0.13	2.50	2.22	6.07	1.15	2.02	0.48	4.54	98.33					
hbgr 15	2429	39.12	13.10	10.72	0.21	4.03	13.15	3.78	0.32	1.13	0.21	12.04	87.84	3.29	0.03	0.06	0.04	11.72
hbgr 16	2431	48.27	10.68	24.51	0.29	3.08	2.67	0.09	1.89	1.03	0.10	6.40	99.05					
hbgr 17	2437	45.05	9.24	26.54	0.58	3.09	3.35	0.06	0.38	1.01	0.10	9.39	98.82					
hbgr 18	2456	60.51	5.05	20.74	0.36	1.62	2.65	0.02	0.23	0.48	0.06	6.23	97.97					
hbgr 19	2461	33.52	9.51	31.19	0.87	3.09	5.90	0.18	1.06	1.18	0.13	11.78	98.39					
hbgr 20	2495	37.63	8.36	30.54	0.70	2.38	6.15	0.09	0.25	0.97	0.09	11.11	98.31	2.88	4.33	1.12	0.54	4.5
hbgr 21	2544	36.99	15.60	30.53	0.39	3.26	0.36	1.46	1.25	2.19	0.23	6.73	98.99					
hbgr 22	2666	23.33	16.72	42.47	1.05	4.43	1.10	0.09	0.39	1.65	<0.01	6.71	97.99					
hbgr 23	2984	41.03	14.80	15.55	0.15	4.35	7.15	2.30	4.16	2.26	0.62	5.24	97.68					
hbgr 24	3010	51.52	15.80	10.25	0.11	3.18	5.01	3.80	2.52	1.91	0.51	4.34	99.01					
hbgr 25	3047	47.21	14.71	12.30	0.20	5.71	12.70	1.01	0.67	1.52	0.37	3.57	99.96					

Sample numbers correlate with sample depth, in feet

**Appendix Table 1. Continued**  
Values in weight percent.

Code number	Sample number	SiO <sub>2</sub>	Al <sub>2</sub> O <sub>3</sub>	Fe <sub>2</sub> O <sub>3</sub>	MnO	MgO	CaO	Na <sub>2</sub> O	K <sub>2</sub> O	TiO <sub>2</sub>	P <sub>2</sub> O <sub>5</sub>	LOI	total %	C/total	S/total	Organic C	C as granite	CO <sub>2</sub>
hbgr 26	3149	51.34	9.21	20.69	0.50	2.22	5.89	0.09	0.10	1.52	0.11	6.83	98.53					
hbgr 27	3277	47.10	11.66	18.86	0.27	4.61	9.42	0.95	1.40	2.78	0.28	1.70	99.10					
hbgr 28	3485	50.17	6.84	32.24	0.25	2.37	2.16	0.23	0.47	1.31	0.09	4.20	100.33					
hbgr 29	3623	45.87	14.26	22.41	0.25	4.12	4.16	0.68	2.54	2.35	0.14	1.89	98.72					
hbgr 30	3818	50.74	14.43	15.45	0.21	5.02	6.77	3.75	0.49	2.16	0.39	1.33	100.75					
hbgr 31	3938	35.79	10.72	37.88	0.56	3.22	2.01	0.41	2.65	1.02	0.10	6.19	100.59					
hbgr 32	4016	47.19	8.34	13.60	0.19	2.46	10.81	1.04	3.19	1.01	0.06	10.89	98.81	4.12	1.57	1.16	0.2	10.12
hbgr 33	4134	60.65	9.27	16.45	0.33	2.25	6.61	0.89	0.85	0.99	0.09	2.57	100.93					
hbgr 34	4332	52.83	14.63	12.02	0.17	4.92	7.75	3.08	1.43	1.83	0.38	1.35	100.36					
hbgr 35	4411	49.04	13.35	13.77	0.26	4.74	9.71	3.90	0.77	2.10	0.40	2.29	100.33					
hbgr 36	4652	47.33	13.46	11.92	0.22	5.24	7.57	3.40	1.98	1.98	0.21	7.04	100.36					
hbgr 37	4845	70.17	6.82	2.52	0.03	6.92	7.88	2.24	1.00	0.19	0.03	2.65	100.46					
hbgr 38	4934	13.26	0.30	1.46	0.08	17.66	27.88	<0.01	0.02	<0.01	<0.01	38.38	99.04	10.76	0.06	<0.03	0.01	39.42
hbgr 39	5067	56.55	13.76	4.26	0.03	3.68	5.22	0.29	7.69	0.55	0.07	6.38	98.48					
hbgr 40	5115	56.33	18.79	11.76	0.11	2.28	0.27	2.25	5.67	0.62	0.10	2.44	100.62					
hbgr 41	5118	84.93	3.94	6.02	0.18	0.91	1.25	0.38	1.02	0.09	0.99	0.65	100.36					
hbgr 42	5181	90.60	2.23	2.91	0.08	0.42	0.96	0.01	1.00	0.03	0.19	0.93	99.36					
hbgr 43	5256	8.64	0.25	1.57	0.10	18.60	27.07	0.02	0.10	<0.01	<0.01	42.48	98.84	11.98	0.03	0.03	0.01	43.79
hbgr 44	5284	9.96	0.43	2.52	0.10	18.07	30.67	<0.01	0.02	0.02	<0.01	37.54	99.34	9.83	0.03	0.03	0.06	35.74
hbgr 45	5411	49.12	19.96	11.91	0.05	2.91	2.38	0.13	8.44	1.48	0.31	3.50	100.20					
hbgr 46	5532	77.88	1.61	1.07	0.07	1.98	9.56	0.01	0.88	0.09	0.05	7.55	100.75					
hbgr 47	5549	55.25	18.22	10.97	0.04	2.40	3.73	5.24	2.47	0.97	0.10	1.40	100.79					
hbgr 48	5606	56.49	19.92	7.54	0.03	3.49	1.19	3.09	5.66	0.84	0.13	2.08	100.44					
hbgr 49	5652	47.04	15.30	14.04	0.21	6.68	9.72	2.66	0.23	1.66	0.13	2.89	100.60					
hbgr 50	5831	33.05	9.72	5.34	0.17	13.10	18.30	0.07	4.80	0.56	0.06	14.43	99.60					
hbgr 51	6120	50.84	16.77	5.35	0.14	2.88	9.54	6.33	0.84	0.77	0.05	6.90	100.41					
hbgr 52	6812	18.04	3.65	46.18	0.34	3.46	11.34	0.08	0.47	0.14	0.89	13.14	97.73	2.61	20.55	0.1	0.02	9.13
hbgr 53	6833	55.47	13.51	16.99	0.56	5.26	1.70	0.98	2.53	0.62	0.41	2.55	100.58					
hbgr 54	7046	57.59	21.79	7.64	0.06	2.24	0.21	0.66	5.33	0.67	0.07	3.77	100.03					
hbgr 55	7317	71.60	2.81	6.40	0.15	1.13	8.51	0.23	1.25	0.11	0.02	8.72	100.97					

Sample numbers correlate with sample depth, in feet



**Appendix Table 1. Continued**

Values in parts per million, except Au and Ir in parts per billion.

Code number	Sample number	Pb	Zn	Ag	Ni	Cd	Bi	V	Be	Au	As	Br	Co	Cr	Cs	Hf	Hg	Ir
hbgr 1	1126	<5.0	70.0	<0.4	79.0	<0.5	<5.0	184.0	<2.0	<5	<2	<1	34	130	<0.5	2.6	8	<5
hbgr 2	1416	5.0	98.0	<0.4	59.0	0.7	<5.0	174.0	<2.0	<5	<2	<1	33	146	0.9	2.2	<1	<5
hbgr 3	1682	5.0	118.0	<0.4	77.0	0.7	<5.0	228.0	<2.0	<5	<2	<1	42	290	<0.5	2.4	<1	<5
hbgr 4	1793	<5.0	21.0	0.5	82.0	<0.5	<5.0	3.0	<2.0	<5	<2	<1	29	14	<0.5	<0.5	3	<5
hbgr 5	1818	16.0	10.0	0.5	133.0	0.8	<5.0	167.0	<2.0	8	4	<1	24	647	1.8	1.8	<1	<5
hbgr 6	1845	1.0	368.0	<0.4	69.0	1.1	<5.0	192.0	<2.0	<5	<2	<1	28	110	4.9	2.7	<1	<5
hbgr 7	1855	20.0	110.0	<0.4	62.0	<0.5	<5.0	125.0	<2.0	<5	<2	<1	11	86	<0.5	3.3	<1	<5
hbgr 8	1862	6.0	127.0	<0.4	71.0	0.5	<5.0	221.0	<2.0	<5	4	<1	37	37	1.9	2.6	<1	<5
hbgr 9	1870	18.0	75.0	<0.4	73.0	0.5	<5.0	191.0	<2.0	<5	<2	<1	10	100	1.6	3.1	<1	<5
hbgr 10	1947	18.0	58.0	<0.4	70.0	<0.5	7.0	189.0	<2.0	<5	<2	<1	17	100	1	3.7	<1	<5
hbgr 11	2010	5.0	95.0	<0.4	33.0	<0.5	<5.0	225.0	<2.0	<5	<2	<1	32	32	<0.5	1.9	<1	<5
hbgr 12	2192	6.0	88.0	0.4	67.0	<0.5	6.0	241.0	<2.0	<5	6	<1	39	145	0.6	2	<1	<5
hbgr 13	2263	<5.0	72.0	<0.4	76.0	<0.5	<5.0	200.0	<2.0	<5	<2	<1	36	140	<0.5	1.8	<1	<5
hbgr 14	2334	9.0	112.0	<0.4	39.0	0.5	<5.0	170.0	<2.0	<5	3	<1	19	52	1.1	3.4	<1	<5
hbgr 15	2429	9.0	59.0	<0.4	76.0	<0.5	<5.0	213.0	<2.0	<5	11	<1	30	47	<0.5	1.2	<1	<5
hbgr 16	2431	<5.0	89.0	<0.4	46.0	<0.5	<5.0	160.0	3.0	7	<2	<1	20	31	3.3	5.3	<1	<5
hbgr 17	2437	<5.0	77.0	<0.4	36.0	0.7	<5.0	148.0	4.0	<5	<2	<1	15	32	1.2	4.1	<1	<5
hbgr 18	2456	<5.0	48.0	<0.4	57.0	<0.5	<5.0	82.0	2.0	6	<2	<1	30	23	1.2	2.1	<1	<5
hbgr 19	2461	6.0	96.0	<0.4	37.0	<0.5	<5.0	123.0	10.0	20	<2	<1	32	31	3.1	4.3	<1	<5
hbgr 20	2495	6.0	76.0	<0.4	69.0	<0.5	<5.0	129.0	2.0	<5	<2	<1	38	35	<0.5	3.8	<1	<5
hbgr 21	2544	5.0	124.0	<0.4	32.0	<0.5	<5.0	186.0	11.0	<5	<2	<1	25	50	2.2	6.1	<1	<5
hbgr 22	2666	9.0	121.0	<0.4	52.0	<0.5	<5.0	228.0	<2.0	<5	<2	<1	36	58	2.4	5.5	<1	<5
hbgr 23	2984	5.0	171.0	<0.4	51.0	<0.5	<5.0	317.0	<2.0	<5	<2	<1	27	17	1.6	4	<1	8
hbgr 24	3010	9.0	139.0	<0.4	34.0	<0.5	<5.0	309.0	<2.0	6	<2	<1	11	31	1.8	3.7	<1	<5
hbgr 25	3047	6.0	89.0	<0.4	43.0	<0.5	<5.0	224.0	<2.0	<5	10	<1	36	40	1	2.2	<1	<5

**Appendix Table 1.** Continued

Values in parts per million, except Au and Ir in parts per billion.

Code number	sample number	Pb	Zn	Ag	Ni	Cd	Bi	V	Be	Au	As	Br	Co	Cr	Cs	Hf	Hg	Ir
hbgr 26	3149	<5.0	77.0	<0.4	34.0	<0.5	<5.0	109.0	<2.0	<5	<2	<1	18	45	<0.5	4	<1	<5
hbgr 27	3277	<5.0	137.0	<0.4	49.0	<0.5	<5.0	328.0	<2.0	9	<2	<1	49	24	2.2	4	<1	<5
hbgr 28	3485	<5.0	54.0	<0.4	89.0	<0.5	<5.0	103.0	3.0	<5	<2	<1	58	35	1.3	3.4	<1	<5
hbgr 29	3623	<5.0	49.0	<0.4	45.0	0.5	<5.0	206.0	3.0	<5	<2	<1	19	54	2.3	7	<1	<5
hbgr 30	3818	5.0	97.0	<0.4	23.0	<0.5	<5.0	280.0	2.0	<5	<2	<1	37	32	0.9	237	<1	<5
hbgr 31	3938	<5.0	128.0	<0.4	51.0	<0.5	<5.0	151.0	<2.0	<5	<2	<1	23	30	5.8	4.3	<1	<5
hbgr 32	4016	<5.0	58.0	<0.4	26.0	<0.5	<5.0	106.0	<2.0	<5	<2	<1	12	26	2.6	3.9	<1	<5
hbgr 33	4134	7.0	62.0	<0.4	17.0	<0.5	6.0	129.0	<2.0	<5	<2	<1	9	26	1	4.1	<1	<5
hbgr 34	4332	5.0	96.0	<0.4	18.0	<0.5	<5.0	226.0	2.0	<5	<2	<1	24	24	<0.5	3.7	<1	<5
hbgr 35	4411	5.0	114.0	<0.4	22.0	0.8	<5.0	274.0	2.0	<5	<2	<1	34	39	0.6	3.9	<1	<5
hbgr 36	4652	5.0	36.0	<0.4	23.0	0.5	<5.0	265.0	<2.0	<5	<2	<1	28	39	1.8	3.5	<1	<5
hbgr 37	4845	7.0	20.0	<0.4	36.0	<0.5	<5.0	27.0	<2.0	<5	4	<1	6	46	<0.5	0.7	<1	<5
hbgr 38	4934	<5.0	7.0	<0.4	6.0	<0.5	<5.0	2.0	<2.0	<5	<2	<1	<1	5	<0.5	<0.5	<1	<5
hbgr 39	5067	10.0	108.0	<0.4	61.0	0.5	<5.0	91.0	<2.0	<5	<2	<1	11	94	3.8	2.4	<1	<5
hbgr 40	5115	<5.0	87.0	<0.4	28.0	<0.5	<5.0	85.0	2.0	<5	<2	<1	5	87	9.3	2.8	<1	<5
hbgr 41	5118	8.0	28.0	<0.4	13.0	<0.5	<5.0	13.0	<2.0	<5	<2	<1	8	34	3	1.7	<1	<5
hbgr 42	5181	6.0	8.0	<0.4	9.0	<0.5	<5.0	6.0	<2.0	<5	<2	<1	3	16	0.5	1.2	<1	<5
hbgr 43	5256	<5.0	70.0	<0.4	8.0	<0.5	<5.0	2.0	<2.0	<5	<2	<1	<1	2	<0.5	<0.5	<1	<5
hbgr 44	5284	<5.0	136.0	<0.4	4.0	<0.5	<5.0	2.0	<2.0	<5	<2	<1	<1	3	<0.5	<0.5	<1	<5
hbgr 45	5411	13.0	94.0	<0.4	46.0	<0.5	<5.0	86.0	2.0	<5	2	<1	26	100	2.7	7.2	<1	<5
hbgr 46	5532	5.0	25.0	<0.4	11.0	<0.5	<5.0	6.0	<2.0	<5	5	<1	8	13	0.7	<0.5	<1	<5
hbgr 47	5549	5.0	28.0	<0.4	58.0	<0.5	<5.0	44.0	2.0	<5	3	<1	14	78	1.5	4.8	<1	<5
hbgr 48	5606	11.0	41.0	<0.4	57.0	<0.5	<5.0	78.0	2.0	<5	<2	<1	14	127	3.2	6.9	<1	<5
hbgr 49	5652	5.0	98.0	<0.4	143.0	<0.5	<5.0	205.0	<2.0	8	<2	<1	49	210	<0.5	2.1	<1	<5
hbgr 50	5831	8.0	137.0	0.4	35.0	<0.5	<5.0	34.0	2.0	<5	3	<1	48	59	4.4	3.3	<1	<5
hbgr 51	6120	7.0	46.0	<0.4	46.0	0.5	<5.0	55.0	<2.0	<5	<2	<1	13	95	2.1	6.1	<1	<5
hbgr 52	6812	9.0	44.0	<0.4	286.0	0.7	<5.0	23.0	<2.0	10	<2	<1	82	25	1	0.6	<1	<5
hbgr 53	6833	7.0	128.0	<0.4	77.0	<0.5	<5.0	105.0	<2.0	<5	<2	<1	38	260	5.6	2.6	<1	<5
hbgr 54	7046	22.0	83.0	<0.4	52.0	<0.5	<5.0	96.0	2.0	<5	<2	<1	18	154	3.3	2.5	<1	<5
hbgr 55	7317	34.0	52.0	<0.4	114.0	<0.5	<5.0	16.0	<2.0	<5	<2	<1	27	26	0.8	<0.5	<1	<5

**Appendix Table 1. Continued**  
Values in parts per million.

Code number	Sample number	Mo	Rb	Sb	Sc	Se	Ta	Th	U	W	La	Ce	Nd	Sm	Eu	Tb	Yb	Lu
hbgr 1	1126	<5	<10	<0.2	26	<3	2	2.4	<0.5	<3	13.2	30	17	3.7	1.2	0.7	2.2	0.37
hbgr 2	1416	<5	<10	<0.2	26	<3	<1	1.4	<0.5	<3	10.6	20	14	2.9	0.9	<0.5	2.0	0.27
hbgr 3	1682	<5	<10	<0.1	38	<3	<1	1.5	<0.5	<3	10.1	25	12	3.1	101	0.7	2.2	0.31
hbgr 4	1793	<5	11	<0.2	0.6	<3	<1	<0.5	<0.5	4	0.5	<3	<5	0.1		<0.5	<0.1	<0.05
hbgr 5	1818		72	0.3	9.1	<3	<1	5.8	6.9	<3	23.1	38	18	2.9	0.6	<0.5	0.9	0.21
hbgr 6	1845	<5	186	0.2	25	<3	2	4.2	1.5	<3	15.1	33	19	3.6	0.8	<0.5	1.6	0.28
hbgr 7	1855	<5	96	<0.2	11	<3	<1	9.7	5	<3	28.8	46	21	3	0.8	<0.5	0.9	0.18
hbgr 8	1862	<5	58	<0.2	29	<3	<1	3	1.3	<3	15.6	32	17	3.8	1.1	0.8	2.2	0.35
hbgr 9	1870	<5	139	<0.2	13	<3	<1	9.2	6.2	<3	24.8	45	23	3.7	0.8	<0.5	1.0	0.19
hbgr 10	1947	11	89	<0.2	10	<3	1	10.1	7.2	<3	27.3	48	19	3.1	0.9	<0.5	1.0	0.15
hbgr 11	2010	<5	<10	<0.2	28	<3	<1	1.6	<0.5	<3	12.6	27	14	3.3	0.9	<0.5	1.5	0.23
hbgr 12	2192	<5	<10	<0.2	33	<3	<1	1.5		<3	16.1	37	19	3.9	1.4	0.6	2.0	0.28
hbgr 13	2263	<5	<10	<0.2	27	<3	<1	1.6	<0.5	<3	14.9	30	20	3.4	1	<0.5	1.5	0.25
hbgr 14	2334	<5	36	<0.2	22	<3	1	6.3	4	<3	63.1	123	60	9.8	3	1.0	1.8	0.28
hbgr 15	2429	<5	<10	<0.2	24	<3	1	1	<0.5	<3	9.3	20	9	2.5	0.9	<0.5	0.9	0.17
hbgr 16	2431	<5	69	<0.2	17	<3	3	9.3	3.5	<3	29.6	56	24	4.6	1.2	<0.5	2.9	0.44
hbgr 17	2437	<5	32	<0.2	16	<3	2	7.4	3.5	<3	34.7	68	33	5.6	1.2	0.9	2.7	0.39
hbgr 18	2456	<5	<10	<0.2	8.7	<3	<1	3.7	1.7	<3	19.9	38	19	3.4	0.8	0.6	1.4	0.23
hbgr 19	2461	5	50	0.3	15	<3	2	6.9	2.5	<3	37.1	75	33	5.3	1.3	0.9	2.9	0.39
hbgr 20	2495	<5	<10	<0.2	15	<3	<1	6.7	3.6	<3	32.8	62	28	5.1	1.2	<0.5	2.3	0.36
hbgr 21	2544	6	63	<0.2	24	<3	2	10.8	5	<3	54.1	96	44	7.8	1.8	1.2	2.8	0.44
hbgr 22	2666	<5	<10	0.2	24	<3	2	9.3	2.9	<3	39.5	80	36	6.2	1.6	1.2	5.0	0.76
hbgr 23	2984	5	61	0.2	29	<3	2	3.5	1.8	<3	52.3	92	48	8.1	2.1	1.0	2.0	0.35
hbgr 24	3010	9	62	<0.2	26	<3	<1	3.7	7.5	<3	51.8	99	56	8.9	2.2	0.9	2.5	0.37
hbgr 25	3047	<5	<10	0.3	29	<3	<1	1.8	<0.5	<3	24.9	55	28	5	1.6	0.6	1.5	0.2

**Appendix Table 1. Continued**  
Values in parts per million.

Code number	Sample number	Mo	Rb	Sb	Sc	Se	Ta	Th	U	W	La	Ce	Nd	Sm	Eu	Tb	Yb	Lu
hbgr 26	3149	<5	<10	<0.2	15	<3	2	5.5	2.1	3	24.3	47	22	4.1	1.1	0.6	2.1	0.35
hbgr 27	3277	<5	54	<0.2	39	<3	1	3.1	0.8	<3	20.1	45	19	5.8	1.8	1.2	4.1	0.62
hbgr 28	3485	<5	22	0.2	11	14	2	5.4	1.1	<3	25.7	47	21	3.6	1.1	<0.5	2.0	0.31
hbgr 29	3623	<5	80	<0.2	25	<3	2	10	2.6	<3	39.9	78	34	6.3	2.1	0.9	3.4	0.53
hbgr 30	3818	<5	<10	<0.2	27	<3	2	3	<0.5	<3	25.1	52	21	5.3	1.5	0.6	2.0	0.28
hbgr 31	3938	5	111	<0.2	12	<3	2	8.5	4.1	<3	24.7	63	27	5.2	1.1	1.0	3.0	0.54
hbgr 32	4016	<5	87	<0.2	13	<3	1	6.7	2.8	<3	27.5	53	24	4.3	1.1	0.6	2.2	0.36
hbgr 33	4134	<5	22	<0.2	14	<3	2	7	2.6	<3	31.7	60	25	4.2	1.1	0.7	2.8	0.38
hbgr 34	4332	<5	28	<0.2	23	<3	2	5.1	1	<3	40.9	74	34	6.8	2.3	1.0	2.7	0.36
hbgr 35	4411	<5	18	<0.2	28	<3	1	4.1	<0.5	<3	30.2	68	35	6.5	1.9	<0.5	2.5	0.36
hbgr 36	4652	<5	42	<0.2	28	<3	<1	3.1	<0.5	<3	20.2	48	23	5.2	1.4	1.0	2.2	0.3
hbgr 37	4845	<5	22	<0.2	4.5	<3	<1	2.4	1.3	<3	6.6	13	<5	1	0.3	<0.5	0.4	0.06
hbgr 38	4934	<5	<10	<0.2	0.3	<3	<1	0.6	<0.5	<3	4.4	6	<5	0.6	0.1	<0.5	0.3	<0.05
hbgr 39	5067	<5	98	<0.2	11	<3	<1	8.1	3.1	<3	28.3	52	25	4.1	1	<0.5	1.5	0.25
hbgr 40	5115	<5	162	<0.2	14	<3	<1	11	1.9	<3	27.6	45	18	3	0.6	<0.5	0.8	0.14
hbgr 41	5118	<5	27	<0.2	2.5	<3	<1	2.5	0.8	<3	10	28	11	1.4	0.4	<0.5	0.4	0.06
hbgr 42	5181	<5	22	<0.2	1	<3	<1	1.4	<0.5	<3	4.1	11	6	0.5	0.1	<0.5	0.2	<0.05
hbgr 43	5256	<5	<10	<0.2	0.4	<3	<1	<0.5	<0.5	<3	1.5	<3	<5	0.2	<0.1	<0.5	<0.1	<0.05
hbgr 44	5284	<5	<10	<0.2	0.4	<3	<1	<0.5	0.6	<3	3.7	5	<5	0.4	0.1	<0.5	0.1	<0.05
hbgr 45	5411	<5	155	<0.2	21	<3	1	12.9	1.8	<3	73.6	148	67	10.4	2.9	1.5	3.1	0.49
hbgr 46	5532	<5	17	<0.2	1.3	<3	<1	1.1	<0.5	<3	4.4	10	5	0.7	0.1	<0.5	0.5	0.07
hbgr 47	5549	<5	57	0.3	20	<3	2	10	1	<3	101	176	74	11	2.6	1.2	2.3	0.37
hbgr 48	5606	<5	134	<0.2	14	<3	2	13.5	2	<3	54.5	113	53	7.8	1.7	1.1	2.6	0.37
hbgr 49	5652	<5	<10	<0.2	33	<3	<1	1.7	<0.5	<3	10.3	23	14	3.2	1	<0.5	2.2	0.34
hbgr 50	5831	<5	100	<0.2	8.4	<3	<1	8.2	0.7	<3	28.5	57	25	3.4	0.7	<0.5	1.4	0.2
hbgr 51	6120	<5	<10	<0.2	111	<3	<1	11	0.6	<3	11.1	25	15	3.9	0.6	0.9	2.1	0.35
hbgr 52	6812	9	33	<0.2	5.7	6	<1	1.1	0.9	<3	7.1	19	7	1.4	0.6	<0.5	1.3	0.21
hbgr 53	6833	<5	96	<0.2	19	<3	<1	3.8	1	<3	14	45	19	3.7	0.9	<0.5	2.0	0.32
hbgr 54	7046	<5	159	<0.2	19	<3	<1	11.2	2.2	<3	47.4	95	39	5.8	1.4	<0.5	1.5	0.22
hbgr 55	7317	<5	22	<0.2	2.4	<3	<1	1.1	<0.5	<3	4.8	11	<5	1.3	0.5	<0.5	1.5	0.24